

A thesis submitted to Royal Holloway, University of London for the
degree of

Doctor of Philosophy

Non-equilibrium dynamics in models of selection and recombination: heteroclinic cycles, networks and chaos

by

TIMOTHY W. RUSSELL

2019



Supervisor: Professor Vincent A. A. Jansen

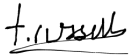
School of Biological Sciences

Royal Holloway
University of London

Declaration

I, Timothy W. Russell, hereby declare that this thesis and the work presented in it is my own. Where I have consulted the work of others, or a piece of work was done in collaboration with others, this is always clearly stated

Signed:

A handwritten signature in black ink, appearing to read "T. Russell", written over a horizontal line.

Date: September 6, 2020

Acknowledgements

My foremost thanks must go to my supervisor, Vincent Jansen. From the very start, he has provided me with scientific mentorship of the highest quality. On top of that, he was able to guide me through difficult decisions as smoothly as possible, always with my best interests at heart. I have thoroughly enjoyed working closely with him, especially when in front of the blackboard tackling difficult mathematical modelling problems in real-time. His speed of thought and his ability to visualise complicated dynamics have been a constant source of motivation.

Secondly, I thank my brother Matt Russell. He has aided me for so long in mathematics and computing, to the point where he is not just a mentor and a brother, but a coauthor! Combining mathematics, computing, music and socialising in the way that we have been for many years is a source of utmost joy for me and I hope it continues for as long as possible.

My collaborator, Francisco Úbeda requires an enormous thanks for providing me with the initial interest and ideas and ultimately the initial formulations of the models used in our papers. The interesting discussions throughout my PhD were very valuable and were the source of inspiration for many research avenues.

Thanks to all of the members of the EEB research group who made my time at Royal Holloway very enjoyable; especially Dan Sankey and Francesco Santi. Sharing our work, collaborating and talking about it in-depth at the pub has allowed me to gain more access to the experimental side of what is done in the group.

The rest of my family, especially my parents, have been wonderful. A constant source of support, never failing to remind me how proud they are. Without their support, especially throughout my Undergraduate and Masters degrees, I am certain I would not have been able to complete a PhD.

I would like to thank all of my incredible friends and loved ones. I am sure to miss some, but those I would like to thank by name are: Lizzy Iredale, Paul Macleod, Sam Smith, Arman Salimian, Gemma Tong, Jeri Smith-Cronin, Tom King, Alastair Gordon, Dan Iley-Williamson, Claire Hall, Josh Cannell, Sarah Sutton and Katherine Hannaford. I would like to especially thank those with whom I've been able to discuss my scientific work and my career with: Liam Shaw, Joel Hellewell, John Lees, Ben Tappin and Rox Middleton. Your academic success, on top of everything else that you do, has greatly inspired me.

Abstract

The dynamics of gene frequencies are extraordinarily complex. Disentangling and abstracting away this complexity often requires a mathematical approach. Traditionally, theoretical population genetics has primarily focused on models which are simple enough to be amenable to analysis, or too complex for any analytic progress to be made — the latter relying heavily on numerical methods. We seek to make progress by analysing models which are in the middle ground: mechanistically derived and amenable to detailed analytic analysis, yet complex enough for the dynamic behaviours to be non-equilibrial. For example, Chapter 3 sees advances from empirical knowledge of the molecular action of a protein, known as PRDM9, on its target site, and associated potential fertility benefits, in a two-locus two-allele model. The recency of the empirical details of this action led to the model being truly novel. Plus, it has interesting dynamic consequences, such as the existence of a degenerate bifurcation and an attracting heteroclinic cycle. Furthermore, we have been able to go beyond the endpoint for many classical analyses: finding equilibria and determining their linear stability. We do so in Chapter 5, where we: find a Lyapunov function for a special case of the two-locus two-allele system, find an approximate closed-form expression for a well-known invariant manifold in population genetics and, using this expression, prove stability of a heteroclinic cycle bounded by the edges in the reduced system. We extended existing models in Chapters 4 and 6. The extensions are of models of recombination hotspot evolution and segregation distorters (respectively). Mathematically, they boil down to systems of eight and nine coupled difference equations. The resulting models were both more biologically realistic and capable of complex dynamics — the second model exhibiting chaotic-like dynamics nearby a heteroclinic network. In these models, we are able to calculate analytic polymorphic equilibria expressions in both (the first being an approximation, but a highly accurate one; the second being exact). Chapter 2, the review, framework and methodology chapter, named *the selection-recombination equation*, contributes a clear and verbose guide through some of what is known about the equation including some technical details from the recent advances. We analyse the models presented without the need for the almost ubiquitous *weak selection approximation*, an assumption that produces a small selection parameter (relative to the other parameters) — a common technique for simplifying models in applied dynamical systems.

Contents

1	Introduction	13
1.1	Biological background	14
1.1.1	The genetic code	14
1.1.2	The laws of Mendelian inheritance	15
1.1.3	The forces behind changes in gene frequencies	17
1.1.3.1	Selection	17
1.1.3.2	Recombination	18
1.1.3.3	Recombination hotspots, <i>PRMD9</i> and the protein PRMD9	18
1.1.3.4	Genetic drift	21
1.1.3.5	Mutation	22
1.1.4	Selfish genetic elements	22
1.1.4.1	Segregation distorters and meiotic drivers	23
1.2	Mathematical background	24
1.2.1	Dynamical systems	24
1.2.1.1	Continuous-time	24
1.2.1.2	Discrete time	25
1.2.1.3	Equilibria	26
1.2.1.4	Linear stability	27
1.3	Goals and structure of the thesis	28
1.4	Additional materials	29
2	The selection-recombination equation	31
2.1	Introduction	33
2.2	The model	34
2.2.1	Two-locus n-alleles	34
2.2.1.1	Discrete-time	34
2.2.1.2	Continuous-time	35
2.2.2	Two-locus two-allele	35
2.2.2.1	The evolution of recombination hotspots model	36

2.3	Reviewing known results	39
2.3.1	Two-locus two-alleles	40
2.3.1.1	Equilibria	40
2.3.1.2	Invariant subspaces	41
2.3.1.3	Invariant line	42
2.3.1.4	Stable cycles	43
2.3.1.5	The quasi-linkage equilibrium manifold	43
2.3.1.6	Coordinate transformation	44
2.4	Conclusions	46
3	PRDM9 and the evolution of recombination hotspots	49
3.1	Introduction	52
3.2	Methods	54
3.2.1	Two-locus n-alleles model	54
3.2.2	Two-locus two-allele model	58
3.3	Results	60
3.3.1	Equilibria	60
3.3.2	Stability	62
3.3.2.1	Corner equilibria	65
3.3.2.2	Heteroclinic orbit	66
3.3.2.3	Internal equilibrium	68
3.3.3	Dynamics	70
3.4	Discussion	72
4	Stable yet distinct linkage disequilibria between sexes due to sexually-antagonistic recombination hotspot evolution	83
4.1	Introduction	85
4.2	Methods	87
4.2.1	Two-locus n-alleles model	87
4.2.2	Cases of biological interest	88
4.2.2.1	No viability effects no sex-antagonistic break	89
4.2.2.2	No viability effects sex-antagonistic break	89
4.2.2.3	Sex-specific viability effects but not sexually antagonistic	90
4.2.2.4	Sex-antagonistic viability	90
4.2.3	Two-locus two-alleles model	90
4.2.4	Simplified model with sex-antagonistic viability	92
4.3	Results	93
4.3.1	Equilibria	93

4.3.1.1	Edge equilibria	93
4.3.1.2	Polymorphic equilibria	93
4.3.1.3	Approximating the interior equilibrium	98
4.3.2	Stability	98
4.3.2.1	Edge equilibria	100
4.3.2.2	Polymorphic equilibria	101
4.4	Discussion	102
5	Stable cycling in quasi-linkage equilibrium: Fluctuating dynamics under gene conversion and selection	109
5.1	Introduction	111
5.2	The model	113
5.3	Analysis and results	115
5.3.1	Change of variables	115
5.3.2	Equilibria and local stability	116
5.3.3	Global stability: a Lyapunov function and heteroclinic cycle . . .	119
5.3.3.1	A continuous-time approximate model	119
5.3.3.2	Lyapunov function	120
5.3.3.3	Discrete-time heteroclinic cycle	121
5.3.4	The QLE manifold	123
5.3.5	Simplification by reducing to allele frequencies	124
5.3.6	Stability of heteroclinic cycle in discrete-time model	126
5.3.7	Justifying the use of D_S derived from the continuous-time model	129
5.4	Discussion	130
6	Chaotic evolutionary dynamics predict faster-than-drift divergence	143
6.1	Main text	145
6.2	Methods	153
6.2.1	The in-patch dynamics	153
6.2.1.1	Equilibria	154
6.2.1.2	Invariant subspaces and heteroclinic connections	155
6.2.2	The spatial model	156
6.3	Supplementary material	156
6.3.1	Model description and motivatoin	156
6.3.2	The models	157
6.3.3	The two-allele model explicitly	157
6.3.4	The three-allele model explicitly	158
6.3.4.1	Matrix notation	160

6.3.5	Some analysis of the two-allele model	160
6.3.5.1	Corner and side equilibria	162
6.3.6	Projection function	164
7	Conclusion	165
7.1	Summary	166
7.1.1	Overview of the models used: their novelty and complexity . . .	166
7.1.2	Details of the analyses	167
7.2	Further work	168
7.3	Concluding remarks	169

List of Figures

1.1	<i>from Wikimedia Commons (2013). The structure of DNA as a double helix along with the individual nucleotide bases and how they bond.</i>	16
1.2	<i>from Seymenoglu (2019). Depiction of a single cross-over event</i>	17
1.3	<i>from Myers et al. (2005). A high resolution map of the rate of recombination across a chromosome</i>	19
1.4	The effects of genetic drift on the frequency of a single allele in different sized populations	21
2.1	Visualising two coordinate transformations used in the study of the selection-recombination equations	45
3.1	Model for recombination initiated by specificity of the double-strand break	55
3.2	Equilibria and heteroclinic cycle	61
3.3	Dynamics of the system	63
3.4	Correspondence between infinite and finite population dynamics	71
3.5	Evolutionary game	74
4.1	The dynamics of the system: an attracting limit cycle	94
4.2	The dynamics of the system: an attracting interior equilibrium	96
4.3	Numerically assessing the accuracy of the approximate polymorphic equilibrium	102
5.1	Time series showing examples of the two types of behaviour of the discrete-time model	117
5.2	The basin of attraction of the heteroclinic cycle against β for the discrete-time model	122
5.3	The approximate quasi-linkage equilibrium manifold, and the approach to it by two typical trajectories of the discrete-time model	123
5.4	The fast approach to the QLE manifold shown using a Poincaré section	125

5.5	The simplification of the system by using the approximate slow manifold, D_{QLE}	127
5.6	Relative error of our approximate manifold D_S	129
6.1	The dynamics of the two-allele model	146
6.2	The dynamics of the three-allele model	148
6.3	The next driver map	150
6.4	A snapshot of the spatial three-allele model	152

List of Tables

2.1	The assumptions, and their consequences mathematically, behind the selection-recombination equations	35
3.1	Stability	67
5.1	Haplotype to allelic frequency relationship	115
5.2	Eigenvalues of the saddle equilibrium between which the heteroclinic cycle travels	128
5.3	The eigenvalues of the equilibria Φ_1 and Φ_4	139
5.4	The eigenvalues of the equilibria Φ_2 and Φ_3	139

Chapter 1

Introduction

Contents

1.1	Biological background	14
1.1.1	The genetic code	14
1.1.2	The laws of Mendelian inheritance	15
1.1.3	The forces behind changes in gene frequencies	17
1.1.4	Selfish genetic elements	22
1.2	Mathematical background	24
1.2.1	Dynamical systems	24
1.3	Goals and structure of the thesis	28
1.4	Additional materials	29

The living world is shaped by genetics and how gene frequencies change over time within populations. The totality of the forces guiding such changes are typically bewilderingly complex. However, once such forces are abstracted away mathematically, conclusions about the resulting success, or failure, of certain genes can begin to be drawn. Theoretical population genetics achieves this using broad yet mathematically precise definitions, phenomenologically capturing such categories of processes. This framework allows one to enter the realm of mathematical modelling, where it is possible to, under certain sets of well-defined assumptions, predict the future trajectory of the gene frequencies within a population.

Theoretical population genetics lies at the intersection between complex mathematics and in-depth biology. Therefore, this introduction provides the necessary background for both. The biological background covers the basics of genetics, mostly from an evolutionary genetics perspective, introducing the jargon used throughout the thesis. More specifically, the biological background includes introductions to: the genetic code, the products of the genetic code, meiotic recombination, selection, mutation, selfish genetic elements and ideas behind gene flow on the scale of populations. After which, we introduce the necessary mathematical concepts, such as: dynamical systems, equilibria and local stability. Lastly, we set out the goals of the thesis and how the structure of the thesis aligns with these goals.

1.1 Biological background

1.1.1 The genetic code

DNA is made up of sequences of nucleotides. Groups of three nucleotide bases, named *codons*, determine which amino acids are produced. These then bind together to form proteins, one of the three classes of biological macromolecule — the other two being carbohydrates and lipids. However, some sections of DNA — known as *introns* — do not code for amino acids. Introns are ubiquitous and are known to perform vital structural functions ensuring the products of the coding regions — *exons* — are formed as error-free as possible. Its biochemistry aside, the broadly accepted definition of a gene is a functional one: sections of DNA which, one way or another, perform a specific task or function. More so, whose function is similar across species, orders and for that matter, any taxonomic group.

The enormous amounts of DNA within each individual is typically stored in efficiently packaged discrete structures called *chromosomes*. The number of chromosomes varies across species, but is well conserved between individuals of the same species. It

it commonly known that healthy humans possess 23 distinct chromosomes. However, given that humans, like many other complex species, are *diploid*, we possess two copies of each distinct chromosome; one from each parent. This idea neatly leads us to two of the most central definitions in population genetics. Namely, that of a *locus* and an *allele*. The former describes the location of a given gene within a chromosome. The latter describes a particular variant of such a gene.

To elucidate both of these definitions, we provide abstract examples of how each would be reported in practice. To state a particular locus, one would need to specify first which chromosome the gene in question was placed on; then one would need to state how far along the chromosome (typically using the genetic unit of *base pairs*, or *kilobase pairs* for large distances) the gene can be found at. This location, within a certain chromosome would be the locus for a gene. To report an allele, one would simply state the sequence of nucleotide bases at a certain locus. Typically only one strand of bases is reported, as the other can be uniquely inferred from the other via the complementary base pairing relationships (see Figure 1.1 for these relationships). The definitions of *genes*, *loci* and *alleles* are three bedrocks of genetics, bioinformatics, evolutionary genetics and population genetics.

The story of the discovery of inherited traits by Gregor Mendel in 1886 (Mendel, 1866; Weiling, 1991) helps shed light on the importance of these definitions. Furthermore, it provides the terminology to discuss how gene frequencies change over time — the central principle of population genetics.

1.1.2 The laws of Mendelian inheritance

Gregor Mendel was a monk from the 19th century, who, like many other monks from this time period, studied aspects of the natural world in his spare time. After some initial experiments and inspired by his professors and colleagues at his monastery, he began to concentrate his wide ranging biological experiments on seven observable traits in pea plants: seed shape, flower colour, seed coat tint, pod shape, unripe pod colour, flower location, and plant height (Mendel, 1866). These traits were chosen as the inheritance of each seemed to be independent of the inheritance of any other trait. Once the pea plants were bred to the point where it was fairly certain each individual was purely of the type corresponding to a given trait — the individuals were now close to being *pure breeds* — Mendel started to cross them with each other. With plenty of replicates, he showed that in the second generation of cross-breeds, a quarter of the resulting plants had one trait, and three quarters had another trait. From these experiments, he was able to deduce the following laws, which have since been coined as *the laws of Mendelian inheritance*:

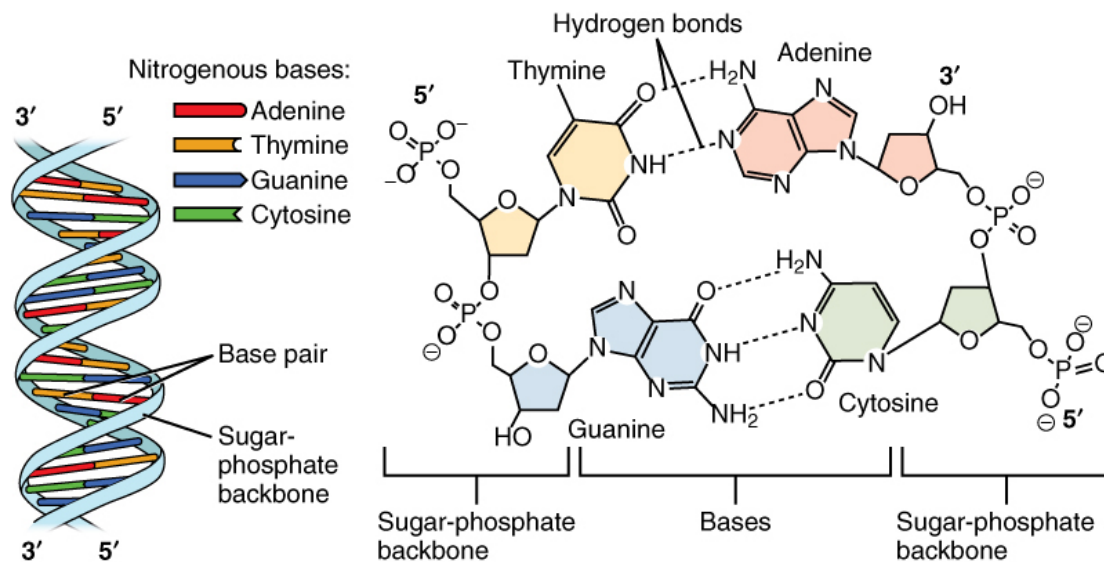


Figure 1.1: *from Wikimedia Commons (2013)*. **The structure of DNA as a double helix along with the individual nucleotide bases and how they bond.** Left: a pictorial representation of the double helix structure of DNA. Right: both the sugar-phosphate backbone of DNA — which remains unchanged for all nucleotides — and the bases, which vary between nucleotides. It also shows how the nucleotides bond and the specific number of hydrogen bonds between each pairing.

Law of segregation: *this law describes how alleles from each copy of DNA in diploid organisms organise themselves when gametes are formed.* It states that the two alleles each individual possesses for a gene segregate uniformly at random, so each gamete carries one allele each.

Law of independent assortment: *this law describes how different genes organise themselves when gametes are formed.* The probability that a certain gene is passed on into a gamete, does not depend on the probability of any other gene being passed on into the same gamete.

Law of dominance: *this law describes how the two alleles present in a diploid interact and, more specifically, which of the two alleles is ultimately expressed phenotypically.* Alleles which obey Mendel's law of dominance are either dominant or recessive. Dominant alleles are always expressed. Recessive alleles are only expressed if both alleles at a given locus are recessive.

However, as is all too often the case with the natural world, the behaviour of most empirical genetic systems are more complex than these laws describe. Their simplicity means they provide a fantastic benchmark against which certain genetic systems can be tested. In fact, their simplicity means very simple mathematical models can be derived which

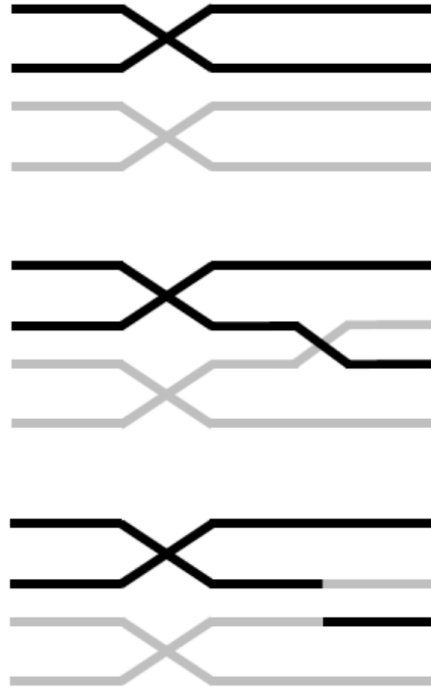


Figure 1.2: *from Seymenoglu (2019)*. **Depiction of a single cross-over event.** Homologous chromosomes, one paternally inherited, one maternally inherited cross over during meiotic cell division causing an exchange of genetic material, producing a potentially novel genetic sequence.

represent systems that do obey these laws. Then it becomes a simple task to test the dynamics of an empirical system, or the dynamics of a more complex model, against these hypothetical systems to test how close a system is to being *Mendelian*. Furthermore, it can often be quantified *how much* certain genetic systems deviate from these laws. We will see in Chapter 6, for example, a model for the dynamics of meiotic drivers; a genetic element which is defined by its ability to deviate from Mendel's first law. The biological background for these are introduced in Section 1.1.4.1 of the Introduction.

1.1.3 The forces behind changes in gene frequencies

At the start of the introduction, we discussed broad categories which guide the changes in gene frequencies over time. Here we list the main categories and describe verbally how each is translated into a component of a resulting mathematical model.

1.1.3.1 Selection

Selection, or *natural selection* is the effect of differential success of individuals, whereby success is measured by the ability to survive until reproductive age and reproduce, creating viable offspring. Individual differences are expressed phenotypically and are caused

by the combined effects of mutations and recombination on the genotype. Differences clearly are not necessarily beneficial to the individual and if the changes are sufficiently deleterious so that the individual is not able to survive long enough to be able to reproduce viable offspring, the genes responsible are removed from the gene pool. This process was famously posited by Charles Darwin in the 19th century and forms the basis for this *theory of natural selection*, which sought to explain how living organisms were so well adapted to their environment (Darwin, 2004).

Given the breadth of modelling procedures in modern population genetics, nowadays there exist many varied ways in which selection is implemented. However, within frequency-independent models from classical theoretical population genetics, selection typically boiled down to a parameter or phenotype-dependent variable within a dynamical system describing the relative advantage/disadvantage an individual receives based on their phenotype. Furthermore, frequency-dependent models classically allow for the parameter to be a function of the relative frequencies of whichever genes or haplotypes are being described. It typically results in a more complex model, but with markedly more flexibility.

1.1.3.2 Recombination

During meiosis, the maternally inherited chromosome can interact with the paternally inherited chromosome in a process called *homologous recombination* or more simply, just *recombination*. Occurring after an event known as a *double-strand break (DSB)* — whereby both sister chromatids of one of the homologous chromosomes are broken apart — recombination is one of the three possible pathways these DSBs are repaired by. The other two repair pathways are known as non-homologous end joining (NHEJ), microhomology-mediated end joining (MMEJ). The details of the latter two pathways are beyond the scope of this thesis and are therefore omitted.

Recombination in its generality is a broad and fascinating topic. To focus on what is required by the content in this thesis, specifically the content in Chapters 3 and 4, we concern ourselves with the elements of recombination known as crossing-over (see Figure 1.2) and gene conversion. The former sees the homologous chromosomes cross-over, resulting in a swap of genetic material. The latter sees the non-broken chromosome used as a template to repair the broken chromosome. Both crossing over and gene conversion have the potential to create novel sequences of genetic material.

1.1.3.3 Recombination hotspots, *PRMD9* and the protein PRMD9

Advances in molecular biology have revealed that the location of these recombination events is not uniformly distributed across whole genomes. On the contrary, it is concen-

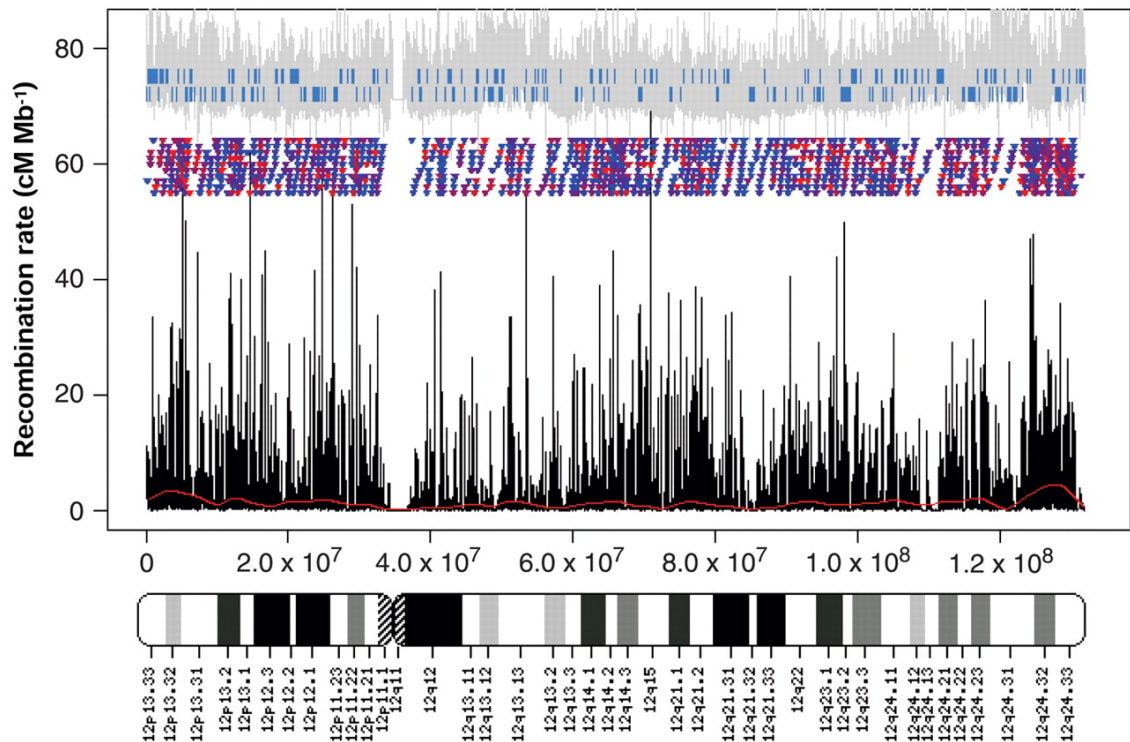


Figure 1.3: *from Myers et al. (2005)*. **A high resolution map of the rate of recombination across a chromosome.** This figure helps show the existence and whereabouts of areas of the genome known as recombination hotspots: locations where recombination is significantly higher than the average rate across a chromosome.

trated in small regions come to be known as *recombination hotspots* (Myers et al., 2005). These hotspots are an active area of research. We address questions pertaining to the evolution of recombination hotspots in Chapter 3 and 4. Figure 1.3 plots the recombination rate against location within a chromosome — the peaks within the figure are the hotspots. A large portion of the biological background for recombination hotspots and their evolution is covered in the Introduction in Chapter 3. We give a short survey here on the missing details.

The evolutionary persistence of such hotspots was proposed as paradoxical in Boulton et al. (1997). Succinctly, the paradox asks how can genetic elements - which control the position recombination occurs at - persist over evolutionarily timescales, if the sequence which initiates the process is nearby the hotspot and therefore very likely to be recombined? Such a genetic dynamic would be self-destructive (Boulton et al., 1997; Ubeda and Wilkins, 2011; Úbeda et al., 2019). It is the discovery of the initiating gene (*PRDM9*) the protein it produces (PRDM9) and many of its molecular biological details that is widely accepted to resolve the paradox. Indeed, its diversity and ability to undergo rapid selective sweeps allow it to persist in different locations across a genome over short evolutionary timescales (Lichten and Goldman, 1995).

It has been estimated that in mouse genomes there are in excess of 15,000 recom-

bination hotspots (Grey et al., 2018); furthermore, estimates for human genomes propose around 30,000 hotspots exist (Baudat et al., 2010; Grey et al., 2018) — both were found by detecting the number of sequences known to be associated with recombination hotspots. However, when more direct methods are used to detect the consequence of the initiation of recombination, i.e. the number of DSBs is measured, in the range of 200-400 such events are observed (per cell). The implication for this striking difference is that most cells only use a fraction of the available hotspots and which hotspots are used varies from cell to cell (Grey et al., 2018).

Another approach taken to determine the number of PRDM9-target binds that take place is achieved by measuring the number of PRDM9 foci — which can be used as an indicator for the number of successful PRDM9-target binds — in mice spermatocytes (Grey et al., 2018). Doing so reveals that thousands of such binds take place, which when compared to the number of DSB events taking place in the same genomes (200-400 per cell) implies that PRDM9-target binds are occurring that do not result in detectable DSBs and that these binds are in excess. To complicate matters further, the level of PRDM9-binds ranges between individuals by significant amounts (at least double) before the number of DSBs caused by the hotspots which rely on the action of PRDM9 is reduced a detectable amount (Grey et al., 2018). This provides some evidence that different PRDM9 polymorphisms — of which there are many, as it is undergoing rapid evolution (Ponting, 2011) — bind to different sites. However, this is difficult to detect directly due to the presence of multiple other proteins associated with recombination hotspots (see Figure 3 in Grey et al. (2018)).

With an aim of quantifying how often recombination and recombination hotspots are initiated, causing DSBs — and therefore potential crossing over events — estimates have found that in human genomes, each hotspot on average has around one crossing over event per 1,300 meiotic divisions (Myers et al., 2006). There is some variation in this figure between different hotspots where some are known to have a rate of roughly one crossover event per 110 meiotic divisions. Recall that crossing over is one of the pathways of repairing a DSB within the canonical model of DSB repair (Ubeda and Wilkins, 2011). These quantities help shed light on the centimorgan: the functionally defined unit of length within genetics. The exact length of a centimorgan — which is measured given in base pairs (bps) or mega base pairs (Mbps) — varies between different species (NIH, 2015). This is because it is defined as the average length of DNA within a chromosome that corresponds to a 1% chance of crossover. When this length is calculated for humans, it results in a measurement of around 1Mbp as a centimorgan, but this number varies between different areas of the genome, as different chromosomes have different levels of recombination and crossover.

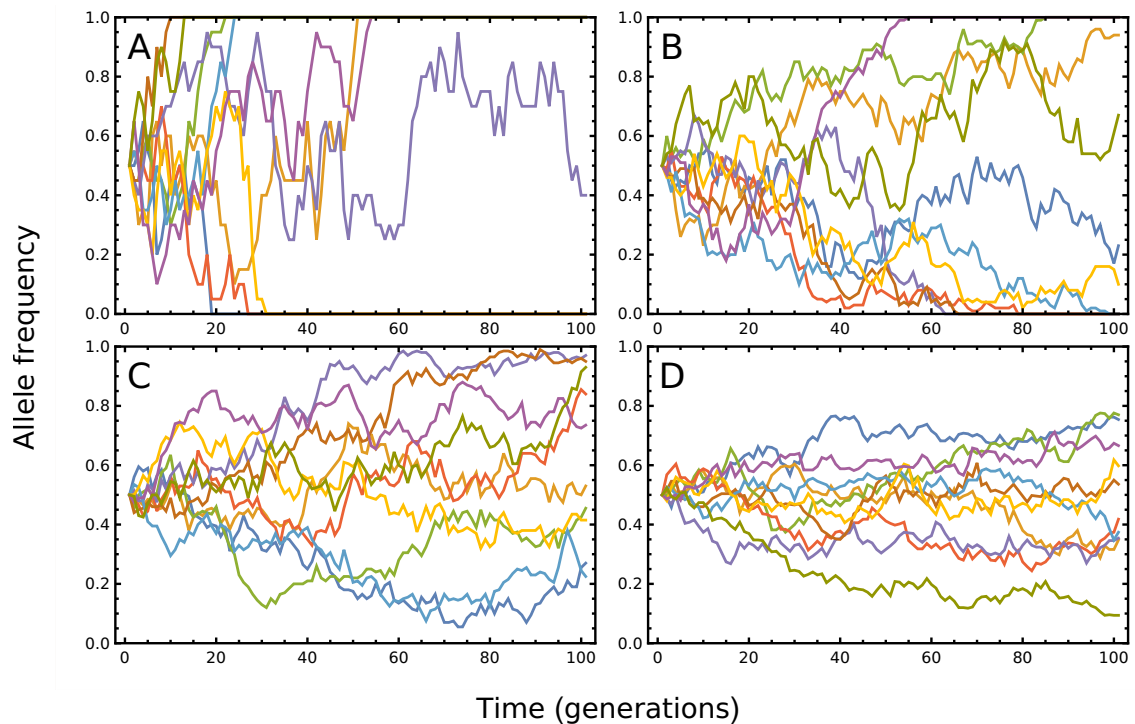


Figure 1.4: **The effects of genetic drift on the frequency of a single allele in different sized populations.** Each panel shows 10 independent simulations of genetic drift acting on a single allele in a randomly mating population. The total population size is varied between the panels. The population sizes used were 20, 100, 200 and 500 from panels A to D respectively. The probability of the success of the allele plotted was 0.5 for each simulation and in each panel. If only the population size is varied, it becomes clear that these stochastic effects are the greatest when the population is small. Only one simulation was not at either extinction or fixation by 100 generations for a population size of 20. In contrast, when the population size was 500, all simulations saw the frequency of the allele somewhere between extinction and fixation.

The advances in understanding the causes and consequences of recombination hotspots are ongoing, and highly complex. We describe the details of PRDM9 required to understand the motivation and the details of the models whose evolution they describe (Chapter 3 and Chapter 4). However, a detailed discussion on the molecular biology of recombination hotspots is far beyond the scope of this mathematically focused thesis. More details on the low level processes governing the evolution of recombination hotspots can be found in the following review articles [Lichten and Goldman \(1995\)](#); [Paigen and Petkov \(2010\)](#).

1.1.3.4 Genetic drift

The effects stochasticity has on the ultimate survival or extinction of specific alleles is known as *genetic drift*. Discussions of this process are primarily concerned with how stochastic effects vary with the population size — i.e. its effects can be more dramatic

when populations are small (see Figure 1.4). This can cause the relative frequencies of alleles to move very low or very high over time, which can cause extinction or fixation of the allele (respectively). Mathematically, this is modelled using a iterated binomial random variable (for a single allele) or an iterated multinomial random variable when multiple alleles are concerned. The probability of success parameter(s) for these distributions is interpreted biologically as the survival and passing on of the allele in question.

Our models of PRDM9 and recombination hotspots in Chapter 3 and our model of meiotic drivers in Chapter 6 include genetic drift, using multinomial sampling of the alleles between generations.

1.1.3.5 Mutation

Mutations typically occur as a result of an error when DNA is replicated, which occurs during both mitosis and meiosis. The rates at which these errors occur is higher during meiosis than mitosis (Rodgers and McVey, 2016). Mutation events result in altered nucleotide sequences. If this occurs during meiosis, it provides a source of variation between gametes and therefore between offspring. Mutation rates are relatively constant among individuals from the same species, where current estimates for humans are in the region of 1.1×10^{-8} per nucleotide site per generation (Roach et al., 2010).

Mathematically, mutations are modelled by including a term describing one allele slightly reducing in frequency and another slightly increasing, proportional to a mutation rate parameter. Our models of recombination hotspots in Chapters 3 and our models of PRDM9 and recombination hotspots in Chapter 3 and our model of segregation distorters in Chapter 6 include mutations.

1.1.4 Selfish genetic elements

Throughout most of the 20th century, the prevailing view of the evolutionary forces described so far was that they sought to increase the fitness — the ability to survive and reproduce — of individuals. Paved by the mathematical underpinnings of population genetics by Sewall Wright, Ronald Fisher and J. B. S. Haldane, many evolutionary biologists began to posit, during the 1950s and beyond, that the gene may have an evolutionary agenda of its own. The eminent figures within this paradigm shift were W. D. Hamilton (Hamilton, 1963, 1964), George C. Williams (Williams, 1966) and Colin Pittendrigh (Pittendrigh, 1958). Finally, these ideas were popularised in *The Selfish Gene* (Dawkins, 1976). Since then, there have been major advances in the discovery of genes which seem to be favouring their own fitness rather than the individuals. This shift in thinking is one of utmost importance across biological subdisciplines, as it allows the

true unit on which natural selection acts to be elucidated, the gene.

Genes which do not benefit, or even cause a reduction in fitness to individuals whilst seeking to increase their own transmission are known as *selfish genetic elements* (SGEs). There are many genetic elements which fit this broad class and an in-depth description of them all is beyond the scope of this thesis. We list the main categories of SGEs, omitting that of segregation distorters, as it is the focus of the following subsection:

- i Homing endonucleases: these are genes which code for any enzyme that is able to cause double-strand breaks (DSBs) at specific sequences of nucleotides. The repair mechanism uses the homologous strand as a template which necessarily contains the homing endonuclease gene. This is how it increases its own transmission (Burt and Koufopanou, 2004);
- ii Transposable elements: these are any genes with the ability to move, or *transpose*, to a new location within whichever genome they are in. Changing location and replacing whatever nucleotide sequence which might have been their before means they can easily disrupt the genome they reside in, typically for their own benefit;
- iii Genomic imprinting: this is the name given to the inherent asymmetry between maternally inherited and paternally inherited genes. More specifically, the competition for *expression* between the maternal and paternal DNA. This is the known cause of several serious human diseases, one such example is Prader-Willi syndrome (Buiting et al., 1995);
- iv Greenbeard genes: these are genes which code some ability to recognise itself but in other individuals and after recognition, it then favours these individuals. By favouring individuals with similar conspicuous tags, it can increase its relative frequency in a population.

1.1.4.1 Segregation distorters and meiotic drivers

Segregation distorters (SDs) are genes are able to disrupt the frequency of the transmission of other genes, thereby increasing their own relative frequency in a population. Specifically, SDs are able to disrupt the Mendelian law of segregation via a variety of mechanisms, each specific to the genetic system in question (Larracuente and Presgraves, 2012). If the distortion occurs during meiosis, then it is known as *meiotic drive* and the element responsible is known as the *meiotic driver*. We'll discuss one such example and refer to one specific model, as the model in Chapter 6 is an extension of it.

The example we discuss comes from the well-studied *Drosophila melanogaster*. On chromosome 2 (out of 4 pairs), there is a locus which can have either an *SD* allele or

any number of wild type alleles, which following convention, we will denote as SD^+ . Within heterozygous males, i.e. males with alleles SD/SD^+ at this locus, the spermatid which segregate with the SD^+ allele fail to complete a key stage in spermatogenesis. This means most (95%) of the successful sperm that develop are carrying the SD allele, clearly disrupting or *distorting* the ratios which would ensue if the Mendelian laws were obeyed.

The well-known model of [Charlesworth and Hartl \(1978\)](#) describes this interaction, showing a stable polymorphic equilibria to exist between the male SD gene and the responder gene Rsp , with damped oscillatory behaviour towards this equilibrium. The similar results we found in our models of the evolution of recombination hotspots in Chapters 3 and 4 when the polymorphic equilibria is stable. The model of [Stadler \(1996\)](#) finds stable heteroclinic cycles in models of segregation distorters, guiding the work in Chapter 6. The models in Chapter 6 are that of two-loci but three-alleles and therefore have a high dimensional state space. Due to this high dimension, build by extending models with heteroclinic cycles, there exists a stable heteroclinic network.

The evolutionary dynamics of meiotic drivers, due to the balance of strong positive and negative selective forces, can be complex. For example, they have been observed undergoing selective sweeps and other non equilibrium behaviours such as recurring cycles and damped oscillations ([Lindholm et al., 2016](#); [Núñez et al., 2018](#)). There is strong theoretical support for such behaviours when the interplay between selective forces are modelled ([Haig and Grafen, 1991](#); [Stadler, 1996](#)). In fact, these theoretical results involve heteroclinic cycles, in which both recurrent cycles and strong selective sweeps between the cycles are present, suggesting that cycling and heteroclinic trajectories and the evolutionary forces behind meiotic drivers — and other SGEs for that matter, for example homing endonucleases ([Yahara et al., 2009](#)) — could be closely linked.

1.2 Mathematical background

This section is dedicated to providing the relevant mathematical knowledge to interpret, at the very least, the models used in the thesis and their numerical results.

1.2.1 Dynamical systems

1.2.1.1 Continuous-time

An (autonomous) dynamical system is a mathematical construction typically consisting of coupled first-order ordinary differential equations (ODEs) and enough initial/boundary conditions for the initial value problem (IVP) to be *well-posed*. Indeed, this means that

the solution exists, is unique and varies continuously as the initial conditions change as proved by the Picard–Lindelöf theorem ([Coddington and Levinson, 1955](#)).

Real dynamical systems are what we are concerned with throughout this thesis. They are systems in which the dependent variables in the coupled ODEs are real-valued (rather than complex-valued). We focus on autonomous dynamical systems — systems where the functions on the right hand side (1.1) depend only on the independent variable and not the dependent variables. This is not particularly restrictive, as almost all non-autonomous systems can be transformed into autonomous ones by defining extra variables and equations. All of the systems we are concerned with are autonomous.

If we let $\mathbf{x}(t)$ be our vector of real-valued dependent variables, we can describe the state space, S , for a real dynamical system as $x \in S \subseteq \mathbb{R}^n$. The independent variable, which we denote with t , typically refers to time — this is the case throughout this thesis — but it can refer to anything in principle. Mathematically, this description looks like

$$\frac{d\mathbf{x}}{dt} = \mathbf{f}(\mathbf{x}), \quad \mathbf{f}(\mathbf{x}) : S \subseteq \mathbb{R}^n \rightarrow \mathbb{R}^m, \quad \mathbf{x} \in \mathbb{R}^n, \quad t \in \mathbb{R}_{\geq 0}. \quad (1.1)$$

The dimension of a dynamical system is given by the minimum total number of dependent variables in the system. In science and applied dynamical systems, it is common to have other identities holding for all time, such as conservation laws and other similar relations. This reduces the dimension, as this relation means one variable can always be written in terms of the others. This occurs in all of our models, as the variables represent haplotype frequencies implying the sum of all the variables is identically one.

There are certainly more technical definitions of a dynamical system than the one provided here, involving semi-groups and manifolds. These facilitate the study of such systems in their own right, but they are not necessary for the content in this thesis. Alas, they would just confuse matters with far more technicalities than are required.

1.2.1.2 Discrete time

If the independent variable — typically *time* — is integer valued, rather than real valued, the system is known as a discrete-time dynamical system. Such systems are defined by determining a law for how the next generation of the system depends on the current generation. For a dependent variable \mathbf{y} , this rule for the next generations values based on the current generation is denoted by

$$\mathbf{y}(n+1) = \mathbf{g}(\mathbf{y}(n)) \quad \mathbf{g}(\mathbf{y}) : S \subseteq \mathbb{R}^n \rightarrow \mathbb{R}^m, \quad \mathbf{y} \in \mathbb{R}^n, \quad n \in \mathbb{N}. \quad (1.2)$$

Such systems can be more simple to derive than their continuous-time analogues.

Furthermore, they are more simple to numerically simulate, as solutions consist of many iterations, rather than some complex numerical integration scheme. However, they are often far more difficult to analyse analytically due to particular mathematical oddities that occur which never do when time is continuous. Plus, even though implementing a numerical simulation of such a system is simple, they are often far more computationally intense than solving their continuous-time analogues. This is in part due to the fact that the mathematics behind solving continuous-time systems — numerical integration — is a more mathematically natural process than iteration. This leads to the existence of very efficient algorithms for 'well-behaved' continuous-time systems (such as the well-known and widely used Runge-Kutta collection of numerical integration schemes [DeVries and Wolf \(1994\)](#)). Put simply, it means that, for example, the solution to a continuous-time dynamical system does not change particularly much between two fixed time-steps (in a crude fixed time-step solving regime), a more sophisticated regime could exploit this and far more efficiently find the solution by varying the time-step used. Such schemes do exist for discrete-time systems, but they are rare and far more complex given their less natural mathematical nature. Therefore when dealing with large systems or simulating over large ranges of parameters, continuous-time systems are often more agreeable.

1.2.1.3 Equilibria

Most applied dynamical systems are nonlinear, which means attaining a general solution is typically not possible. At the very least, it is far from guaranteed, but it can be done for particular models. When a general solution is out of reach, other methods are required. A standard approach is to look for time-independent solutions, i.e. *equilibria* of the system. These are points within the full solution for which the system of differential equations — which usually would need to be solved — reduces to a system of algebraic equations. Generally speaking, solutions can be found, or at least, well approximated, for such algebraic systems.

The equilibria of the continuous-time system (1.1) are given by the solutions, \mathbf{x}^* to the system

$$\frac{d\mathbf{x}^*}{dt} = \mathbf{f}(\mathbf{x}^*) = 0, \quad (1.3)$$

and the equilibria of the discrete-time system (1.2) are given by the solutions, \mathbf{x}^* to the system

$$\mathbf{x}^* = \mathbf{f}(\mathbf{x}^*). \quad (1.4)$$

Related continuous-time and discrete-time systems are used within this thesis, in Chapter 5. The similarity of the specific discrete and continuous-time models used in this thesis results in them both having the same equilibria. This is clearly not true in general,

however, it is often the case with applied dynamical systems.

1.2.1.4 Linear stability

Using the equilibria of a system, a qualitative picture of the full solution can begin to be pieced together. This is achieved by determining the linear stability of equilibria, informing whether trajectories starting "close" to such equilibria will converge (or diverge) towards (or away) from the equilibria. We show how linear stability calculations are carried out by studying how solutions which are just a small perturbation away from an equilibrium change over time. To begin, we define our solution close to an equilibrium in the following way

$$\mathbf{x} = \mathbf{x}^* + \epsilon =: \delta \mathbf{x}, \quad \epsilon \ll 1, \quad (1.5)$$

which means (1.1) becomes

$$\mathbf{f}(\mathbf{x}) = \mathbf{f}(\mathbf{x}^* + \epsilon). \quad (1.6)$$

Taylor expanding (1.6) gives the following infinite sum

$$\mathbf{f}(\mathbf{x}^* + \epsilon) = \mathbf{f}(\mathbf{x}^*) + \epsilon \frac{\partial}{\partial \mathbf{x}} \mathbf{f}(\mathbf{x}^*) + \frac{1}{2} \epsilon^2 \frac{\partial^2}{\partial \mathbf{x}^2} \mathbf{f}(\mathbf{x}^*) + O(\epsilon^3). \quad (1.7)$$

The first term in this expansion is identically zero, given that we are evaluating the right hand side of the dynamical system at equilibrium, which is, by definition, zero. Truncating this series at $O(\epsilon)$, which serves as a good approximation close to the equilibrium in question, as each term is an order of magnitude smaller than the last in (1.8) gives

$$\begin{aligned} \mathbf{f}(\mathbf{x}^* + \epsilon) &= \cancel{\mathbf{f}(\mathbf{x}^*)}^{=0} + \epsilon \frac{\partial}{\partial \mathbf{x}} \mathbf{f}(\mathbf{x}^*) \\ &= J_{\mathbf{x}} \mathbf{f}(\mathbf{x})|_{\mathbf{x}=\mathbf{x}^*} \end{aligned} \quad (1.8)$$

which denotes the Jacobian of (1.1) evaluated at equilibrium.

Clearly, perturbations nearby equilibria grow according to

$$J_{\mathbf{x}} \mathbf{f}(\mathbf{x})|_{\mathbf{x}=\mathbf{x}^*} \quad (1.9)$$

to first-order. Therefore, studying how perturbations near equilibria grow, i.e. the stability properties of an equilibrium, comes down to finding eigenvalues of the Jacobian matrix evaluated at equilibrium. We outline the typical procedure used to study stability

1. Find equilibria, by solving $\mathbf{f}(\mathbf{x}^*) = 0$;
2. Evaluate the Jacobian matrix at this equilibrium $J_{\mathbf{x}} \mathbf{f}|_{\mathbf{x}=\mathbf{x}^*}$;

3. Determine the eigenvalues λ of this matrix by solving the characteristic equation $\det(J|_{x=x^*} - \lambda I) = 0$
4. Determine whether the real part of the eigenvalues are positive or negative. If all are positive, the equilibrium is locally attracting. If not, it is repelling. If the eigenvalues are identically zero, a higher order analysis is required where more terms in (1.8) are needed to determine how perturbations grow.

1.3 Goals and structure of the thesis

The central aim of this thesis is twofold: to study deterministic and stochastic genetic systems modelling novel processes or with a novel number of alleles; to analyse systems which are similar to those that exist, but to a level of analysis beyond linear stability if possible. We now lay out which of these broad aims, and any others, each chapter addresses.

- Chapter 3 builds a model including novel knowledge of the action of a gene *PRDM9* on a target site at a different loci. We associate a fitness benefit to such an action within this model and find complex behaviours arising from the model. We then analyse the model to the point of a linear stability analysis. The aim satisfied by this chapter is that of building a biologically novel system and analysing it numerically and analytically to the point where its dynamics can be qualitatively fully characterised.
- Chapter 4 sees the model built in Chapter 3 extended to allow for the sex-specific effects of the target site to which the protein PRDM9 binds to. This means doubling the size of the dynamical system and breaking up the population into a male population and a female population. We then proceed to find a stable polymorphic equilibria for which linkage disequilibrium is different between the sexes. Again, the model in this chapter is biologically novel. Its complexity means full analytic analysis is difficult, but with some approximation techniques, we can analytically find equilibria. We find its stability numerically.
- Chapter 5 involves a model inspired by the system studied in Chapter 3. However, in Chapter 5, we relax the dependency of the simplifying parameters on the original biological parameters. We are able to analyse the model to a higher degree than was possible in Chapter 3 by noticing there was an attracting invariant manifold. We find an approximate closed-form for this manifold and prove stability of the heteroclinic cycle found in Chapter 3 in the reduced system, constrained to the manifold.

- Chapter 6 is based on a model for segregation distortion, a specific type of selfish genetic element. We generalise a model derived originally in Charlesworth and Hartl (1978) to allow for n -alleles. We then study in detail the dynamics when three alleles are possible. We find an attracting heteroclinic network, close to which, chaotic-like dynamics are possible. We study the dynamics of this system in a metapopulation context by coupling many instances of the system together on a lattice. Within this context, we are able to see that chaotic in-patch dynamics cause faster divergence rates of subpopulations than regular in-patch dynamics. We suggest this could be a novel evolutionary dynamic which, if genetic systems include multiple variants interacting at specific loci, could be generic.
- Chapter 2, mainly a framework and review chapter, lays out the general model used in all other chapters. It describes the common techniques used to study the general system and reviews some of the known results about the system. We also show how the models used in Chapters 3, 4 and 5 are special cases of this general model.

1.4 Additional materials

All of the additional materials referred to throughout this thesis, whether they are C++ code, Mathematica notebooks or animations, can be found at the following shared Dropbox folder: <https://tinyurl.com/y6caeto6>. However, if GitHub is easier, they can also be found at the following GitHub repository: <https://github.com/thimotei/thesis-additional-materials>. A GitHub account is required for to add you as a collaborator, as the repository is private. Email timothywilliamrussell@gmail.com for access as a collaborator or for it to be shared a different way if it is easier. Once all of the work is published, the repository will be make public. On request, I can share the materials a different way if the readers do not use Dropbox or GitHub.

Chapter 2

The selection-recombination equation

Author contributions

Myself and Vincent A. A. Jansen conceived of the research and carried out the analysis. I wrote the first draft of the manuscript.

Contents

2.1	Introduction	33
2.2	The model	34
2.2.1	Two-locus n-alleles	34
2.2.2	Two-locus two-allele	35
2.3	Reviewing known results	39
2.3.1	Two-locus two-alleles	40
2.4	Conclusions	46

The selection-recombination equation

Timothy W. Russell^{a,*}, Vincent A.A. Jansen^a

^a*School of Biological Sciences, Royal Holloway University of London, Egham, Surrey, TW20 0EX, UK*

Abstract

In theoretical population genetics, the selection-recombination equations, or variants on these equations, have been central to understanding how gene frequencies change over time. More so, they have helped mould mathematically rigorous but broad definitions of the range of processes behind these changes. Indeed, these definitions, like selection, recombination, marginal fitness et cetera, now have well understood mathematical definitions helping to disentangle the complexities involved in the dynamics of genetic systems. Much is known about this system of nonlinear difference, or differential equations — depending on whether non-overlapping or overlapping generations are under consideration (respectively). We briefly survey the known results, adding to them where possible with several pieces of modern work. Global stability within the system, for example, has seen good progress in the last few years. We show some of the common techniques used to study the system in-depth, such as common coordinate transformations and techniques. We also show the breadth of the system with some simple proofs which show how some modern models can be re-written as a member of the general system. Finally, we provide some ideas for potential future research avenues.

Keywords:

Mean fitness, Two-locus two-allele, Nonlinear dynamics, Coordinate transformation, Linkage disequilibrium

*Corresponding author

Email address: `timothy.russell.2015@rhul.ac.uk` (Timothy W. Russell)

1. Introduction

The general system of equations known in theoretical population genetics as the *selection-recombination equations* have been a central tenet of the field for decades (Hastings, 1981; Bürger, 2011). This widely studied system of equations describes how the haplotype frequencies in a population change over time. The equations track the outcome of every possible pairing of haploid gametes $p_{i,j}$ and associate with each haplotype pairing a fitness benefit, $a_{i,j;k,l}$ which describes a selective advantage any given pair of haplotypes, $p_{i,j}$ and $p_{k,l}$, may confer to the resulting diploid individual.

The equations also describe the effects of recombination has on the population of haplotypes. Recombination is a genetic process which occurs during meiotic cell division, whereby diploid individuals with specific combinations of alleles on sister chromatids can transfer alleles from one to another. This complex genetic process results in a shuffling of alleles in the segregating chromosomes, altering the resulting haplotype relative frequencies. Hence, recombination is a necessary component for a reliable model of the evolution of haplotype frequencies within a population. A more detailed discussion about the background biology governing this process can be found in Bürger (2011). Classically, in these equations, the rate at which this happens is denoted by r and is bounded by $r \in [0, \frac{1}{2}]$.

As far as the authors are aware, the two-locus two-allele version of the model was first suggested — in continuous-time — by Kimura (1956). The model has since been generalised to arbitrary loci and allele numbers; one well-known example of such a generalisation is given — in discrete-time — by Nagylaki (1993). Table 1 states the assumptions that are used to derive system (1), using the standard theoretical population genetics terms, along with how the statements translate into mathematics.

The aims of this paper are:

- to give an overview of the different implementations of the model, for example discrete vs continuous-time;
- describe the assumptions behind the model;
- give some basic results showing how some recent models, especially those used to study the evolution of recombination hotspots, fall into the category of the selection-recombination equations;
- review the literature, describing many of the results known about the system of equations — especially for the two-locus two-allele and two-locus three-allele cases;

- show how the mathematical results from this thesis fit within some of the known results from the literature;

Given that each of the models within the thesis this paper is originally from (Russell, 2019) is either: trivially a member of the class of selection-recombination equations; or, with some work, can be shown to fall into the class, we treat the general model as the linchpin of the thesis. Therefore, the overarching aim of this paper is to provide the mathematical framework — and the biological assumptions used to build such a framework — that the rest of the thesis is built upon.

2. The model

2.1. Two-locus n-alleles

2.1.1. Discrete-time

We only present the system of equations describing the interaction between two loci and not for higher numbers. We do so because all of the models considered in this thesis concern the interaction of the products of two loci only and the structure of the expanded equations changes considerably as more loci are considered. In discrete-time, for n -distinct allelic variants at each locus, the general system is given by

$$p'_{i,j} = \bar{w}^{-1} \left(p_{i,j} \sum_{k,l=1}^n a_{i,j;k,l} p_{k,l} - r \sum_{k,l=1}^n (p_{i,j} p_{k,l} - p_{i,l} p_{k,j}) \right), \quad (1)$$

where $p'_{i,j}$ is shorthand for the frequency of $p_{i,j}$ in the next generation, the $a_{i,j;k,l}$ parameters correspond to the fitness of an individual formed by the pairing of haplotypes with alleles i, j from one gamete and k, l from the other and

$$\bar{w} = \sum_{i,j,k,l=1}^n a_{i,j;k,l} p_{i,j} p_{k,l}, \quad (2)$$

is known as the *population mean fitness*. Mathematically, it is a normalisation term, used to maintain the interpretation of each variable as a frequency. A consequence of which is that

$$\sum_{i,j} p_{i,j}(t) = 1, \quad \forall t \in \mathbb{N}_+. \quad (3)$$

This implies the state space for the model is the n -simplex, defined by

$$\Delta_n = \{(p_{1,1}, \dots, p_{n,n}) \in \mathbb{R}^n : p_{i,j} \geq 0, \sum_{i,j} p_{i,j} = 1\}. \quad (4)$$

Assumption	Modelling consequences
Infinite population size	The model is deterministic — typically a dynamical system on a subset of the real numbers — as there is no need to track the time evolution of each individual when the population is infinite.
Random union of gametes: <i>panmixia</i>	Only need to keep track of four haplotypes, rather than 16 distinct genotypes.
Variables are <i>frequencies</i> of haplotypes	The sum of all the variables is identically one, achieved by subtracting or dividing, for continuous and discrete-time (respectively), the right hand side of each equation by the <i>population mean fitness</i> given by \bar{w} : defined as the sum of the right-hand sides of the system of equations.
No parent-of-origin effects	Whether an allele came from a sperm or an egg is irrelevant to the fitness of the resulting individual

Table 1: The assumptions, and their consequences mathematically, behind the selection recombination equations.

2.1.2. Continuous-time

In continuous-time, we present the equations in the following form

$$\dot{p}_{i,j} = \bar{m}^{-1} \left(p_{i,j} \sum_{k,l=1}^n m_{i,j;k,l} p_{k,l} - r \overbrace{\sum_{k,l=1}^n (p_{i,j} p_{k,l} - p_{i,l} p_{k,j})}^{=:D} \right) - p_{i,j}, \quad (5)$$

where the variables are now functions of time as a real number and as is standard, a dot is used to denote the derivative with respect to some unique independent variable — typically *time*, which is clearly what it is with respect to in this case and throughout this thesis. This is not the most common form of the continuous-time equations however; usually, for the classic two-locus two-allele model, the system is written as

$$\dot{p}_{i,j} = p_{i,j} \left(\sum_{k,l=1}^n m_{i,j;k,l} p_{k,l} - \bar{m} \right) - r \sum_{k,l=1}^n (p_{i,j} p_{k,l} - p_{i,l} p_{k,j}). \quad (6)$$

It is easy to see however, that these two systems, (5) and (6), are almost equivalent — there is a difference in the scaling of time and the second is more restrictive. We prefer the first for these reasons. Furthermore, it more clearly elucidates the difference between the discrete and continuous-time models. Notationally, the fitness parameters are now denoted by $m_{i,j;k,l}$ for *Malthusian fitness* and the population mean fitness — which is given by the same function as the discrete-time formulation — is denoted by \bar{m} .

2.2. Two-locus two-allele

Most of this paper is focused on the discrete-time formulation of the selection-recombination equations. However, we discuss in detail the known results of both the discrete and continuous-time systems in Section 3. Moreover, we cover the similarities and differ-

ences of the two models in this section.

The term delineated by the over brace in equation (5) is a well-known quantity throughout population genetics. It is known as the *linkage disequilibrium*, it is typically denoted by D and, for two-loci and two-alleles, it is given by

$$D = p_{1,1}p_{2,2} - p_{1,2}p_{2,1}. \quad (7)$$

When $n = 2$, the second term in (5) — defined above the over brace as D — the sum is expanded and the resulting expression is simplified, reduces to (7).

For mathematical convenience, we briefly switch from double to single subscript notation in the following way $p_{i,j} =: x_{i+n(j-1)}$ for the haplotype frequencies, $a_{i,j;k,l} = w_{i+n(j-1),k+n(l-1)} =: w_{\bar{i},\bar{j}}$ for the selection parameters and $m := n^2$ for the summation index — the two here comes from the number of loci under consideration. Doing so gives the following system of equations

$$x'_i = \bar{w}^{-1} \left(x_i \sum_{j=1}^m w_{\bar{i},\bar{j}} x_j + \epsilon_i r D \right), \quad i \in \{1, \dots, 4\}. \quad (8)$$

The new parameter ϵ is introduced so that the sign of the linkage disequilibrium term remains correct when written using the same term for each equation. Specifically,

$$\epsilon_i^* = \begin{cases} 1, & i = 1, 4; \\ -1, & i = 2, 3. \end{cases} \quad (9)$$

This system, the two-locus two-allele governing equations (8) are a system of four coupled nonlinear difference equations. A general solution is almost certainly out of reach. However, we discuss some of what is known about this system, including bifurcation patterns, potential behaviours and special cases in Section 3.

2.2.1. The evolution of recombination hotspots model

The deterministic model developed and presented in [Úbeda et al. \(2019\)](#), representing the evolution of *recombination hotspots* - a collection of genes involved in the genetic control of recombination, is a special case of the selection-recombination equations (1). To see precisely how, we begin from the general form that all of the different instances of the hotspot models took. Indeed, we observed that the processes we were modelling, under many different sets of biological assumptions — outlined in the supplementary

*Under the double subscript notation, this definition becomes $\epsilon_{i,j} = 1$ if $i = j$ and -1 if $i \neq j$.

material of [Úbeda et al. \(2019\)](#) —resulted in many models, all of this generic form

$$p'_{i,j} = \bar{w}^{-1} \left(\sum_{k,l=1}^n a_{i,j;k,l} p_{i,j} p_{k,l} + \sum_{k,l=1}^n b_{i,j;k,l} p_{i,l} p_{k,j} \right)^{\dagger}. \quad (10)$$

We wish to show that (10) can be written in the form of (8). Specifically, we wish to show that (10) can be reduced to the following system

$$p'_{i,j} = \bar{w}^{-1} \left(1 + \epsilon_{i,j} \beta p_{i,j} - \epsilon_{i,j} \gamma p_{i,l} \right) p_{i,j} - \epsilon_{i,j} \delta D, \quad (11)$$

which, following the notation of the original version in both [Úbeda et al. \(2019\)](#) and [Russell et al. \(2019\)](#), reads as

$$\begin{aligned} x_1 &= \frac{1}{\bar{w}} \left[x_1 (1 + \beta x_1 - \gamma x_2) - \delta D \right], \\ x_2 &= \frac{1}{\bar{w}} \left[x_2 (1 - \beta x_2 + \gamma x_1) + \delta D \right], \\ x_3 &= \frac{1}{\bar{w}} \left[x_3 (1 - \beta x_3 + \gamma x_4) + \delta D \right], \\ x_4 &= \frac{1}{\bar{w}} \left[x_4 (1 + \beta x_4 - \gamma x_3) - \delta D \right]. \end{aligned} \quad (12)$$

Both indexes are expanded and presented in single subscript form. The population mean fitness is now given by

$$\bar{w} = x_1 + x_2 + x_3 + x_4 + \beta(x_1^2 + x_4^2 - x_2^2 - x_3^2). \quad (13)$$

We have also defined new parameters, which are functions of the original $a_{i,j;k,l}$ and $b_{i,j;k,l}$ parameters, simplifying the resulting equations greatly. The following mathematical steps describe explicitly how we defined these new parameters.

Given that the indices, for the two-locus two-allele model, only take values of either one or two, we define s as the value this is not i , for a given i . Similarly, let be t the value that is not j . Mathematically, this can be stated as $s := i \pmod{2} + 1$ and $t = j$

[†]We switch back to the double subscript notation from here onwards, as it aids with the following steps showing that this system falls, under some generic assumptions of the parameters $a_{i,j;k,l}$ and $b_{i,j;k,l}$, into the class of selection-recombination equations.

(mod 2) + 1. Using these definitions, we can rewrite (8) as

$$\begin{aligned}
 \bar{w}p'_{i,j} &= p_{i,j} \sum_{k,l=1}^n a_{i,j;k,l} p_{k,l} + \sum_{k,l=1}^n b_{i,j;k,l} p_{i,l} p_{k,j} \\
 &= p_{i,j} \sum_{k,l=1}^n a_{i,j;k,l} p_{k,l} + \sum_{k,l=1}^n b_{i,j;k,l} p_{i,j} p_{k,l} + \sum_{k,l=1}^n b_{i,j;k,l} (p_{i,l} p_{k,j} - p_{i,j} p_{k,l}) \quad (14) \\
 &= p_{i,j} \sum_{k,l=1}^n (a_{i,j;k,l} + b_{i,j;k,l}) p_{k,l} + b_{i,j;s,t} (p_{i,t} p_{s,j} - p_{i,j} p_{s,t}).
 \end{aligned}$$

If we assume that

$$a_{i,j;s,j} + b_{i,j;s,j} = a_{i,j;s,t} + b_{i,j;s,t} =: c_{i,j;s} = c_{i,j;t}, \quad (15)$$

we are able to write (14) as

$$\begin{aligned}
 \bar{w}p'_{i,j} &= p_{i,j} \sum_{l=1}^n (a_{i,j;i,l} + b_{i,j;i,l}) p_{i,l} + p_{i,j} \sum_{l=1}^n (a_{i,j;s,l} + b_{i,j;s,l}) p_{s,l} + b_{i,j;s,t} (p_{i,s} p_{s,j} - p_{i,j} p_{s,t}) \\
 &= p_{i,j} \sum_{l=1}^n (a_{i,j;i,l} + b_{i,j;i,l}) p_{i,l} + c_{i,j;s} p_{i,j} \sum_{l=1}^n p_{s,l} + b_{i,j;s,t} (p_{i,t} p_{s,j} - p_{i,j} p_{s,t}) \\
 &= p_{i,j} \sum_{l=1}^n (a_{i,j;i,l} + b_{i,j;i,l}) p_{i,l} + p_{i,j} c_{i,j;s} (1 - \sum_{l=1}^n p_{i,l}) + b_{i,j;s,t} (p_{i,t} p_{s,j} - p_{i,j} p_{s,t}) \\
 &= p_{i,j} \left[c_{i,j;s} + \sum_{l=1}^n (a_{i,j;i,l} + b_{i,j;i,l} - c_{i,j;s}) p_{i,l} \right] + b_{i,j;s,t} (p_{i,t} p_{s,j} - p_{i,j} p_{s,t}). \quad (16)
 \end{aligned}$$

With this general form, if we choose

$$\begin{aligned}
 \beta &:= \frac{1}{c_{i,j;s}} \left(a_{i,j;i,j} + b_{i,j;i,j} - c_{i,j;s} \right), \\
 \gamma &:= \frac{1}{c_{i,j;s}} \left(a_{i,j;i,t} + b_{i,j;i,t} - c_{i,j;t} \right), \\
 \delta &:= \frac{1}{c_{i,j;s}} b_{i,j;s,t},
 \end{aligned} \quad (17)$$

and switch back to the single subscript notation, we recover (12).

The specific expressions for the new parameters can be found by calculating the $a_{i,j;p,k}$ and $b_{i,j;k,l}$ terms from the biological formulation of the recombination hotspots

model in [Úbeda et al. \(2019\)](#). Doing so gives

$$\begin{aligned}\beta &= \frac{\frac{1}{4}bf}{\frac{1}{4}b + \frac{1}{2}(1 - \frac{1}{2}b)(1 - f)}, \\ \gamma &= \frac{\frac{1}{8}bc}{\frac{1}{4}b + \frac{1}{2}(1 - \frac{1}{2}b)(1 - f)}, \\ \delta &= \frac{\frac{1}{8}b \left[\frac{1}{2}c + (1 - c)r \right]}{\frac{1}{4}b + \frac{1}{2}(1 - \frac{1}{2}b)(1 - f)},\end{aligned}\tag{18}$$

as stated, but not derived, in [Úbeda et al. \(2019\)](#). Here, we followed ([Russell et al., 2019](#)) and normalised the parameters in [Úbeda et al. \(2019\)](#) by the parameter α for mathematical simplicity.

In contrast to the treatment in [Úbeda et al. \(2019\)](#) which obeys the biological constraints on the parameters, the analysis of the simplified system (12) in [Russell et al. \(2019\)](#) treats the parameters β , γ and δ independently. Therefore, apart from the assumption given by (15), the analysis in [Russell et al. \(2019\)](#) is a general analysis of the system (8). In the context of recombination hotspots, this assumption can be interpreted as: if a haplotype produces only one allelic variant of the recombinogenic protein, acting on two target sites, the rate of breakage is equal to when two different allelic variants of the protein are produced and each protein acts on a different target site.

3. Reviewing known results

We begin this section with some remarks about which parts of the literature serve as excellent reference and survey material. For the classic continuous-time viability selection-recombination model, the textbook [Akin \(1979\)](#) gives a full account of the dynamics, cast in terms of the Shahshahani gradient ([Shahshahani, 1979](#)): a metric which allows global stability of the continuous-time model to be determined; for both the discrete and the continuous-time systems, the paper [Bürger \(2011\)](#) gives a full account of the equilibria and behaviour of both models and describes the differences with clarity — the weak selection approximation is particularly well discussed, with a simple derivation of the model under weak selection included.

We use this section to pick apart what is currently known about the system (1) and its counterpart in continuous-time (6) and place the results from this thesis within these results. The pool of knowledge is deeper for the continuous-time model, which is not particularly surprising, given that continuous-time models are typically more amenable to analysis; discrete-time models often throw up mathematical oddities with require an enor-

mous amount of work to prove analogous results. The scope and the limits of known results for the two-locus two-allele continuous-time model is best described in Sub-section 3.1.5. Generally speaking, being able to prove existence of invariant manifolds within dynamical systems tends to be a highly powerful tool for characterising the dynamics, as it allows for global stability properties to be determined along with, occasionally, a reduction in dimension (Kuehn, 2015).

3.1. Two-locus two-alleles

3.1.1. Equilibria

The equilibria of the discrete and continuous-time models are equivalent, with a short, simple proof of this in Bürger (2011). Equilibria of the system (1) are given when

$$\mathbf{p}'|_{p=p^*} = \mathbf{f}(\mathbf{p}^*) = \mathbf{p}^* \quad (19)$$

and the equilibria are given by \mathbf{p}^* , which are the solutions to (19). For the two-locus two-allele system, this is a system of 4 coupled nonlinear polynomials that need to be solved. However, the conservation law (3) applies and therefore, the true number of equations to be solved is three. The equations are of order two, i.e. each term is no more than quadratic and can be solved, occasionally giving relatively simple closed-form solutions for certain special cases of the general system, which typically make simplifying assumptions on the general parameters (Úbeda et al., 2019; Russell et al., 2019).

The four vertices of the tetrahedron are equilibria for the general system, without the need for simplifying assumptions to guarantee this. These equilibria, the edges of the tetrahedron, are given by

$$\begin{aligned} p_{1,1}^* &= (1, 0, 0, 0), \\ p_{1,2}^* &= (0, 1, 0, 0), \\ p_{2,1}^* &= (0, 0, 1, 0), \\ p_{2,2}^* &= (0, 0, 0, 1). \end{aligned} \quad (20)$$

The other equilibria for the general model exist only under certain conditions on the systems parameters, conditions which are unwieldy and complicated. Conditions for the existence of a unique polymorphic equilibria are equally unwieldy. However, many special cases exist and are able to show when such an equilibria exists. Typically, these analyses go further and prove when such equilibria are linearly (or occasionally globally) stable.

3.1.2. Invariant subspaces

Each of the six edges of the 4-simplex, the *tetrahedron*, can be parameterised using a single variable. This is due to the fact that on each edge, two variables are identically zero, and one of the two non-zero variables can always be written in terms of the other, by making use of the conservation law (3), which is now comprised of only two variables.

The following is a list of particular parameterisations of the six edges, using the double subscript notation for the variables

$$\begin{aligned}
 E_{1,2} &= (p_{1,1}, 1 - p_{1,1}, 0, 0) = E_{2,1}, \\
 E_{1,3} &= (p_{1,1}, 0, 1 - p_{1,1}, 0) = E_{3,1}, \\
 E_{1,4} &= (p_{1,1}, 0, 0, 1 - p_{1,1}) = E_{4,1}, \\
 E_{2,3} &= (0, p_{1,2}, 1 - p_{1,2}, 0) = E_{3,2}, \\
 E_{2,4} &= (0, p_{1,2}, 0, 1 - p_{1,2}) = E_{4,2}, \\
 E_{3,4} &= (0, 0, p_{2,1}, 1 - p_{2,1}) = E_{4,3}.
 \end{aligned} \tag{21}$$

The edges $E_{1,2}$, $E_{2,4}$, $E_{4,3}$ and $E_{4,1}$ are invariant with respect to both the general system given as a flow (6) and given as a map (1). The remaining two edges, $E_{1,3}$ and $E_{2,3}$, are not invariant with respect to either the general system (1), or our special case model (12).

Lemma 3.1. *The subspace $E_{1,2}$ is invariant with respect to the dynamics of the map (1).*

Proof. The dynamics constrained to the first of these subspaces, $E_{1,2}$, with the equations expanded, is given by

$$\begin{aligned}
 p'_{1,1} &= \bar{w}^{-1} p_{1,1} \left[p_{1,1}(a_{1,1;1,1} + b_{1,1;1,1}) + p_{1,2}(a_{1,1;1,2} + b_{1,1;1,2}) \right], \\
 p'_{1,2} &= \bar{w}^{-1} p_{1,2} \left[p_{1,1}(a_{1,2;1,1} + b_{1,2;1,1}) + p_{1,2}(a_{1,2;1,2} + b_{1,2;1,2}) \right], \\
 p'_{2,1} &= 0, \\
 p'_{2,2} &= 0,
 \end{aligned} \tag{22}$$

where \bar{w} constrained to this subspace is given by

$$\begin{aligned}
 \bar{w} &= p_{1,1}^2(a_{1,1;1,1} + b_{1,1;1,1}) + p_{1,2}^2(a_{1,2;1,2} + b_{1,2;1,2}) \\
 &\quad + p_{1,2}x_{1,1}(a_{1,1;1,2} + a_{1,2;1,1} + b_{1,1;1,2} + b_{1,2;1,1}).
 \end{aligned} \tag{23}$$

Recall that the subspace under consideration is given by $(p_{1,1}, 1 - p_{1,1}, 0, 0)$. Therefore, to show the invariance of this subspace with respect to the dynamics of the map (1), it

suffices to show that

$$p'_{1,1} + p'_{1,2} = 1, \quad (24)$$

which can be easily verified by substituting $p_{1,2} = 1 - p_{1,1}$ into the condition (24) to give

$$\begin{aligned} \bar{w}^{-1} \left[p_{1,1} \left(p_{1,1}(a_{1,1;1,1} + b_{1,1;1,1}) + p_{1,2}(a_{1,1;1,2} + b_{1,1;1,2}) \right) \right. \\ \left. + p_{1,2} \left(p_{1,1}(a_{1,2;1,1} + b_{1,2;1,1}) + p_{1,2}(a_{1,2;1,2} + b_{1,2;1,2}) \right) \right] = \frac{\bar{w}}{\bar{w}}. \end{aligned} \quad (25)$$

As the left hand side of the condition reduces identically to 1, (24) is satisfied. \square

Remark. The proofs of the invariance of $E_{2,4}$, $E_{4,3}$ and $E_{4,1}$ with respect to either (1) or (5) are trivially similar and are therefore omitted.

The invariance of these four edges of the tetrahedron is a result of both the Kolmogorov form of the selection term — that each variables selection term is proportional to its own frequency — and that the linkage disequilibrium term $p_{1,1}p_{2,2} - p_{1,2}p_{2,1}$ is identically zero along the four invariant edges. Along $E_{2,3}$ and $E_{2,4}$ however, the linkage disequilibrium term equals $p_{1,1}(1 - p_{1,1})$ and $p_{1,2}(p_{1,2} - 1)$ respectively, causing these edges not to be invariant with respect to either (1) or (5). This indicates that if searching for behaviour reliant on invariant subspaces, such as: equilibria, homoclinic connections or heteroclinic connections; the four subspaces outlined here are likely candidates, as they are invariant for any specific implementation of the general model, in both continuous and discrete-time.

3.1.3. Invariant line

The subspace parameterised by

$$\begin{aligned} p_{1,1} &= p_{2,2} \\ p_{1,2} &= p_{2,1} \end{aligned} \quad (26)$$

describes a straight line from the middle of the edge $E_{1,4}$ and the edge $E_{2,3}$, whose midpoint intersects the Wright manifold. This line is invariant with respect to specific recombination hotspots model (Russell et al., 2019) given by equation (10). This does not carry over to the general case and relies on the assumption (15) build into the recombination hotspots model (15). Precise conditions for the invariance of this line, derived from the general model (1), are possible. However, without a simplifying assumption — for example (15) — they are arduous and not particularly illuminating, given the high number of parameters.

3.1.4. Stable cycles

Stable cycles, in the form of limit cycles, have been shown to exist: numerically in discrete-time (1) by Hastings (1981) and analytically in continuous-time (6) by Akin (1979, 1982, 1983, 1987). Stable cycles, in the form of heteroclinic cycles, have been shown to exist in the discrete-time model by Haig and Grafen (1991); Úbeda et al. (2019) and have been proved to be stable by Stadler (1996); Russell et al. (2019). A Hopf bifurcation, and nearby stable limit cycles, were determined to exist by Hofbauer (1985) in a nearby model: namely, the *selection-mutation equation*.

3.1.5. The quasi-linkage equilibrium manifold

For the two-locus n -allele case, a globally attracting invariant manifold known as the *quasi-linkage equilibrium* (QLE) *manifold* is known to exist, if the well-known population genetics assumption — known as the *weak selection approximation* — is satisfied (Nagylaki et al., 1999). In the context of the selection-recombination equations, this assumption means selection is weak relative to recombination, hence producing a small parameter in the system.

Several attempts have been made to determine the existence, attraction and closed-form expressions for such manifolds, without the need for necessarily small parameters:

- In the continuous-time two-locus two-allele model (6), sufficient conditions on the parameters for the existence of the QLE manifold, in a slightly simplified version of the model have been recently determined in Seymenoglu (2019).
- In the two-locus two-allele discrete-time model, with assumption (15), the QLE manifold has been shown to exist under some parameter regimes. When it does, it can be globally attracting, shown using a combination of numerical and analytic results. Furthermore, an approximate closed-form was determined as a graph of the linkage disequilibrium function — analytically determined change on a faster time-scale than the other variables (Russell et al., 2019). Both of these approaches, and many others throughout the study of applied dynamical system, employ coordinate transformations, making the analysis possible by disentangling as much of the complexity as possible of coupled nonlinear systems. Two of the many transformations used are discussed below.

3.1.6. Coordinate transformations

To study the continuous-time two-locus two-allele model, [Seymenoglu \(2019\)](#) defined the following coordinate transformation $\Phi_1 : \Delta_4 \rightarrow \mathbb{R}_+^3$

$$\mathbf{p} \mapsto \mathbf{u} = \Phi_1(\mathbf{p}) := \begin{pmatrix} p_{1,1} + p_{1,2} \\ p_{1,1} + p_{1,3} \\ p_{1,1} + p_{1,4} \end{pmatrix}^T, \quad (27)$$

where $\mathbf{p} = (p_{1,1}, p_{1,2}, p_{2,1}, p_{2,2})$ and $\mathbf{u} = (u, v, w)$. The map $\Phi_1(x)$ has the inverse $\Phi_1^{-1}(\mathbf{u})$ given by

$$\mathbf{u} \mapsto \mathbf{p} = \Phi_1^{-1}(\mathbf{u}) = \frac{1}{2} \begin{pmatrix} u + v + q - 1 \\ u - v - q + 1 \\ -u + v - q + 1 \\ -u - v + q + 1 \end{pmatrix}^T. \quad (28)$$

This transformation is also known to at least have been used in [Wagner and Bürger \(1985\)](#).

The first two new variables u and v are equivalent to the variables defined in [Russell et al. \(2019\)](#). The transformation from the tetrahedron to a subset of \mathbb{R}^3 is also similar. However, the third variable chosen in [Russell et al. \(2019\)](#) does change the resulting geometry somewhat. Let the mapping chosen by [Russell et al. \(2019\)](#) be named here as $\Phi_2 : \Delta_4 \rightarrow \mathbb{R}^3$. It is defined as

$$\mathbf{p} \mapsto \mathbf{y} = \Phi_2(\mathbf{p}) := \begin{pmatrix} p_{1,1} + p_{1,2} \\ p_{1,1} + p_{1,3} \\ p_{1,1}p_{1,4} - p_{1,2}p_{2,1} \end{pmatrix}^T. \quad (29)$$

where we follow notation from the paper and let $\mathbf{y} = (A, B, D)$. The interpretation of these variables is: the frequency of allele A_1 , the frequency of allele B_1 and the amount of linkage disequilibrium between the two, respectively. The second map, $\Phi_2(x)$, has the inverse $\Phi_2^{-1}(\mathbf{u})$ given by

$$\mathbf{y} \mapsto \mathbf{p} = \Phi_2^{-1}(\mathbf{y}) = \begin{pmatrix} AB + D \\ A(1 - B) - D \\ (1 - A)B - D \\ (1 - A)(1 - B) + D \end{pmatrix}^T. \quad (30)$$

This transformation was certainly used in [Karlin et al. \(1970\)](#). However, we believe it to

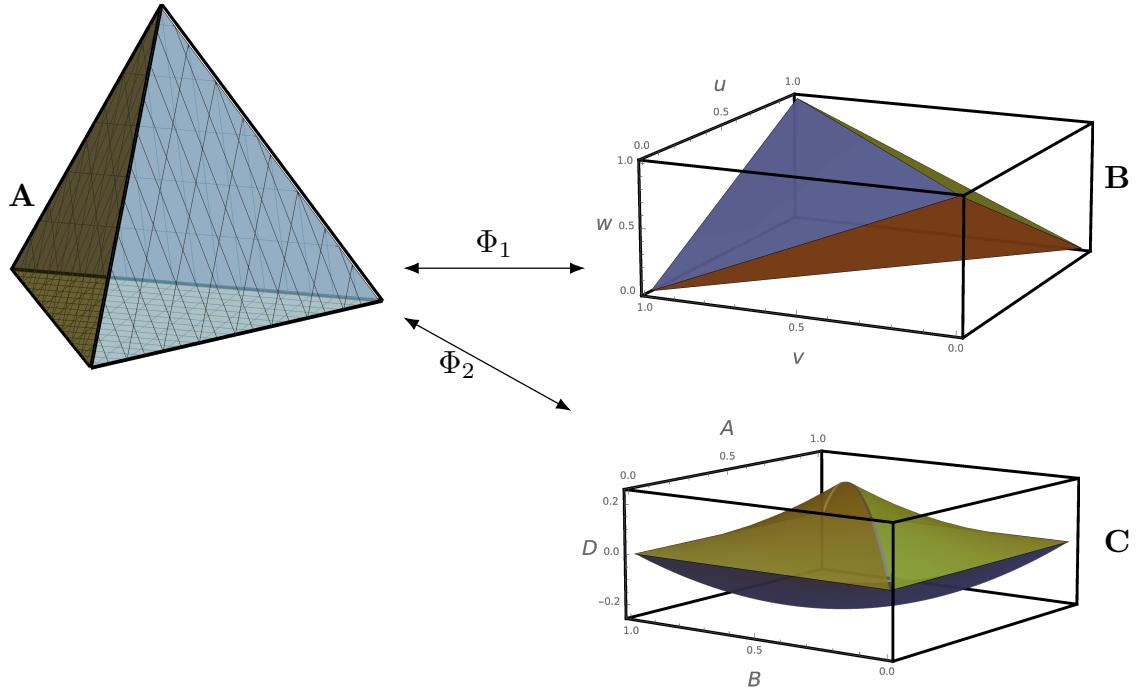


Figure 1: **Visualising two coordinate transformations used in the study of the selection-recombination equations.** The state space for the two-locus two-allele system, represented in three different coordinate systems and the relationship between them. Panel A is Δ_4 , the 4-simplex or the tetrahedron, which is typically how the selection-recombination equations are represented. Panel B is the resulting representation of the state space after mapping Φ_1 transforms the space. Similarly, Panel C is the space after the map Φ_2 has transformed the state space. Both B and C are subsets of \mathbb{R}^3 .

be a widely known transformation.

The second transformation, Φ_2 , was chosen to approximately study the QLE manifold as Nagylaki et al. (1999) observed that the QLE manifold, under the weak selection approximation, was a perturbation of the Wright manifold. The Wright manifold, Σ_W , is defined as the subset of the state space for which

$$p_{1,1}p_{2,2} - p_{1,2}p_{2,1} = 0 \quad (31)$$

(Rice, 2004). It is easy to see that Σ_W is given, in terms of \mathbf{y} coordinates, by

$$\Sigma_W = \{\mathbf{y} = (A, B, D) \in \mathbb{R}^3 : 0 \leq A \leq 1, 0 \leq B \leq 1, D = 0\}. \quad (32)$$

Since the QLE manifold was determined to be a perturbation of the Wright manifold in Nagylaki et al. (1999), which can be thought of as the subspace where $D = 0$, we conjectured that D would be small if the QLE manifold existed and was attracting. Therefore, the second coordinate choice was employed to find an approximate closed-form for the QLE manifold using a quasi-steady state assumption (Russell et al., 2019). The difference in coordinate choice Φ_1 and Φ_2 reflects the difference in approach: the first found

explicit sufficient parameter conditions which ensure the existence of the QLE manifold (Seymenoglu, 2019); whereas, the second used approximate techniques from multiple time-scale analysis to find a graph of a function approximating the QLE manifold.

4. Conclusions

We discuss the selection-recombination equation in its generality, for two-loci and n -alleles. We elaborate, giving details of known results for the two-locus two-allele implementation of the model and outline some of the techniques used to prove these results. Much of the results on the dynamics of the two-locus two-allele model comes from studying special cases, with some specific biological interpretation. This is in part due to the complexity of the model in general. More recent general results are discussed too, where the model in its fullest form is studied.

A clear take-home message from the work in this paper (and the discussed specific instances of the selection-recombination equations discussed) is that the biological formulation of the model with double subscript notation and up to 16 parameters for the two-locus two-allele model (and far more possible for higher locus or allele numbers) is that it can be notationally cumbersome. The simplification procedure undergone here for the models of recombination hotspot evolution would apply to other special cases of this system and, as can be seen by the relative simplicity of resulting system (12), others models may be reducible to a far simpler version if a similar procedure is employed.

The combined effects of selection and recombination can produce complex dynamics (Russell et al., 2019). Instances of the model which converge, either via damped oscillations or monotonically towards a stable equilibrium have been more commonly studied than those which produce more complex dynamics (limit cycles, heteroclinic cycles, chaotic-like dynamics, bistability etc). We believe this is partly due to simplifying assumptions — i.e. the *weak selection approximation* — and partly due to focussing on instances which only allow for low numbers (less than two) of both loci and alleles possible at each locus. Speaking generally, dynamical systems of low dimension can only exhibit dynamics of certain levels of complexity. Only in higher dimensions are many of the discussed complex dynamics possible.

References

- Akin, E., 1979. The geometry of population genetics. *Notes Biomath* 31.
- Akin, E., 1982. Cycling in simple genetic systems. *Journal of Mathematical Biology* 13, 305–324.
- Akin, E., 1983. Hopf bifurcation in the two locus genetic model. *American Mathematical Soc.*
- Akin, E., 1987. Cycling in simple genetic systems: Ii. the symmetric cases, in: *Dynamical Systems*. Springer, pp. 139–153.
- Bürger, R., 2011. Some mathematical models in evolutionary genetics, in: *The Mathematics of Darwin's Legacy*. Springer, pp. 67–89.
- Haig, D., Grafen, A., 1991. Genetic scrambling as a defence against meiotic drive. *Journal of theoretical Biology* 153, 531–558.
- Hastings, A., 1981. Stable cycling in discrete-time genetic models. *Proceedings of the National Academy of Sciences* 78, 7224–7225.
- Hofbauer, J., 1985. The selection mutation equation. *Journal of mathematical biology* 23, 41–53.
- Karlin, S., Feldman, M.W., et al., 1970. Linkage and selection: two locus symmetric viability model. *Theoretical population biology* 1, 39–71.
- Kimura, M., 1956. A model of a genetic system which leads to closer linkage by natural selection. *Evolution* , 278–287.
- Kuehn, C., 2015. Multiple time scale dynamics. volume 191. Springer.
- Nagylaki, T., 1993. The evolution of multilocus systems under weak selection. *Genetics* 134, 627–647.
- Nagylaki, T., Hofbauer, J., Brunovský, P., 1999. Convergence of multilocus systems under weak epistasis or weak selection. *Journal of mathematical biology* 38, 103–133.
- Rice, S.H., 2004. *Evolutionary theory: mathematical and conceptual foundations*. Sinauer Associates Sunderland, MA.
- Russell, T.W., 2019. Non-equilibrium dynamics in models of selection and recombination: heteroclinic cycles, networks and chaos. Ph.D. thesis. Royal Holloway, University of London.

- Russell, T.W., Russell, M.J., Úbeda, F., Jansen, V.A., 2019. Stable cycling in quasi-linkage equilibrium: fluctuating dynamics under gene conversion and selection. *Journal of theoretical biology* 477, 84–95.
- Seymenoglu, B., 2019. Invariant manifolds of models from Population Genetics. Ph.D. thesis. UCL (University College London).
- Shahshahani, S., 1979. A new mathematical framework for the study of linkage and selection. *American Mathematical Soc.*
- Stadler, B.M., 1996. Heteroclinic cycles and segregation distortion. *Journal of theoretical biology* 183, 363–379.
- Úbeda, F., Russell, T.W., Jansen, V.A., 2019. Prdm9 and the evolution of recombination hotspots. *Theoretical population biology* 126, 19–32.
- Wagner, G.P., Bürger, R., 1985. On the evolution of dominance modifiers ii: a non-equilibrium approach to the evolution of genetic systems. *Journal of theoretical Biology* 113, 475–500.

Chapter 3

PRDM9 and the evolution of recombination hotspots

Publication

This work has been published as

PRDM9 and the evolution of recombination hotspots (Úbeda et al., 2019)

Francisco Úbeda, Timothy W. Russell, Vincent A. A. Jansen

Theoretical Population Biology: 126, 19-32 (2019)

doi: <https://doi.org/10.1016/j.tpb.2018.12.005>

Author contributions

Francisco Úbeda conceived the research and formulated the model. Myself and Vincent A. A. Jansen analysed the model with feedback from Francisco Úbeda. I carried out the numerical analysis and Francisco Úbeda wrote the paper with feedback from myself and Vincent A. A. Jansen.

Contents

3.1	Introduction	52
3.2	Methods	54
3.2.1	Two-locus n-alleles model	54
3.2.2	Two-locus two-allele model	58
3.3	Results	60
3.3.1	Equilibria	60
3.3.2	Stability	62
3.3.3	Dynamics	70
3.4	Discussion	72

PRDM9 and the evolution of recombination hotspots

Francisco Úbeda^{a,*}, Timothy W. Russell^a, Vincent A.A. Jansen^a

^a*School of Biological Sciences, Royal Holloway University of London, Egham, Surrey, TW20 0EX, UK*

Abstract

Recombination in mammals is not uniformly distributed along the chromosome but concentrated in small regions known as recombination hotspots. Recombination starts with the double-strand break of a chromosomal sequence and results in the transmission of the sequence that does not break (preventing recombination) more often than the sequence that breaks (allowing recombination). Thus recombination itself renders individual recombination hotspots inactive and over time should drive them to extinction in the genome. Empirical evidence shows that individual recombination hotspots die but, far from being driven to extinction, they are abundant in the genome: a contradiction referred to as the Recombination Hotspot Paradox. What saves recombination hotspots from extinction? The current answer relies on the formation of new recombination hotspots in new genomic sites driven by viability selection in favour of recombination. Here we formulate a population genetics model that incorporates the molecular mechanism initiating recombination in mammals (PRDM9-like genes), to provide an alternative solution to the paradox. We find that low selection allows individual recombination hotspots to become inactive (die) while saving them from extinction in the genome by driving their re-activation (resurrection). Our model shows that when selection for recombination is low, the introduction of rare variants causes recombination sites to oscillate between hot and cold phenotypes with a recombination hotspot dying only to come back. Counter-intuitively, we find that low viability selection leaves a hard selective sweep signature in the genome, with the selective sweep at the recombination hotspot being the hardest when fertility selection is the lowest. Our model can help to understand the rapid evolution of PRDM9, the co-existence of two types of hotspots, the life expectancy of hotspots, and the volatility of the recombinational landscape (with hotspots rarely being shared between closely related species). From a more applied perspective our findings suggest ways of determining the strength of fertility driving the evolution of recombination and the need to account for the variability in fitness effects between subpopulations when using

*Corresponding author

Email address: f.ubeda@rhul.ac.uk (Francisco Úbeda)

genetic markers to predict diseases (genome wide association studies).

Keywords:

Recombination Hotspot Paradox, PRDM9, Population genetics, Gene conversion, viability selection, Heteroclinic cycles

1. Introduction

The distribution of recombination in the genome - and thus crossover events - is key to our understanding of the molecular mechanisms controlling recombination, the role of recombination on evolution, and the implementation of tests linking genetic markers with human disease (genome-wide association studies) (Boulton et al., 1997; Hey, 2004; Rosenberg et al., 2010). In many mammals, recombination is not uniformly distributed in the genome but concentrated in small chromosomal regions - known as recombination hotspots - where recombination is ten to a thousand times more frequent than the genome's average (Lichten and Goldman, 1995; Petes, 2001; Myers et al., 2005; Paigen and Petkov, 2010). While recombination hotspots are abundant in the mammalian genome (for example, in the human genome there are more than twenty five thousand), their mere existence is paradoxical and their life cycle is not fully understood (Boulton et al., 1997; Pineda-Krch and Redfield, 2005; Myers et al., 2005).

Recombination is initiated by a double-strand break (DSB) and may result in the conversion of the allelic sequence that breaks (active allele, enabling recombination) into the allelic sequence that does not break (inactive allele, disabling recombination) (Lichten and Goldman, 1995; Petes, 2001). The conversion of the allele that enables recombination into the one that disables recombination should be faster in genomic regions where recombination is higher (recombination hotspots). As a result individual recombination hotspots should become inactive (this process is often referred as the death of a hotspot; Coop and Myers (2007)) and, over evolutionary time, recombination hotspots should disappear from the genome (Boulton et al., 1997; Pineda-Krch and Redfield, 2005). Empirical work shows that individual recombination hotspots die (Ptak et al., 2004, 2005; Winckler et al., 2005; Coop et al., 2008; Myers et al., 2010; Stevison et al., 2015) but, despite their self-destructive nature, recombination hotspots are abundant in the mammalian genome (Myers et al., 2005; Baudat et al., 2013), thus posing the Recombination Hotspot Paradox (Boulton et al., 1997; Pineda-Krch and Redfield, 2005): what saves recombination hotspots from extinction?

Due to its molecular, evolutionary and medical implications the Recombination Hotspot Paradox has received much attention. Initial work aimed to test whether the known beneficial effects of recombination - in particular how recombination may favor proper chromosomal segregation during meiosis; thus avoiding the formation of aneuploidy gametes (Hassold et al., 2000; Louis and Borts, 2003; Brick et al., 2012; Alves et al., 2017)- can solve the paradox (Boulton et al., 1997; Pineda-Krch and Redfield, 2005; Calabrese, 2007; Peters, 2008). These mathematical models found that the strength of viability selection needed to

maintain active alleles at recombination hotspots over evolutionary time was too high to be realistic (Boulton et al., 1997; Pineda-Krch and Redfield, 2005; Calabrese, 2007; Peters, 2008). Furthermore, in these models when viability selection prevents the extinction of hotspots in the genome, it does so by preventing the death of individual hotspots, which is contrary to empirical observations (Ptak et al., 2004, 2005; Winckler et al., 2005; Coop et al., 2008; Myers et al., 2010; Stevison et al., 2015). Therefore, far from providing solutions to the Recombination Hotspot Paradox, previous work demonstrates that the paradox is well grounded.

Recent advances in our understanding of the molecular mechanisms initiating recombination include the identification of gene PRDM9 in humans (and many mammals) coding for protein PRDM9 that may bind a specific sequence at a target recombination hotspot (Myers et al., 2010; Baudat et al., 2010). Binding specificity between PRDM9 and its target site is required for the initiation of recombination (Myers et al., 2010; Baudat et al., 2010). This finding led to the verbal argument that when a target site has its binding motif (active allele) replaced by the non-binding motif (inactive allele) due to biased gene conversion, a mutant PRDM9 could create a new target site by coding for a new binding motif (Myers et al., 2010; Baudat et al., 2010). Natural selection would thus favor this rare mutant PRDM9 as long as recombination is advantageous for the individual (Myers et al., 2010; Baudat et al., 2010). Lacking a mathematical model to back this claim, it remained unclear whether selection would favor such mutant to the extent of allowing the formation (henceforth birth) of new recombination hotspots before an inactive allele arose. Furthermore, would the strength of selection required for the birth of new hotspots be too high to be realistic?

Úbeda and Wilkins (2011) modelled a trans acting modifier locus with binding specificity - like PRDM9 - showing that, for a strength of selection lower than in previous models, new recombination hotspots can be born at new target sites, while existing recombination hotspots die (Úbeda and Wilkins, 2011). These findings were consistent with empirical observations regarding the persistence of recombination hotspots in the genome in spite of the death of individual recombination hotspots (Úbeda and Wilkins, 2011). The Red Queen hypothesis of recombination hotspots evolution refers to the balance between death and birth of new hotspots driven by conversion and viability selection (Myers et al., 2010; Baudat et al., 2010; Úbeda and Wilkins, 2011), and is currently accepted as a possible resolution to the recombination hotspots paradox (Lesecque et al., 2014; Latrille et al., 2017).

In many respects, however, the Red Queen hypothesis needs further theoretical investigation (Latrille et al., 2017). One of these key theoretical aspects is the role of viability

selection in maintaining recombination hotspots, and the evolution of PRDM9 and target sequences (Ségurel et al., 2011; Latrille et al., 2017). Recent models include variables that mask the effect of selection; for example drift, recurrent mutation, and multiple locus targets (Úbeda and Wilkins, 2011; Latrille et al., 2017). While the introduction of these variables is justified to make the models more realistic, they complicate our understanding of the interplay between the key variables of these models, namely conversion and selection.

Here we formulate a population genetics model aimed to explore the interplay between conversion and selection in the resolution of the Recombination Hotspot Paradox. We start by considering an infinite population, without recurrent mutation and with a single target locus, to eliminate the above mentioned confounding variables. We build on the insight gained from this minimal model to interpret the results of an extended model with a finite population and recurrent mutation. In doing so, we find an alternative solution to the Recombination Hotspot Paradox, one that does not require the formation of new hotspots but relies on existing hotspots. Counter-intuitively, in our novel solution, it is low viability selection regimes that allow the persistence of recombination hotspots in spite of the death of individual ones (contrary to all previous models). Furthermore, sometimes, low viability selection accelerates the turnover of hotspots. We also find that viability selection can maintain polymorphisms at the PRDM9 and target loci. We apply these findings to explore the molecular signatures of selection in PRDM9 and target loci and consider their implications for genome-wide association studies.

2. Methods

2.1. Two-locus n-alleles model

We follow the classic Wright-Fisher population genetics framework (Wright, 1969; Bürger, 2000) to formulate a discrete time mathematical model of an infinite population of diploid individuals carrying two loci with an arbitrary number of alleles in each locus.

This model represents the interaction between a gene (PRDM9-like) producing a protein that binds a specific motif at a target recombination site (Figure 1), as it is observed in humans and many mammals (Myers et al., 2010; Baudat et al., 2010, 2013). The modifier locus A may carry alleles A_1, A_2, \dots, A_I each encoding a protein that attempts to bind a motif at a target locus B . Locus B may carry alleles B_1, B_2, \dots, B_K each corresponding to a base pair motif that the protein produced by locus A may attempt to bind. In each generation, both modifier alleles in each diploid individual show the same level of expression producing

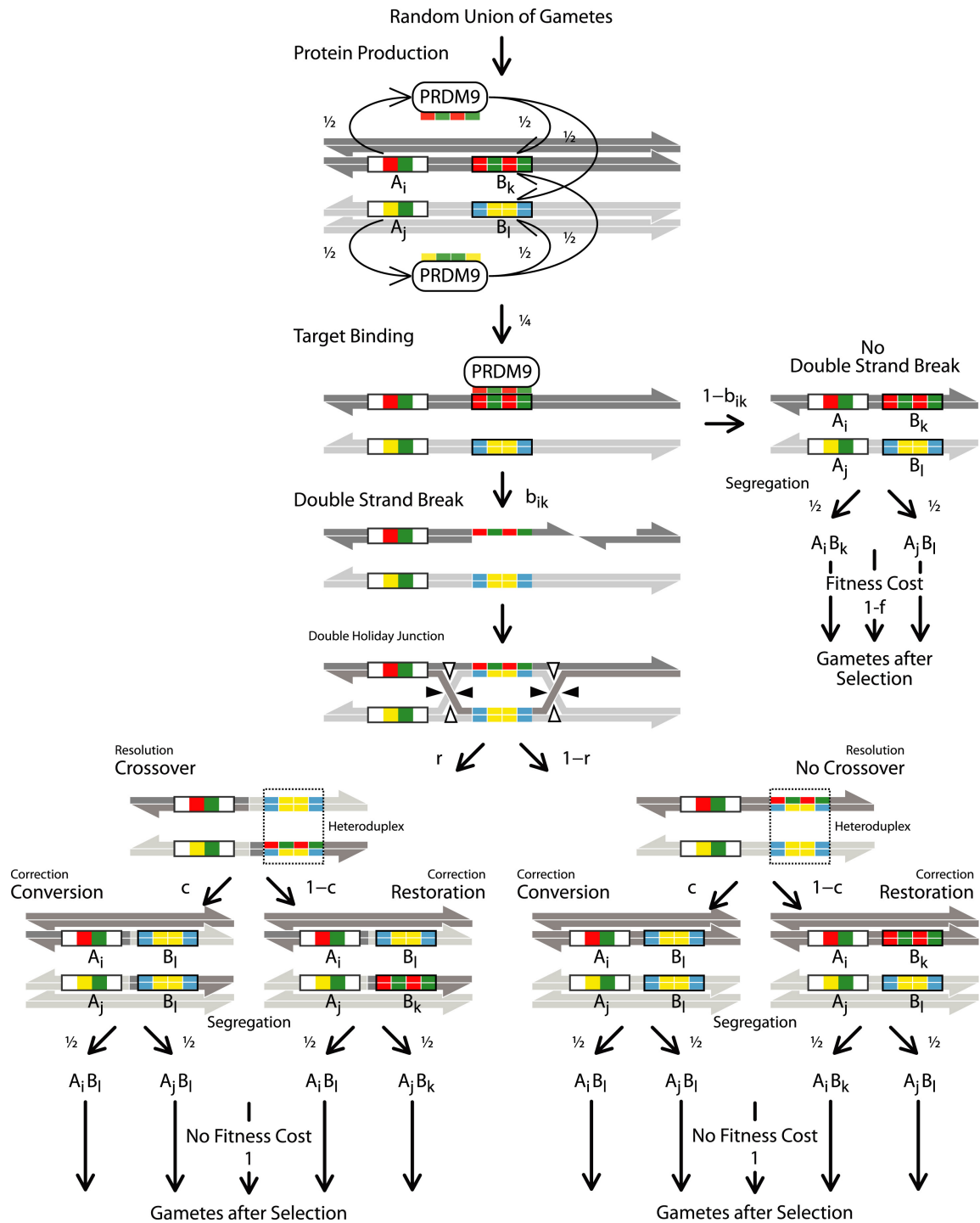


Figure 1 (*previous page*): **Model for recombination initiated by specificity of the double strand break.** Summary of the sequence of events modeled. We start with the production of a PRDM9-like protein with a recognition sequence that may match the target motif (same color sequence in recognition and motif) or not (different color sequence in recognition and motif). If protein and target bind, we follow the canonical DSB repair model for the initiation of recombination (Szostak et al., 1983; Sun et al., 1991). Once recombination (including crossover and conversion effects) has been completed, we model Mendelian segregation of haplotypes with no fitness cost. If protein and target do not bind, there is no recombination and we model Mendelian segregation of haplotypes with a fitness cost. Notice that sister chromatids are represented at the beginning and end of the figure but are omitted from the middle part for clarity.

proteins that have equal probability of binding the two target motifs (Figure 1). Therefore, in an individual with genotype $\frac{A_i B_k}{A_j B_l}$, the probability that a protein produced by alleles A_i or A_j attempts to bind the motif of alleles B_k or B_l is $\frac{1}{4}$ (Figure 1). The binding attempt of the protein A_i to the motif B_k results in binding and a double-strand break of allele B_k with probability $b_{i,k}$. However, the binding attempt may result in failure to bind and lack of any double-strand break with probability $1 - b_{i,k}$ (where $0 < b_{i,k} < 1$) (Figure 1).

A double-strand break initiates recombination and the chromatid that breaks is often repaired using its homologous chromatid as a template (Lichten and Goldman, 1995; Petes, 2001) (Figure 1). During the repair process there might be a crossover event in or near the target locus with probability r and none with probability $1 - r$ (where $0 < r < 1$) (Lichten and Goldman, 1995; Petes, 2001) (Figure 1). In our model, we assume that a crossover event between the modifier and target loci requires a double-strand break at the target locus. However, if the modifier and target loci are far apart in the same chromosome or in separate chromosomes, a crossover event between these loci may not require a double-strand break. Whether a crossover event between the modifier and target loci require a double-strand break at the target locus or not does not change any of the qualitative results of our model (see the Supplemental Material for a formulation of this model and the Discussion section for a summary of the results). During the repair process there might also be conversion of the allelic motif that breaks into the allelic motif that does not break with probability c and restoration to the allelic motif that breaks with probability $1 - c$ (where $0 < c < 1$) (Szostak et al., 1983; Sun et al., 1991; Lichten and Goldman, 1995; Petes, 2001) (Figure 1). Typically c takes the value $\frac{1}{2}$ (Szostak et al., 1983; Sun et al., 1991; Lichten and Goldman, 1995; Petes, 2001). Notice that biased gene conversion results in the over-transmission of the allele that is less likely to break (Boulton et al., 1997; Petes, 2001) (Figure 1).

Recombination ends up with Mendelian segregation of alleles into gametes. Following previous models (Boulton et al., 1997; Pineda-Krch and Redfield, 2005; Peters, 2008; Úbeda and Wilkins, 2011; Latrille et al., 2017), we assume that individuals undergoing recombina-

tion at the target locus have proper chromosomal segregation and do not suffer any fitness cost, while individuals that do not undergo recombination at the target locus have defective chromosomal segregation producing aneuploid (non-viable) gametes with probability f (where $0 < f < 1$) (Figure 1). Therefore, the fitness of individuals experiencing a recombination event is 1 but the fitness of individuals not experiencing a recombination event is $1 - f$ (Figure 1). Proper chromosomal segregation, however, often requires a crossover event rather than a recombination event (Baker et al., 1976; Koehler et al., 1996; Hassold and Hunt, 2001; Louis and Borts, 2003; Brick et al., 2012; Alves et al., 2017). Whether it is a crossover or a recombination event that determine the probability of proper chromosomal segregation does not change any of the qualitative results of our model (see the Supplemental Material for a formulation of this model and the Discussion section for a summary of the results).

Let $x_{i,k}$ be the frequency of haplotype $A_i B_k$ in gametes. Notice that $0 \leq x_{i,k} \leq 1$ and $\sum_{i,k} x_{i,k} = 1$. Random union of gametes results in an embryo with genotype $\frac{A_i B_k}{A_j B_l}$ with frequency $x_{i,k} x_{j,l}$. The probability that this embryo reaches adulthood is independent of its genotype, but its genotype determines the outcome of meiosis in adults. In particular, the probability that during meiosis the protein produced by the modifier locus breaks targets B_k and B_l are $\bar{b}_{i,j,k} = \frac{1}{2}(b_{i,k} + b_{j,k})$ and $\bar{b}_{i,j,l} = \frac{1}{2}(b_{i,l} + b_{j,l})$ respectively, and the probability that it breaks one of the targets is $\bar{\bar{b}}_{i,j,kl} = \frac{1}{2}(\bar{b}_{i,j,k} + \bar{b}_{i,j,l})$. The probability that during meiosis a double-strand break is followed by a crossover event between alleles at locus A and B is r , and the probability that the motif that breaks is converted into the motif that does not break is c . Recombination at the target locus is followed by correct Mendelian segregation of haplotypes into gametes but in the absence of recombination segregation of haplotypes is incorrect with probability f . Haplotype segregation brings us back to the beginning of our census.

The frequency of haplotype $A_i B_k$ in gametes in the next generation is:

$$\begin{aligned} x'_{i,k} = \frac{1}{\bar{w}} \sum_{j,l} \frac{1}{2} [& (\bar{\bar{b}}_{i,j,kl} + (1 - \bar{\bar{b}}_{i,j,kl})(1 - f)) x_{i,k} x_{j,l} \\ & - \frac{1}{4} c (\bar{b}_{i,j,k} x_{i,k} x_{j,l} - \bar{b}_{i,j,l} x_{i,l} x_{j,k}) \\ & - \frac{1}{2} (1 - c) r \bar{b}_{i,j,kl} (x_{i,k} x_{j,l} - x_{i,l} x_{j,k})] \end{aligned} \quad (1)$$

where prime represents the next generation and:

$$\bar{w} = \sum_{i,k} \sum_{j,l} \frac{1}{2} [\bar{\bar{b}}_{i,j,kl} + (1 - \bar{\bar{b}}_{i,j,kl})(1 - f)] x_{i,k} x_{j,l} \quad (2)$$

is the population mean fitness. These changes in haplotype frequency underpin changes in the population mean crossover rate at the target locus

$$\bar{r} = \frac{1}{2}r \sum_{i,k} \sum_{j,l} \bar{b}_{ij,kl} x_{i,k} x_{j,l}, \quad (3)$$

which is the phenotype whose evolution we are interested in.

Our model greatly differs from all other attempts to incorporate binding specificity (PRDM9-like genes) into the mechanism of recombination hotspots (Úbeda and Wilkins, 2011; Latrille et al., 2017), as previous models relied on simulations while we present analytic results (although see Latrille et al. (2017) for a one locus model approximating the frequency of PRDM9-like alleles in an infinite population).

2.2. Two-locus two-allele model

We consider the above model in the particular case when there are two alleles (A_1, A_2) at the modifier locus and two alleles (B_1, B_2) at the only target locus, resulting in four different haplotypes ($A_1B_1, A_1B_2, A_2B_1, A_2B_2$). Henceforth, we assume that a match between the subscripts of the modifier allele producing the binding protein and the allelic sequence that is the target of this protein results in a double-strand break with probability b (where $0 < b < 1$) and a mismatch between the subscripts prevents a double-strand break. For our modelling purposes this translates into:

$$b_{i,k} = \begin{cases} b & \text{if } i = k, \\ 0 & \text{if } i \neq k. \end{cases}$$

Notice that two of these haplotypes (A_1B_1, A_2B_2) correspond to haplotypes producing a protein that matches its own recognition sequence (recombination enabling haplotypes) and the other two (A_1B_2, A_2B_1) correspond to haplotypes producing a protein that does not match its own recognition sequence (recombination disabling haplotypes).

The dynamic system describing the change in frequency over time of each of these haplotypes can be obtained from replacing generic subscripts i and k by specific subscripts 1

and 2 in equation (1). The frequency of haplotype $A_i B_k$ in gametes in the next generation is

$$\begin{aligned}\bar{w}x'_{1,1} &= \left[\frac{1}{4}b + \frac{1}{2}(1 - \frac{1}{2}b)(1 - f) + \frac{1}{4}bf x_{1,1} - \frac{1}{8}bc x_{1,2} \right] x_{1,1} - \frac{1}{8}b \left(\frac{1}{2}c + (1 - c)r \right) D, \\ \bar{w}x'_{1,2} &= \left[\frac{1}{4}b + \frac{1}{2}(1 - \frac{1}{2}b)(1 - f) - \frac{1}{4}bf x_{1,2} + \frac{1}{8}bc x_{1,1} \right] x_{1,2} + \frac{1}{8}b \left(\frac{1}{2}c + (1 - c)r \right) D, \\ \bar{w}x'_{2,1} &= \left[\frac{1}{4}b + \frac{1}{2}(1 - \frac{1}{2}b)(1 - f) - \frac{1}{4}bf x_{2,1} + \frac{1}{8}bc x_{2,2} \right] x_{2,1} + \frac{1}{8}b \left(\frac{1}{2}c + (1 - c)r \right) D, \\ \bar{w}x'_{2,2} &= \left[\frac{1}{4}b + \frac{1}{2}(1 - \frac{1}{2}b)(1 - f) + \frac{1}{4}bf x_{2,2} - \frac{1}{8}bc x_{2,1} \right] x_{2,2} - \frac{1}{8}b \left(\frac{1}{2}c + (1 - c)r \right) D,\end{aligned}\tag{4}$$

where

$$\bar{w} = \frac{1}{4}b + \frac{1}{2}(1 - \frac{1}{2}b)(1 - f) + \frac{1}{4}bf(x_{1,1}^2 + x_{2,2}^2 - x_{1,2}^2 - x_{2,1}^2),\tag{5}$$

is the population mean fitness and

$$D = x_{1,1}x_{2,2} - x_{1,2}x_{2,1},\tag{6}$$

is the linkage disequilibrium.

To simplify the analysis, we define parameters α, β, γ , and δ as follows

$$\begin{aligned}\bar{w}x'_{i,k} &= \underbrace{\left(\frac{1}{4}b + \frac{1}{2}(1 - \frac{1}{2}b)(1 - f) \right)}_{\alpha} \pm \underbrace{\frac{1}{4}bf x_{i,k}}_{\beta} \pm \underbrace{\frac{1}{8}bc x_{i,l}}_{\gamma} x_{i,k} \\ &\quad \pm \underbrace{\frac{1}{8}b \left(\frac{1}{2}c + (1 - c)r \right) D}_{\delta},\end{aligned}\tag{7}$$

which allows us to re-write the system of equations (4) as follows:

$$\begin{aligned}\bar{w}x'_{1,1} &= (\alpha + \beta x_{1,1} - \gamma x_{1,2})x_{1,1} - \delta D, \\ \bar{w}x'_{1,2} &= (\alpha - \beta x_{1,2} + \gamma x_{1,1})x_{1,2} + \delta D, \\ \bar{w}x'_{2,1} &= (\alpha - \beta x_{2,1} + \gamma x_{2,2})x_{2,1} + \delta D, \\ \bar{w}x'_{2,2} &= (\alpha + \beta x_{2,2} - \gamma x_{2,1})x_{2,2} - \delta D,\end{aligned}\tag{8}$$

with population mean fitness

$$\bar{w} = \alpha + \beta(x_{1,1}^2 - x_{1,2}^2 - x_{2,1}^2 + x_{2,2}^2).\tag{9}$$

Notice that $0 < \alpha, \beta, \gamma, \delta < 1$. This two-locus two-allele model shares some similarities with the well-known symmetric viability model of Karlin and Feldman (Karlin et al., 1970; Bürger, 2000).

3. Results

3.1. Equilibria

We apply the equilibrium conditions ($x'_{i,k} = x_{i,k} = x^*_{i,k}$ for all i, k) to system (8) to find five equilibria with biological meaning; where all haplotype frequencies lie between (and including) 0 and 1. Let $\mathbf{x}^{*e} = (x^{*e}_{1,1}, x^{*e}_{1,2}, x^{*e}_{2,1}, x^{*e}_{2,2})$ denote the haplotype frequencies at equilibrium e where e is between one and five.

The first four equilibria correspond to the corners of the three dimensional simplex:

$$\begin{aligned}\mathbf{x}^{*1} &= (1, 0, 0, 0), \\ \mathbf{x}^{*2} &= (0, 1, 0, 0), \\ \mathbf{x}^{*3} &= (0, 0, 1, 0), \\ \mathbf{x}^{*4} &= (0, 0, 0, 1).\end{aligned}\tag{10}$$

Notice that equilibria 1 and 4, \mathbf{x}^{*1} and \mathbf{x}^{*4} , correspond to the fixation of one of the two recombination enabling haplotypes, $x_{1,1}$ and $x_{2,2}$ respectively. Equilibria 2 and 3, \mathbf{x}^{*2} and \mathbf{x}^{*3} , correspond to the fixation of one of the two recombination disabling haplotypes, $x_{1,2}$ and $x_{2,1}$ respectively (Figure 2).

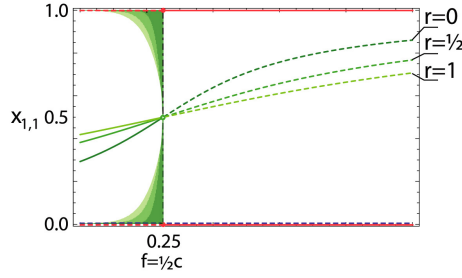
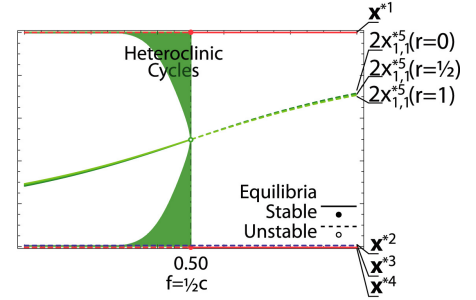
The last equilibrium can be obtained by noticing some symmetries of our model. In particular:

- (i) If at any point $x_{1,1} = x_{2,2}$ and $x_{1,2} = x_{2,1}$, this remains so in the future;
- (ii) If $x_{1,1} = x_{2,2}$ and $x_{1,2} = x_{2,1}$, the difference equations become $x'_{1,1} = x'_{2,2}$ and $x'_{1,2} = x'_{2,1}$ and the changes in $x_{1,1}$ and $x_{1,2}$ are equal to the changes in $x_{2,2}$ and $x_{2,1}$ respectively;
- (iii) If $x_{1,1} = x_{2,2}$ and $x_{1,2} = x_{2,1}$ and keeping in mind that $x_{1,1} + x_{1,2} + x_{2,1} + x_{2,2} = 1$, we also have that $2x_{1,1} + 2x_{1,2} = 1$ and thus $x_{1,2} = \frac{1}{2} - x_{1,1}$

The existence of a one dimensional manifold which is invariant in the interior of the state space implies that there is a symmetric equilibrium. The dynamics on this manifold are

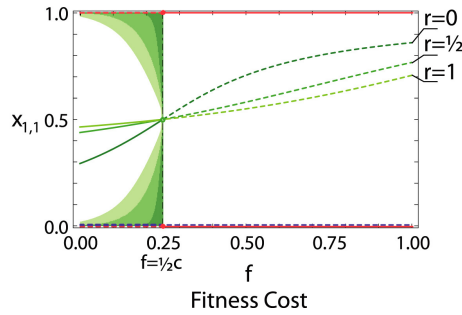
i. Fitness from break

Modifier target crossover require break

 $c = \frac{1}{2}$

 $c \approx 1$


ii. Fitness from break

Modifier target crossover does not require break

 $c = \frac{1}{2}$


iii. Fitness from crossover

Modifier target crossover require break

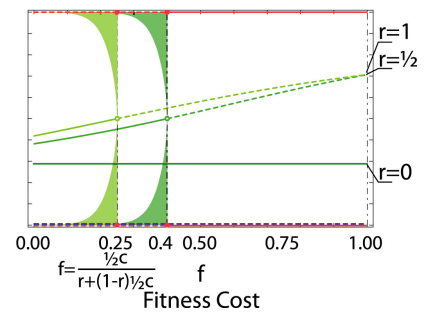
 $c = \frac{1}{2}$


Figure 2: Equilibria and heteroclinic cycle. Summary of the equilibria with biological meaning, their stability and the basin of attraction of the heteroclinic cycle. Each panel corresponds to a different value of the conversion rate $c = \{0, \frac{1}{2}, 1\}$ and shades of green correspond to different values of the crossover rate $r = \{0, \frac{1}{2}, 1\}$ (with darker green corresponding to no-crossover $r = 0$). For each pair of values (c, r) , the equilibrium frequency of haplotype $x_{1,1}^*$ is plotted as a function of the fitness cost f . Red lines depict corner equilibria x^{*1} and x^{*4} corresponding to the fixation of recombination enabling haplotypes (notice that these are independent of the values of c and r). Blue lines depict corner equilibria x^{*2} and x^{*3} corresponding to the fixation of recombination disabling haplotypes (notice that these are independent of the values of c and r). Green lines depict twice corner equilibrium x^{*5} corresponding to a polymorphism between recombination enabling and disabling haplotypes. Continuous lines depict stable equilibria while dashed lines depict unstable equilibria. The green colored area corresponds to the region in the space formed by the initial frequencies $(x_{1,1}^0, 0, 0, 1 - x_{1,1}^0)$ and the fitness cost f where the system tends to the heteroclinic cycle $(\dots x^{*1} \rightarrow x^{*2} \rightarrow x^{*4} \rightarrow x^{*3} \rightarrow x^{*1} \dots)$ as opposed to the internal equilibrium x^{*5} . Shades of green correspond to different values of the crossover rate $r = \{0, \frac{1}{2}, 1\}$ (with darker green corresponding to no-crossover $r = 0$).

described by a single difference equation

$$\bar{w}x'_{1,1} = \left(\alpha + \beta x_{1,1} - \gamma \left(\frac{1}{2} - x_{1,1} \right) \right) x_{1,1} - \delta \left(x_{1,1} - \frac{1}{4} \right), \quad (11)$$

with population mean fitness

$$\bar{w} = \alpha + 2\beta \left(x_{1,1} - \frac{1}{4} \right). \quad (12)$$

Applying the equilibrium condition ($x'_{1,1} = x_{1,1} = x_{1,1}^*$) to the previous equation yields the symmetric equilibrium:

$$\begin{aligned} \mathbf{x}^{*5} &= (x_{1,1}^{*5}, \frac{1}{2} - x_{1,1}^{*5}, \frac{1}{2} - x_{1,1}^{*5}, x_{1,1}^{*5}), \\ x_{1,1}^{*5} &= \frac{1}{4} + \frac{1}{4} \frac{2\delta - \sqrt{(2\delta)^2 + (\gamma - \beta)^2}}{\gamma - \beta}. \end{aligned} \quad (13)$$

At this equilibrium, the linkage disequilibrium is

$$D^* = x_{1,1}^{*5} - \frac{1}{4} = \frac{1}{4} \frac{2\delta - \sqrt{(2\delta)^2 + (\gamma - \beta)^2}}{\gamma - \beta}, \quad (14)$$

and the population mean fitness is

$$\bar{w}^* = \alpha + 2\beta \left(x_{1,1}^* - \frac{1}{4} \right) = \alpha + 2\beta D^*. \quad (15)$$

Notice that equilibrium \mathbf{x}^{*5} corresponds to a polymorphism where all haplotypes (recombination enablers and disablers) are preserved.

Finally, we can re-write the expression for equilibrium \mathbf{x}^{*5} in terms of the original parameters of our model

$$x_{1,1}^{*5} = \frac{1}{4} + \frac{1}{4} \frac{\frac{1}{2}c + (1-c)r - \sqrt{(\frac{1}{2}c + (1-c)r)^2 + (\frac{1}{2}c - f)^2}}{\frac{1}{2}c - f}. \quad (16)$$

3.2. Stability

The stability of an equilibrium \mathbf{x}^{*e} of a map $\mathbf{x}' = \mathbf{g}(\mathbf{x})$ is determined by studying the eigenvalues λ^e of the Jacobian matrix \mathbf{J} of the map evaluated at the equilibrium, that is $\mathbf{J}|_{\mathbf{x}=\mathbf{x}^{*e}}$.

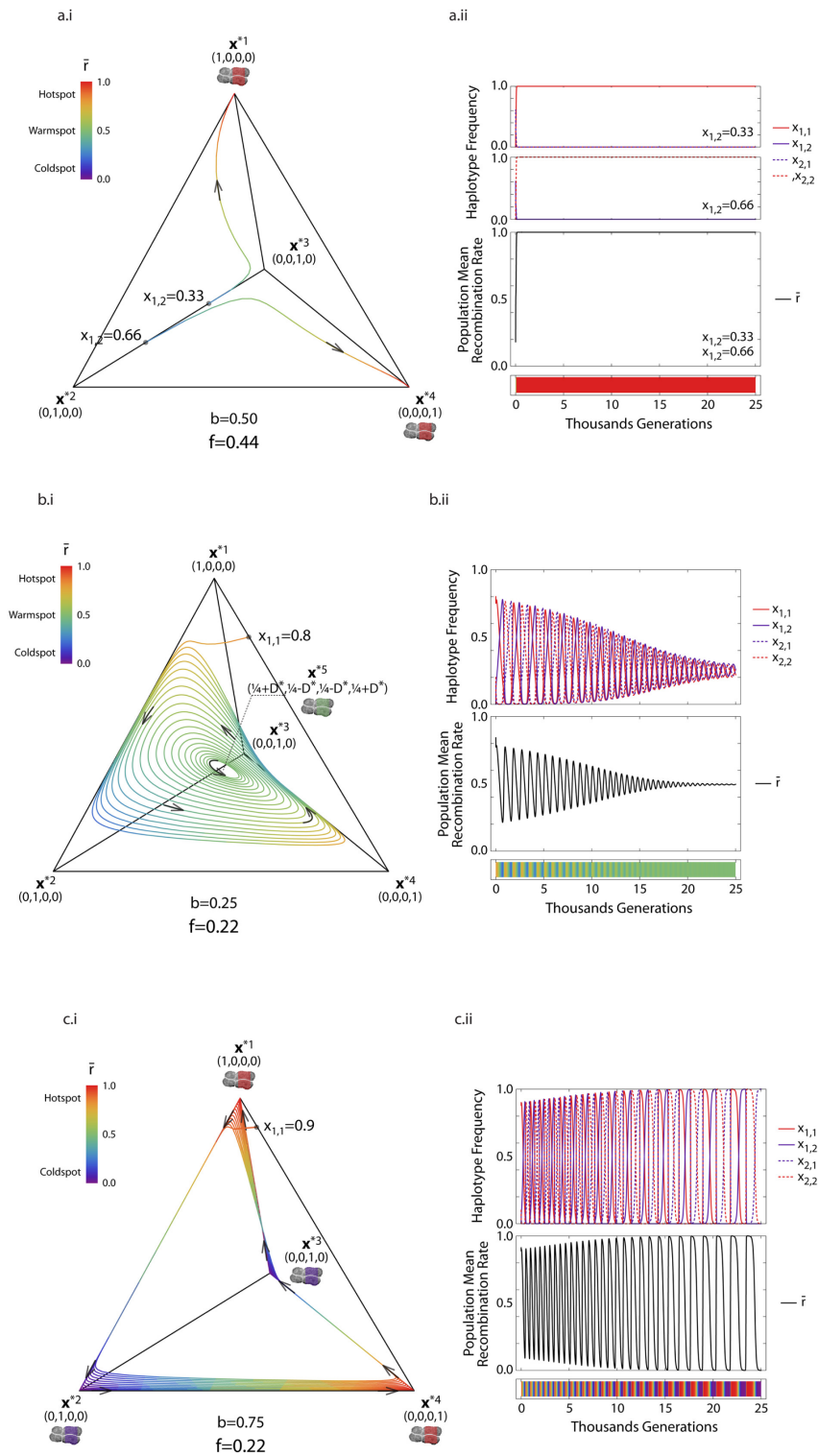


Figure 3 (previous page): *Dynamics of the system.* Examples of the three types of dynamics we find in our system. Each panel corresponds to a different combination of parameter values (f, b) and initial conditions $(x_{1,1}^0, x_{1,2}^0, x_{2,1}^0, x_{2,2}^0)$, while parameter values r, c remain fixed across panels, in particular $(r, c) = (1, \frac{1}{2})$. Subpanel (i) depicts the frequency of all haplotypes $(x_{1,1}, x_{1,2}, x_{2,1}, x_{2,2})$ at time t as a point in the three dimensional simplex. Arrows indicate in which direction the dynamics progress as time goes by. The color of the line depicts the population mean recombination activity of the target (see legend). Subpanel (ii) stacks three plots, namely: each of the haplotype frequencies against generational time, the population mean recombination activity as a line against time, and the population mean recombination activity as heat map against time. Panel (a) corresponds to parameter values $(f, b) = (0.44, 0.50)$ and initial conditions $(0, x_{1,2}^0, 1 - x_{1,2}^0, 0)$ where $x_{1,2}^0 = 0.33$ or $x_{1,2}^0 = 0.66$. (a.i) shows that when the initial condition is $x_{1,2}^0 = 0.33$ the system tends to corner equilibrium \mathbf{x}^{*1} . When the initial condition is $x_{1,2}^0 = 0.66$ the system tends to the other stable corner equilibrium \mathbf{x}^{*4} . In both cases the target site at equilibrium is a recombination hotspot (target colored). (a.ii) shows that when the initial condition is $x_{1,2}^0 = 0.33$ the recombination enabling haplotype $x_{1,1}$ becomes fixed. There are no changes at the modifier locus coding for PRDM9-like proteins. The population mean recombination activity reaches and remains over time at its highest (1). The target site becomes and remains a recombination hotspot over time. Panel (b) corresponds to parameter values $(f, b) = (0.22, 0.25)$ and initial conditions $(x_{1,1}^0, 0, 0, 1 - x_{1,1}^0)$ where $x_{1,1}^0 = 0.80$. (b.i) shows that the system tends to internal equilibrium \mathbf{x}^{*5} where the target site is what we called a recombination warmspot. (b.ii) shows that the frequency of all haplotypes oscillate in their approach to equilibrium where all haplotypes (recombination enabling and disabling) are present. There are oscillations at the locus coding for PRDM9-like proteins in the approach to equilibrium but these changes cease when equilibrium is reached. The population mean recombination activity oscillates between high and low as it approaches an intermediate value (0.5) at equilibrium. The target site oscillates between hot and cold phenotypes as it approaches a warm phenotype at equilibrium. Panel (c) corresponds to parameter values $(f, b) = (0.22, 0.75)$ and initial conditions $(x_{1,1}^0, 0, 0, 1 - x_{1,1}^0)$ where $x_{1,1}^0 = 0.90$. (c.i) shows that the system tends to the heteroclinic cycle $(\dots \mathbf{x}^{*1} \rightarrow \mathbf{x}^{*2} \rightarrow \mathbf{x}^{*4} \rightarrow \mathbf{x}^{*3} \rightarrow \mathbf{x}^{*1} \dots)$. (c.ii) shows that the frequency of all haplotypes oscillate in their approach to the heteroclinic cycle where there is an alternation between near fixation of one of the recombination enabling haplotypes and near fixation of one of the recombination disabling haplotypes. There are oscillations at the locus coding for PRDM9-like proteins, oscillations that become increasingly pronounced as the system approaches the heteroclinic cycle. The population mean recombination activity oscillates between high and low, oscillations that become increasingly pronounced as the system approaches the heteroclinic cycle. The target site oscillates between hot and cold phenotypes with it hot and cold character becoming more marked as the system approaches the heteroclinic cycle.

For brevity, we will refer to the eigenvalues λ_i^e as the eigenvalues of equilibrium \mathbf{x}^{*e} . If the modulus of all eigenvalues of equilibrium \mathbf{x}^{*e} are less than one ($|\lambda_i^e| < 1$ for all $i = 1, \dots, n$), the equilibrium is linearly stable (where $|z|$ denotes the modulus of a number z that may have real $\text{Re}(z)$ and imaginary $\text{Im}(z)$ components and is defined as $|z| = \sqrt{\text{Re}(z)^2 + \text{Im}(z)^2}$). If the modulus of at least one eigenvalue of equilibrium \mathbf{x}^{*e} is greater than one ($|\lambda_i^e| > 1$ for any $i = 1, \dots, n$), the equilibrium is linearly unstable.

The specifics of our model simplify the calculation of the Jacobian at equilibrium. In particular, our model describes changes in haplotype frequencies. To ensure that all frequencies add up to one at all times, the changes in frequency are normalised and the system is of the form

$$\mathbf{x}' = \frac{\mathbf{g}(\mathbf{x})}{\bar{w}(\mathbf{x})}, \quad (17)$$

where $\bar{w}(\mathbf{x}) = \mathbf{1}^T \mathbf{g}(\mathbf{x})$, $\mathbf{1}$ is a vector with all entries equal to one, and subscript T is the transpose operator. The Jacobian of this system is

$$\mathbf{J} = D_x \frac{\mathbf{g}(\mathbf{x})}{\bar{w}(\mathbf{x})} = \frac{D_x \mathbf{g}(\mathbf{x})}{\bar{w}(\mathbf{x})} - \frac{\mathbf{g}(\mathbf{x})}{\bar{w}(\mathbf{x})} \frac{\mathbf{1}^T D_x \mathbf{g}(\mathbf{x})}{\bar{w}(\mathbf{x})}, \quad (18)$$

where D_x is the total derivative with respect to x . Evaluated at equilibrium \mathbf{x}^* the Jacobian reduces to

$$\mathbf{J}|_{\mathbf{x}=\mathbf{x}^*} = \frac{1}{\bar{w}(\mathbf{x}^*)} (\mathbf{I} - \mathbf{x}^* \mathbf{1}^T) D_x \mathbf{g}(\mathbf{x})|_{\mathbf{x}=\mathbf{x}^*}, \quad (19)$$

where \mathbf{I} is the identity matrix.

3.2.1. Corner equilibria

The eigenvalues of corner equilibria \mathbf{x}^{*1} and \mathbf{x}^{*4} are equal and given by

$$\{\lambda_1^1, \lambda_2^1, \lambda_3^1, \lambda_4^1\} = \{\lambda_1^4, \lambda_2^4, \lambda_3^4, \lambda_4^4\} = \left(0, \frac{\alpha}{\alpha+\beta}, \frac{\alpha+\gamma}{\alpha+\beta}, \frac{\alpha-\delta}{\alpha+\beta}\right). \quad (20)$$

All eigenvalues of corner equilibrium \mathbf{x}^{*1} are real numbers, and \mathbf{x}^{*1} is stable if all λ_{1-4}^1 lie between 1 and -1 .

1. Condition $-1 < \lambda_2^1 < 1$ is always satisfied.
2. Condition $-1 < \lambda_3^1 < 1$ implies the satisfaction of:
 - i. $\lambda_3^1 < 1$ which requires that $\beta > \gamma$.
 - ii. $\lambda_3^1 > -1$ which is always satisfied.
3. Condition $-1 < \lambda_4^1 < 1$ implies the satisfaction of:
 - i. $\lambda_4^1 < 1$ which is always satisfied.
 - ii. $\lambda_4^1 > -1$ which requires that $2\alpha + \beta - \delta > 0$ which is always satisfied for the original parameters of our model.

To summarise, corner equilibria \mathbf{x}^{*1} and \mathbf{x}^{*4} are stable ($-1 < \lambda_{2-4}^1 < 1$) if $\beta > \gamma$ ($f > \frac{1}{2}c$ in terms of the original parameters) but unstable (saddles) ($-1 < \lambda_{2,4}^1 < 1$ but $\lambda_3^1 > 1$) if $\beta < \gamma$ ($f < \frac{1}{2}c$) (see Table 1 and Figure 2).

The eigenvalues of corner equilibria \mathbf{x}^{*2} and \mathbf{x}^{*3} are equal and given by

$$\{\lambda_1^2, \lambda_2^2, \lambda_3^2, \lambda_4^2\} = \{\lambda_1^3, \lambda_2^3, \lambda_3^3, \lambda_4^3\} = \left(0, \frac{\alpha}{\alpha-\beta}, \frac{\alpha-\gamma}{\alpha-\beta}, \frac{\alpha-\delta}{\alpha-\beta}\right). \quad (21)$$

All eigenvalues of corner equilibrium \mathbf{x}^{*2} are real numbers, and \mathbf{x}^{*2} is stable if all λ_{1-4}^2 lie between 1 and -1 .

1. Condition $-1 < \lambda_2^2 < 1$ implies the satisfaction of:

- i. $\lambda_2^2 < 1$ which is never satisfied.
- ii. $\lambda_2^2 > -1$ which is always satisfied.

2. Condition $-1 < \lambda_3^2 < 1$ implies the satisfaction of:

- i. $\lambda_3^2 < 1$ which requires that $\beta < \gamma$.
- ii. $\lambda_3^2 > -1$ which is always satisfied for the original parameters of our model.

To summarise, corner equilibria \mathbf{x}^{*2} and \mathbf{x}^{*3} are unstable ($\lambda_2^2 > 1$). If $\beta < \gamma$ ($f < \frac{1}{2}c$) these equilibria are saddles ($\lambda_2^2 > 1$ but $-1 < \lambda_3^2 < 1$) (see Table 1 and Figure 2).

3.2.2. Heteroclinic orbit

Here we show the existence of a heteroclinic orbit between the corner equilibria in our state space: $\dots \mathbf{x}^{*1} \rightarrow \mathbf{x}^{*2} \rightarrow \mathbf{x}^{*4} \rightarrow \mathbf{x}^{*3} \rightarrow \mathbf{x}^{*1} \dots$. To do so, we need to show that the subspaces in which the heteroclinic orbit travels are invariant. A set, $C \subseteq \mathbb{R}^n$, is an invariant set with respect to the map $x' = g(x)$ if, for every orbit ϕ it is true that $\phi_t(x) \in C \implies \phi_\tau(x) \in C$ for all $\tau > t$ where $t, \tau \in \mathbb{N}_+$. The subspaces in which our heteroclinic orbit travels are described by the lines joining each of the corners of our simplex, namely: $(x_{1,1}, 1 - x_{1,1}, 0, 0)$, $(0, x_{1,2}, 0, 1 - x_{1,2})$, $(0, 0, 1 - x_{2,2}, x_{2,2})$, $(1 - x_{2,1}, 0, x_{2,1}, 0)$. Our system can be written in the form

$$\bar{w}x'_{i,k} = (\alpha + \epsilon\beta x_{i,k} - \epsilon\gamma x_{i,l})x_{i,k} - \epsilon\delta(x_{i,k}x_{j,l} - x_{i,l}x_{j,k}), \quad (22)$$

where $\epsilon = 1$ for $(i, k) = (1, 1)$ and $(2, 2)$, and $\epsilon = -1$ for $(i, k) = (1, 2)$ and $(2, 1)$. From the system written in this form, it is easy to see that if $x_{i,k} = 0$ and $x_{i,l} = 0$ or $x_{j,k} = 0$ for $(i, k, j, l) \in 1, 2$ then $x'_{i,k} = 0$. In particular for the heteroclinic orbit we consider, either when $x_{2,2} = 0$ then $x_{2,1} = 0$ and $x'_{2,2} = 0$, when $x_{2,1} = 0$ then $x_{1,1} = 0$ and $x'_{2,1} = 0$, when $x_{1,1} = 0$ then $x_{1,2} = 0$ and $x'_{1,1} = 0$, and when $x_{1,2} = 0$ then $x_{2,2} = 0$ and $x'_{1,2} = 0$. This means that any subspace where $x_{i,k} = 0$ and $x_{i,l} = 0$ or $x_{j,k} = 0$ is invariant and thus all subspaces considered in our system are invariants.

When $\beta < \gamma$ ($f < \frac{1}{2}c$ in terms of the original parameters) all corner equilibria are saddles with one incoming and one outgoing eigenvector situated within the lines connecting the corner equilibria. Under the action of our system, the invariant subspaces have orbits which tend always away from one saddle equilibrium and towards another saddle equilibrium, thus implying the existence of a heteroclinic orbit.

Equilibria	Eigenvalues	Stability: $\beta > \gamma$	Stability: $\beta < \gamma$
$\mathbf{x}^{*1} = (1, 0, 0, 0)$ $\mathbf{x}^{*4} = (0, 0, 0, 1)$	$\lambda_1^{1,4} = 0$ $\lambda_2^{1,4} = \frac{\alpha}{\alpha+\beta}$ $\lambda_3^{1,4} = \frac{\alpha+\gamma}{\alpha+\beta}$ $\lambda_4^{1,4} = \frac{\alpha-\delta}{\alpha+\beta}$	$\lambda_i^{1,4}$ real $-1 < \lambda_{2,4}^{1,4} < 1$ stable	$\lambda_i^{1,4}$ real $-1 < \lambda_{2,4}^{1,4} < 1$ $\lambda_3^{1,4} > 1$ unstable (saddle)
$\mathbf{x}^{*2} = (0, 1, 0, 0)$ $\mathbf{x}^{*3} = (0, 0, 1, 0)$	$\lambda_1^{1,4} = 0$ $\lambda_2^{1,4} = \frac{\alpha}{\alpha-\beta}$ $\lambda_3^{1,4} = \frac{\alpha-\gamma}{\alpha-\beta}$ $\lambda_4^{1,4} = \frac{\alpha-\delta}{\alpha-\beta}$	$\lambda_i^{2,3}$ real $\lambda_{2,3}^{2,3} > 1$ unstable	$\lambda_i^{2,3}$ real $-1 < \lambda_3^{2,3} < 1$ $\lambda_2^{2,3} > 1$ unstable (saddle)
\mathbf{x}^{*5}	$\lambda_1^5 = 0$ $\lambda_2^5 = 1 + \frac{\gamma D^* + \sqrt{\frac{1}{4}(\beta-\gamma) + (D^*\gamma)^2}}{\bar{w}^*}$ $\lambda_3^5 = 1 + \frac{\gamma D^* - \sqrt{\frac{1}{4}(\beta-\gamma) + (D^*\gamma)^2}}{\bar{w}^*}$ $\lambda_4^5 = 1 - \frac{\delta + 2D^*(\beta-\gamma)}{\bar{w}^*}$	λ_i^5 real $-1 < \lambda_{3,4}^5 < 1$ $\lambda_2^5 > 1$ unstable (saddle)	$\lambda_{2,3}^5$ imaginary $-1 < \lambda_4^5 < 1$ $ \lambda_{2,3}^5 < 1$ stable

Table 1

Table 1 (previous page): *Stability*. The *eigenvalue* column contains the eigenvalues corresponding to each equilibrium with biological meaning (\mathbf{x}^{*1-5}). The *stability* column summarises the analysis of the stability of each equilibrium using their eigenvalues. This analysis shows that the stability of all equilibria is determined by a single condition, namely whether $\beta > \gamma$ or not.

3.2.3. Internal equilibrium

Calculating the eigenvalues of the internal equilibrium \mathbf{x}^{*5} using the original Jacobian matrix in (19) leads to intractable results. To attain eigenvalues that are tractable, we transform the vector \mathbf{x} into the vector \mathbf{y} using the linear transformation $\mathbf{y} = \mathbf{M}\mathbf{x}$ where

$$\mathbf{M} = \begin{bmatrix} 1 & 1 & 1 & 1 \\ 1 & -1 & -1 & 1 \\ 1 & 1 & 0 & 0 \\ 1 & 0 & 1 & 0 \end{bmatrix}. \quad (23)$$

This matrix simplifies the eigenvalue calculation, as it almost diagonalises the Jacobian matrix evaluated at the internal equilibrium \mathbf{x}^{*5} . It does so because it is the linearisation of the well-known transformation from haplotype frequencies to allele frequencies [Bürger \(2000\)](#). The linearisation of such a transformation is sufficient to simplify this calculation, as it is the linearised dynamics (linearised around the internal equilibrium) that we are interested in.

The dynamics in the vicinity of the equilibrium for the transformed variables are

$$\mathbf{y}' = \mathbf{M}\mathbf{x}' = \mathbf{M}\mathbf{J}\mathbf{x} = \mathbf{M}\mathbf{J}\mathbf{M}^{-1}\mathbf{y}, \quad (24)$$

where the matrix $\mathbf{M}\mathbf{J}\mathbf{M}^{-1}$ is given by

$$\begin{aligned} \mathbf{M}\mathbf{J}\mathbf{M}^{-1} &= \mathbf{M} \frac{1}{\bar{w}^*} (\mathbf{I} - \mathbf{x}^* \mathbf{1}^T) D_x \mathbf{g}(\mathbf{x})|_{\mathbf{x}=\mathbf{x}^*} \mathbf{M}^{-1} \\ &= \begin{bmatrix} 0 & 0 & 0 & 0 \\ \frac{\beta - \gamma - 8D^*(\bar{w}^* + \delta)}{2\bar{w}^*} & -\frac{4D^*(\beta - \gamma) - 2(\bar{w}^* - \delta)}{2\bar{w}^*} & 0 & 0 \\ -\frac{\bar{w}^* + \frac{1}{2}\beta}{2\bar{w}^*} & 0 & 1 & \frac{\beta}{2\bar{w}^*} \\ -\frac{\frac{1}{2}(\beta - \gamma) + 2D^* + \bar{w}^*}{2\bar{w}^*} & 0 & \frac{\beta - \gamma}{2\bar{w}^*} & \frac{4D^*\gamma + 2\bar{w}^*}{2\bar{w}^*} \end{bmatrix}. \end{aligned} \quad (25)$$

The eigenvalues of the transformed matrix $\mathbf{M}\mathbf{J}\mathbf{M}^{-1}$ are equivalent to the eigenvalues of the original matrix \mathbf{J} but they are easier to find. In particular, the eigenvalues of matrix $\mathbf{M}\mathbf{J}\mathbf{M}^{-1}$

are

$$\{\lambda_1^5, \lambda_2^5, \lambda_3^5, \lambda_4^5\} = \left(0, 1 + \frac{\gamma D^* + \sqrt{\Delta^*}}{\bar{w}^*}, 1 + \frac{\gamma D^* - \sqrt{\Delta^*}}{\bar{w}^*}, 1 - \frac{\delta + 2D^*(\beta - \gamma)}{\bar{w}^*}\right), \quad (26)$$

where $\Delta^* = (\gamma D^*)^2 + \frac{1}{4}\beta(\beta - \gamma)$.

The eigenvalues of internal equilibrium \mathbf{x}^{*5} can be either real or imaginary numbers.

1. Stability conditions derived from the second and third eigenvalues $\lambda_{2,3}^5$.

- (a) Eigenvalues $\lambda_{2,3}^5$ are real numbers when $\Delta^* > 0$. If $\beta > \gamma$, the later condition is always satisfied, eigenvalues $\lambda_{2,3}^5$ are real numbers, and the stability of the internal equilibrium requires that $-1 < \lambda_{2,3}^5 < 1$. This requirement implies the satisfaction of four conditions:
 - i. Condition $\lambda_2^5 < 1$ requires that $\gamma D^* + \sqrt{\Delta^*} < 0$ which is never satisfied.
 - ii. Condition $\lambda_2^5 > -1$ requires that $\gamma D^* + \sqrt{\Delta^*} > -2\bar{w}^*$ which is always satisfied.
 - iii. Condition $\lambda_3^5 < 1$ requires that $\gamma D^* - \sqrt{\Delta^*} < 0$ which is always satisfied because $\gamma D^* < (\gamma D^*)^2 + \frac{1}{4}\beta(\beta - \gamma)$.
 - iv. Condition $\lambda_3^5 > -1$ requires that $\gamma D^* - \sqrt{\Delta^*} > -2\bar{w}^*$ which is always satisfied because $\alpha > \beta$ given the parametrisation of our model.

Notice that $\beta > \gamma$ implies that $D^* > 0$. In particular, from (14) we know that $D^* = \frac{1}{2(\beta - \gamma)} \left(\sqrt{\delta^2 + \frac{1}{4}(\beta - \gamma)^2} - \delta \right)$ and given that $\delta^2 + \frac{1}{4}(\beta - \gamma)^2 > \delta^2$ the sign of D^* is always equal to the sign of $\beta - \gamma$.

- (b) Eigenvalues $\lambda_{2,3}^5$ are complex conjugate numbers when $\Delta^* < 0$ and thus condition $\beta < \gamma$ is necessary for having complex eigenvalues. If $\beta > \gamma$ and the eigenvalues $\lambda_{2,3}^5$ are complex numbers, the stability of the internal equilibrium requires that $|\lambda_{2,3}^5| < 1$. This requirement implies the satisfaction of a single condition.
 - i. Condition $|\lambda_2^5| = |\lambda_3^5| < 1$ requires that $2\gamma\bar{w}^*D^* - \frac{1}{4}\beta(\beta - \gamma) < 0$. Replacing \bar{w}^* and D^* with their definitions from (15) and (14) respectively, yields the new condition $\alpha - \Omega < 4\delta < \alpha + \Omega$ where $\Omega = \frac{(2\gamma - \beta)\sqrt{\gamma(\beta^3 - \beta^2\gamma + \alpha^2\gamma)}}{\beta\gamma}$. The term Ω is equal to α if $\beta = \gamma$ but is greater than α if $\beta < \gamma$. This can be shown by calculating the derivative of Ω with respect to β , $\frac{\partial\Omega}{\partial\beta}$, which is negative when $\beta < \gamma$. This is true when $\alpha > \beta, 2\delta$ as is the case given the parametrisation of our model. Because Ω is greater than α when $\beta < \gamma$, the stability condition $\alpha - \Omega < 4\delta < \alpha + \Omega$ can be replaced by $0 < 4\delta < 2\alpha$ which is always satisfied given the parametrisation of our model. Therefore, when eigenvalues $\lambda_{2,3}^5$ are complex, their modulus is always less than one.

2. Stability conditions derived from the fourth eigenvalue λ_4^5 . Eigenvalue λ_4^5 is a real number and the stability of the internal equilibrium requires that $-1 < \lambda_4^5 < 1$. This requirement implies the satisfaction of two conditions:

- i. Condition $\lambda_4^5 < 1$ requires that $-\delta - 2D^*(\beta - \gamma) < 0$ which is always satisfied because $\beta - \gamma$ and D^* have the same sign and thus their product is always positive.
- ii. Condition $\lambda_4^5 > -1$ requires that $\delta + 2D^*(\beta - \gamma) < 2\bar{w}^*$. Replacing D^* and \bar{w}^* with their definitions from (14) and (15) respectively, yields the new condition $2(\alpha + 2\beta D^*) > \sqrt{\frac{1}{4}(\beta - \gamma)^2 + \delta^2}$. Because $2(\alpha + 2\beta D^*) > 2\alpha - \beta$ and $\frac{1}{2}(\gamma - \beta) + \delta > \sqrt{\frac{1}{4}(\beta - \gamma)^2 + \delta^2}$ the later condition is true when $2\alpha - \beta > \frac{1}{2}(\gamma - \beta) + \delta$ which is always satisfied for the parametrisation of our model.

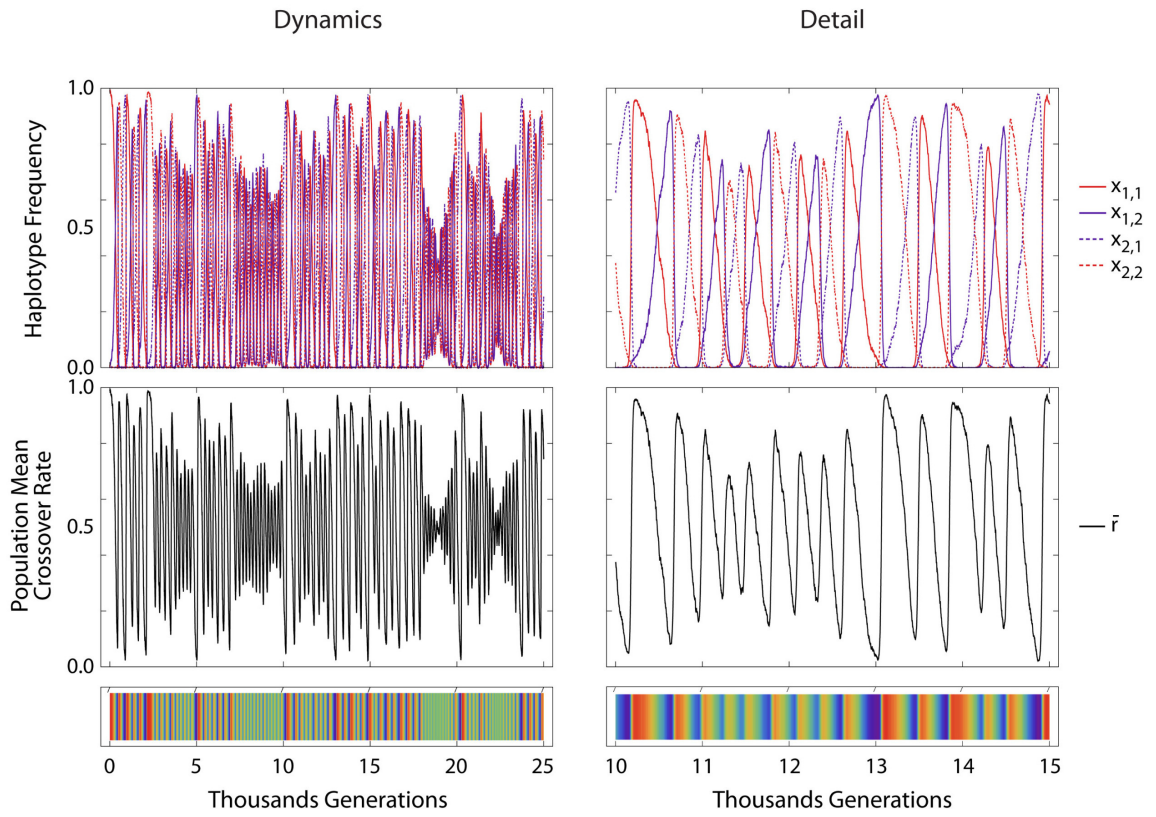
To summarise, internal equilibrium \mathbf{x}^{*5} is unstable (saddle) ($\lambda_2^5 > 1$ but $-1 < \lambda_{3,4}^5 < 1$) if $\beta > \gamma$ ($f > \frac{1}{2}c$) but stable ($|\lambda_{2,3}^5| < 1$ and $-1 < \lambda_4^5 < 1$) if $\beta > \gamma$ ($f < \frac{1}{2}c$) (see Table 1 and Figure 2).

3.3. Dynamics

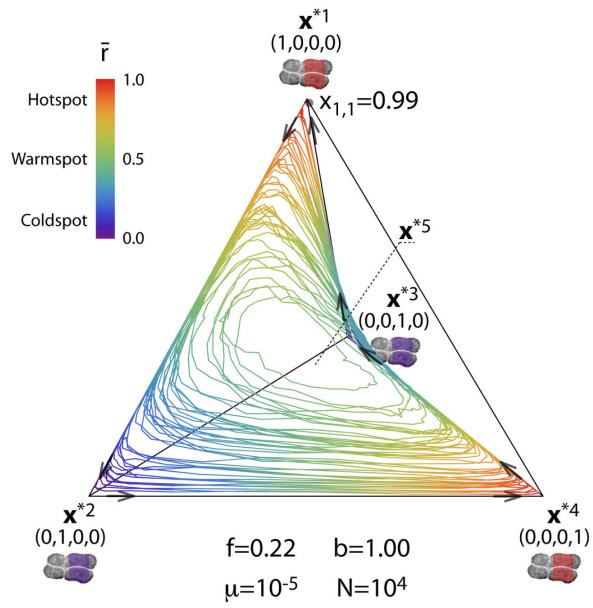
When viability selection is high ($f > \frac{1}{2}c$) the dynamics of our system tend towards the fixation of one of the recombination enabling haplotypes (\mathbf{x}^{*1} or \mathbf{x}^{*4}) (Figure 2 and 3.a). In these two corner equilibria, an individual recombination hotspot remains inactive and the genomic recombinational landscape remains unchanged (Figure 3.a). Furthermore, the PRDM9-like gene does not evolve and remains monomorphic. An unchanging recombinational landscape and a non-evolving PRDM9 gene, are inconsistent with empirical observations on the life history of recombination hotspots controlled by PRDM9 (Ptak et al., 2004, 2005; Winckler et al., 2005; Coop et al., 2008; Myers et al., 2010; Stevison et al., 2015).

When viability selection is weak ($f < \frac{1}{2}c$) and initially all haplotypes are present in the population ($x_{i,k} \not\approx 0$ for any pair (i, k)), the dynamics of our system oscillate towards a polymorphic equilibrium where all haplotypes (enabling and disabling) are present (\mathbf{x}^{*5}) (Figure 2 and 3.b). At this interior equilibrium, an individual recombination hotspot will see their activity reduced but not extinguished and the genomic recombinational landscape remains unchanged (Figure 3.b). Furthermore, the PRDM9-like gene does not evolve but remains polymorphic. An unchanging recombinational landscape and a non-evolving PRDM9 gene, are inconsistent with empirical observations (Ptak et al., 2004, 2005; Winckler et al., 2005; Coop et al., 2008; Myers et al., 2010; Stevison et al., 2015).

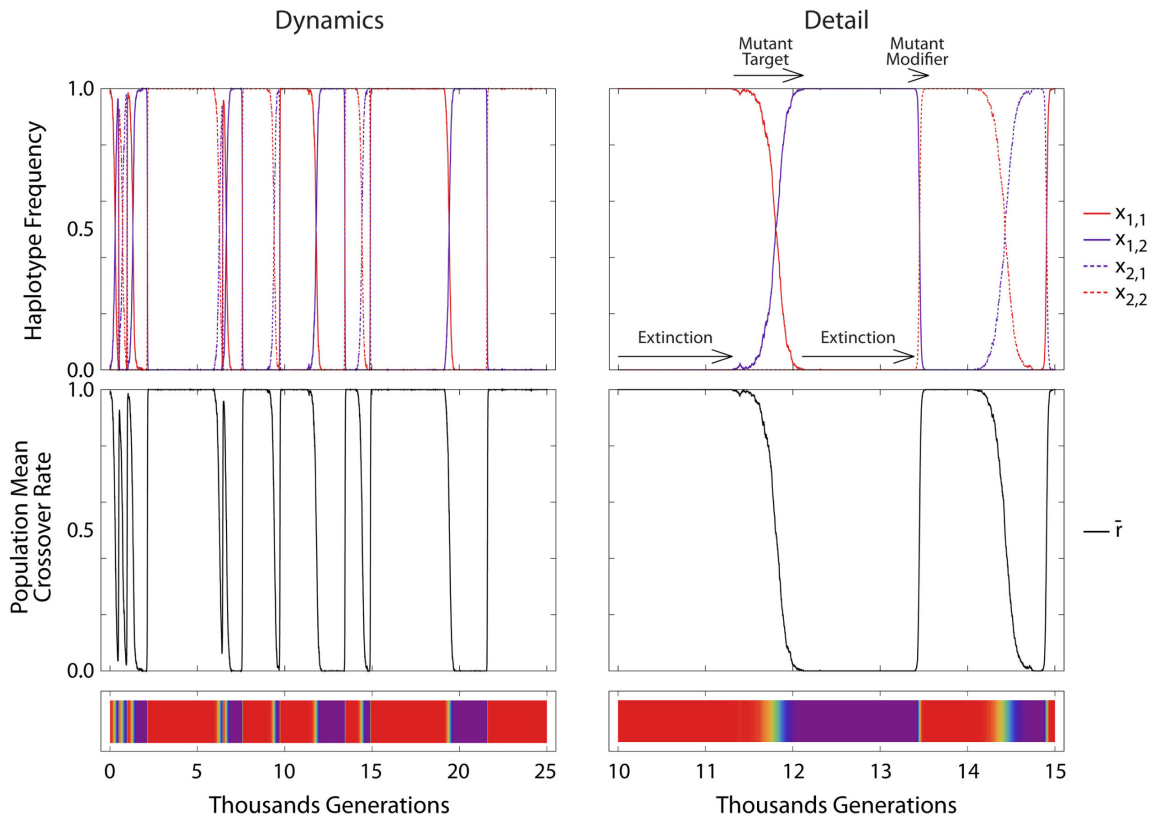
a.i



a.ii



b.i



b.ii

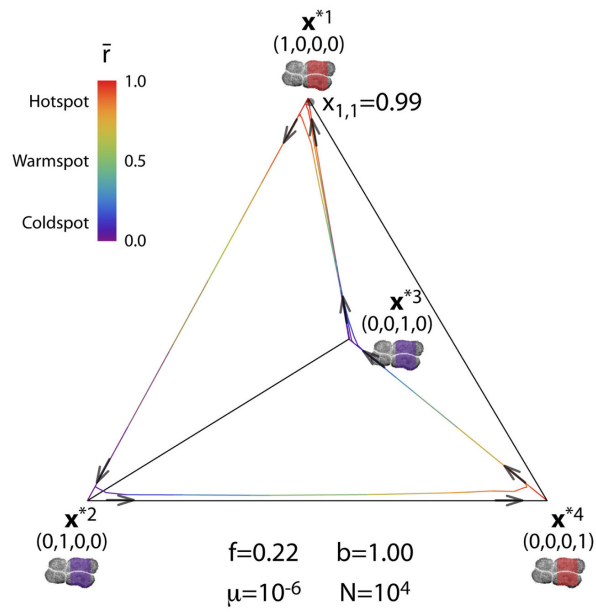


Figure 4 (previous page): *Correspondence between infinite and finite population dynamics.* Examples of the correspondence between dynamics in the infinite and finite population models. Each panel corresponds to a different combination of parameter values (f, b) and (μ, N) where μ is the mutation rate and N is the population size. Parameter values $(r, c) = (1, \frac{1}{2})$ and initial conditions $(x_{1,1}^0, x_{1,2}^0, x_{2,1}^0, x_{2,2}^0) = (0.99, \frac{1}{3}0.01, \frac{1}{3}0.01, \frac{1}{3}0.01)$ remain fixed across panels. Subpanel (i) stacks three plots, namely: each of the haplotype frequencies against generational time, the population mean recombination activity against time, and the population mean recombination activity as a heat map against time. Subpanel (ii) depicts the frequency of all haplotypes $(x_{1,1}, x_{1,2}, x_{2,1}, x_{2,2})$ at time t as a point in the three dimensional simplex. Arrows indicate in which direction the dynamics progress as time goes by. The color of the line depicts the population mean recombination activity of the target site (see legend). Panel (a) corresponds to parameter values $(f, b) = (0.22, 1.00)$ and $(\mu, N) = (10^{-5}, 10^4)$. The target site oscillates between hot and cold phenotypes rapidly and no haplotype becomes fixed. Panel (b) corresponds to parameter values $(f, b) = (0.22, 1.00)$ and $(\mu, N) = (10^{-6}, 10^4)$. The target site oscillates between hot and cold phenotypes slowly and haplotypes often become fixed.

When viability selection is low ($f < \frac{1}{2}c$) and initially one haplotype is present while the others are rare mutants ($x_{i,k} \approx 1$ for one (i, k) while $x_{i,k} \approx 0$ for any other pair (i, k)), the dynamics of our system oscillate towards a (heteroclinic) cycle where fixation of one of the recombination enabling haplotypes alternates with fixation of one of the recombination disabling haplotypes ($\dots \mathbf{x}^{*1} \rightarrow \mathbf{x}^{*2} \rightarrow \mathbf{x}^{*4} \rightarrow \mathbf{x}^{*3} \rightarrow \mathbf{x}^{*1} \dots$) (Figure 2 and 3.c). Other examples of heteroclinic cycles in evolutionary genetics can be found in [Haig and Grafen \(1991\)](#) or [Yahara et al. \(2009\)](#). Along this cycle, an individual recombination hotspot will alternate between becoming inactive (die) and becoming active (resurrect) (Figure 3.c). Therefore, the recombinational landscape becomes highly dynamic (Figure 3.c). Furthermore, the PRDM9-like gene is evolving fast with selective sweeps that are harder when viability selection is higher within the lower range ($f < \frac{1}{2}c$). A changing recombinational landscape and a rapidly evolving PRDM9 gene, are consistent with empirical observations on the life history of recombination hotspots controlled by PRDM9 ([Ptak et al., 2004, 2005](#); [Winckler et al., 2005](#); [Coop et al., 2008](#); [Myers et al., 2010](#); [Stevison et al., 2015](#)).

4. Discussion

We find that strong selection (defined as selection bigger than conversion) fixes haplotypes which enable double-strand breaks (which translates into individual recombination hotspots exhibiting high activity and do not die over time (Figure 3.a)). This finding recovers the result of previous models ([Boulton et al., 1997](#); [Pineda-Krch and Redfield, 2005](#); [Calabrese, 2007](#); [Peters, 2008](#)). In our model however, weak selection (defined as selection smaller than conversion) does not fix any particular haplotype; it either maintains all haplotypes in constant proportions (which translates into individual recombination hotspots that exhibit moderate

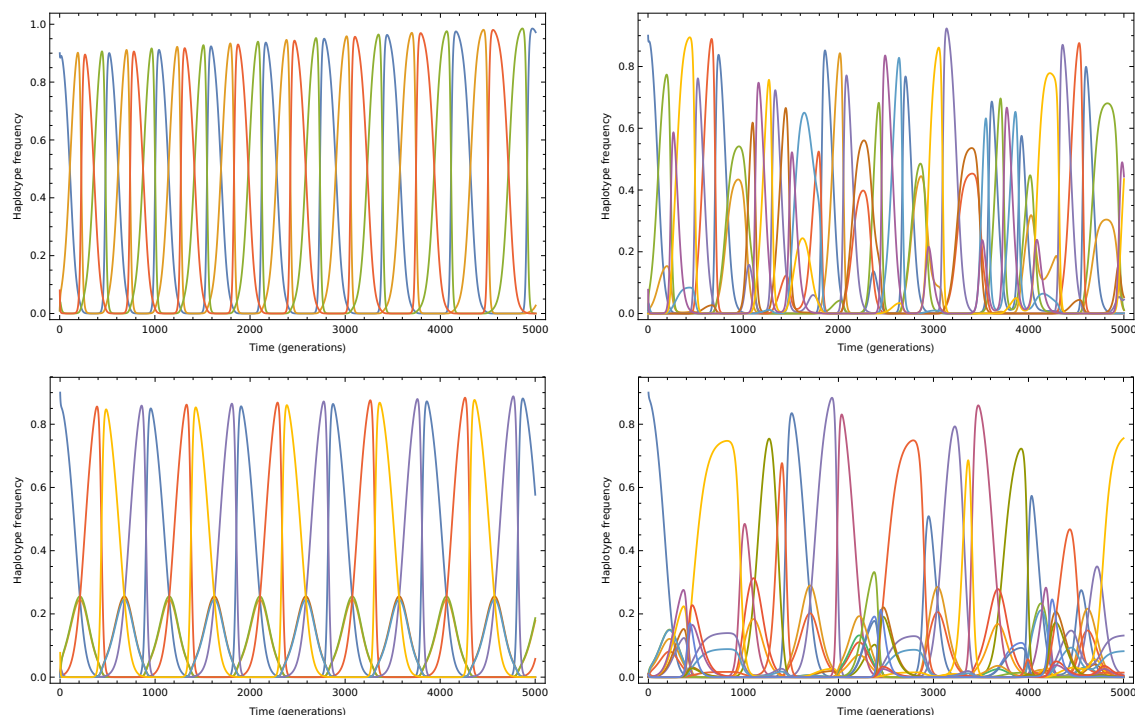


Figure 5: Extending the number of targets and the number of alleles. We simulate extensions of the model numerically to study the nature of the resulting cycles. Top left: a simulation of the heteroclinic cycle present in the two locus two allele model (four equations). Bottom left: A regular heteroclinic cycle in the model with two alleles but three loci (two target loci; 8 equations); the cycling is still regular, but the complexity of the cycle has increased somewhat. Top right: a chaotic solution of the three alleles two loci model (nine equations); cycling is still possible in certain subspaces of the state space (see Chapter 6 for an in-depth analysis of this model). Bottom right: a highly disordered trajectory of the three allele three locus model (27 equations); clearly hotspot turnover is still occurring but in a far less regular and predictable fashion. The parameters used for these simulations were all the same: $f = 0.2$, $c = 0.5$, $b = r = 1$ and the initial conditions were x_1 close to 1 (i.e. $x_1 = 0.99$) and whichever other variables present in the model in question (each model required a different number of initial conditions) almost equal to zero. We omit a key as it is really the nature of the cycles which we wish to emphasise with this figure, not which haplotype is which. Furthermore, the number of haplotypes present varies between each figure and the bottom right panel has a total of 27 possible haplotypes, making a key less than helpful.

activity and do not die (Figure 3.b)), or the proportion of each haplotype cycles over time (which translates into individual recombination hotspots that exhibit low and high activity, dying and resurrecting in a constant cycle (Figure 3.c)). These two types of recombination hotspots are novel. An equilibrium that maintains a polymorphism at a PRDM9-like locus and its target has not been described (Latrille et al., 2017). A cycle whereby the same set of alleles at a PRDM9-like locus and its target site rotate has not yet been described; Úbeda and Wilkins (2011) and Latrille et al. (2017) found through simulations a succession of new alleles at a PRDM9-like locus targeting a large number of new target sites.

It is possible to gain an intuitive interpretation of our formal results if we consider a mutant gene playing a game against another gene from a gamete pool in a diploid individual.

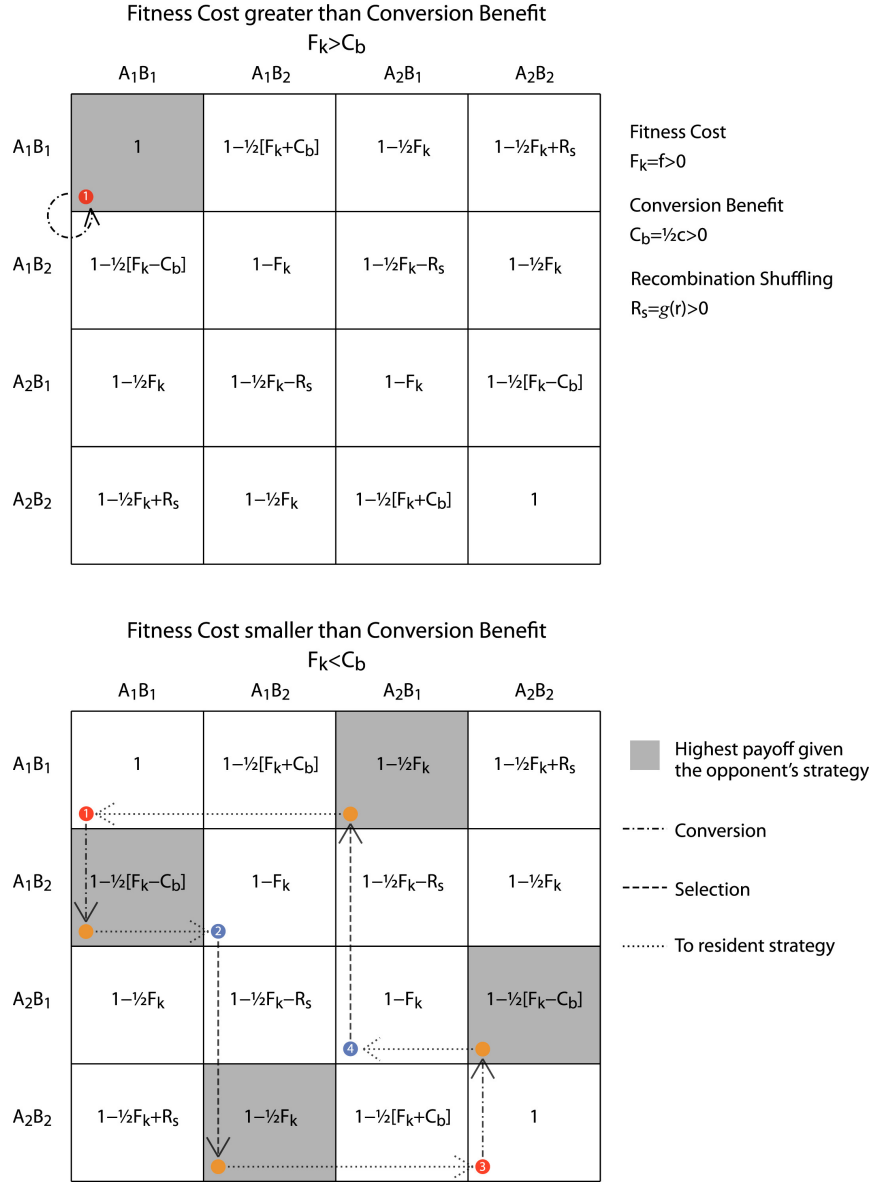


Figure 6: **Evolutionary game.** Payoff matrix of a game played by each haplotype against a haplotype pool. The payoff is determined by the possibility of a diploid genotype containing that haplotype experiencing a fitness cost (F_k) due to the absence of a double-strand break, a conversion benefit (C_b) - or conversion cost ($-C_b$) - due to the conversion of the opponent's haplotype into the player's haplotype or the conversion of the player's haplotype into the opponent's haplotype, and are shuffling benefit or cost due to the generation of the player's or the opponent's haplotype due to the formation of new combinations of alleles. In the first matrix we assume that the fitness cost is greater than the conversion benefit ($F_k > C_b$). Starting with a population fixed for haplotype A_1B_1 , A_1B_1 is the mutant strategy that gives the highest payoff (in gray in the matrix). No mutant haplotype can invade and A_1B_1 is the only evolutionarily stable strategy. In the second matrix we assume that the fitness cost is smaller than the conversion benefit ($F_k < C_b$). Starting with a population fixed for haplotype A_1B_1 , A_1B_2 is the mutant strategy that gives the highest payoff (in gray in the matrix) and should take over the population. When A_1B_2 has become the resident strategy, A_2B_2 is the mutant strategy that gives the highest payoff (in gray in the matrix) and should take over the population. Using the same logic it becomes obvious that in this second game there is no pure evolutionarily stable strategy but a continuous cycling of strategies.

A mutant gene can play four strategies (A_1B_1 , A_1B_2 , A_2B_1 , A_2B_2) and the gamete pool can be formed by the same four strategies. The payoff of each interaction is summarized in the payoff matrix provided in Figure 4 and is determined by the individual fitness cost of not experiencing a DSB ($F_k = f > 0$), the allelic conversion benefit (or cost) of not experiencing (or experiencing) a DSB ($C_b = \frac{1}{2}c > 0$), and a recombination shuffling factor that determines which alleles benefit from conversion in double heterozygotes ($R_s = f(r) > 0$). Let's start by considering a population almost fixed for a recombination enabling haplotype A_1B_1 . If fitness cost is greater than conversion benefit ($F_k > C_b$), our resident population of A_1B_1 cannot be invaded by any alternative strategy ($1 > 1 - \frac{1}{2}F_k + \frac{1}{2}C_b$; Figure 4.a). Therefore strong selection favors highly active permanent recombination hotspots (Figure 3.a). If fitness cost is lower than conversion benefit ($F_k < C_b$; Figure 4.b), our resident population of A_1B_1 can be invaded by the rare mutant A_1B_2 ($1 - \frac{1}{2}F_k + \frac{1}{2}C_b > 1 - \frac{1}{2}F_k + R_s > 1$ when $C_b > 2R_s$; Figure 4.b) as it gains a transmission advantage that more than compensates for its fitness cost; once A_1B_2 becomes the resident haplotype, it can be invaded by rare mutant A_2B_2 ($1 - \frac{1}{2}F_k > 1 - F_k$; Figure 4.b) as it gains a fitness benefit and does not suffer a transmission disadvantage, once A_2B_2 becomes the resident it can be invaded by rare mutant A_2B_1 ($1 - \frac{1}{2}F_k + \frac{1}{2}C_b > 1$; Figure 4.b), and once A_2B_1 becomes the resident it can be invaded by rare mutant A_1B_1 ($1 - \frac{1}{2}F_k > 1 - F_k$; Figure 4.b) thus completing a recurrent cycle. Therefore weak selection and abundance of only one haplotype, can favor recombination hotspots that alternate between low and high activity; dying and resurrecting in a permanent cycle (Figure 3.c). When all haplotypes are frequent in the initial population, the abundance of double heterozygotes results in the shuffling of the transmission advantage between different haplotypes. Depending on intensity of the shuffling either the previous cycle is maintained or the best strategy becomes to play a fixed proportion of each strategy. Therefore weak selection and abundance of all haplotypes, can favor recombination hotspots that exhibit moderate activity and do not die (Figure 3.b), forming an intuitive (non-rigorous) interpretation of our rigorous analysis.

These findings provide an alternative solution to the recombination hotspots paradox (Boulton et al., 1997). In the prevailing explanation (the Red Queen theory), individual recombination hotspots die and are saved from extinction in the genome by the birth of new recombination hotspots at new target sites in the genome (Myers et al., 2010; Baudat et al., 2010). Strong viability selection favors mutant PRDM9 alleles that bind new target sites (Úbeda and Wilkins, 2011; Latrille et al., 2017). In our model, viability selection does not prevent the death of individual recombination hotspots but saves them from extinction in the

genome by driving their resurrection in homozygous targets where the effect of conversion is negligible (Figure 3, 4). Selection favors mutant PRDM9 alleles that bind the alternative target allele within the same target site. Both theories succeed in explaining the life history of recombination hotspots characterized by: i. the death of individual recombination hotspots not leading to their extinction in the genome (notice however that in principle the Red Queen theory would require an infinite number of targets to prevent the extinction); ii. rapid change of the recombinational landscape; iii. rapid evolution of PRDM9. In our model however, this life history is explained by the bottom range of viability selection parameters (which seems more plausible from an empirical perspective) while the Red Queen theory requires the upper range (Úbeda and Wilkins, 2011; Latrille et al., 2017). A more rigorous analysis of the Red Queen model may expand the range of values where it applies though. Furthermore, our model makes novel predictions that the Red Queen (at least in its present formulation) does not; in particular, our model predicts that: i. the molecular signature near some recombination hotspots should be one of multiple recurrent events of high crossover activity evolutionary time as opposed to a single event of high crossover activity; ii. viability selection can maintain polymorphisms in PRDM9 (see Latrille et al. (2017) to put into context the uniqueness of this finding); iii. the same genetic architecture under the same selection regime can result in two different families of recombination hotspots, one family with alternation of high and low activity and another family with constant intermediate activity.

For the purpose of characterizing the interplay between selection and conversion on the evolution of recombination hotspots, our model makes a series of simplifying assumptions provided in the Methods section. Many of these assumptions are standard in population genetics models and relaxing all of them is beyond the scope of this research. However, relaxing some of them will help us to better understand the empirical relevance of our model. In particular, we relax three types of assumptions, specifically those relating to:

- i Selection and cross-over;
 - ii Number of alleles and target loci;
 - iii Population size.
-
- i Selection and cross-over: in our research, we focus on the case where viability selection is caused by a DSB and crossover between PRDM9-like and target loci requires a DSB in the latter. In the Methods section however, we show that all results we present hold when assuming that viability selection is caused by crossover events and when crossover between PRDM9-like and target loci does not require a DSB in the latter. This change in assumptions changes the exact value of the polymorphic equilibrium, and the range of

initial conditions that lead to the heteroclinic cycle (its basin of attraction), but not the qualitative results. The case that we discuss in the main text is the one where the basin of attraction of the heteroclinic cycle is smallest and thus least favorable to the arguments we develop.

- ii Number of alleles and target loci: in the main text, we modelled the cases of two locus two alleles as the minimal expression of the biological process we were interested in researching. In humans there are multiple alleles segregating at PRDM9 and multiple alleles at each of many target sites. Here we carried out some numerical analysis of a two locus (1 target) three alleles model to gain insight on how multiple alleles at a PRDM9-like and target loci would affect our conclusions from the main text. The typical dynamics are summarized in Figure 5, (bottom left). In this figure it can be observed that the cycling remains with a rapid alternation of hotspots and coldspots. The most striking difference with its two locus two alleles counterpart is that the fluctuations are no longer regular; the expected lifetime and temperature of the hotspot cannot be predicted in general. This is consistent with intuition as in this extended model it is not one but multiple alleles that can be favored by selection and conversion in each oscillation taking the dynamics in different trajectories, albeit always fluctuating, trajectories. In addition, we carried out some numerical analysis of the corresponding three locus (2 targets) two alleles models to gain insight on how multiple target loci would affect our conclusions from the main text. The typical dynamics are summarized in Figure 5 (top right). In this figure it can be observed that - once again - the cycling remains with a rapid alternation of hotspots and coldspots. The most interesting feature is that each of the two targets can fluctuate concordantly, or independently. In this extended model, alleles of PRDM9 that match the allele at one of the targets but not the other are also favored by natural selection. The introduction of three alleles in this three locus model brings about a combination irregular fluctuations within and between target locus (Figure 5, bottom right).
- iii Population size: we modelled the cases of an infinite population without recurrent mutation, to better characterize the interaction between selection and conversion. In nature however, the population is finite and mutations are introduced recurrently. Therefore, we carried out some numerical analysis of a model for a finite population with recurrent mutations at the modifier and target locus to gain insight on the effect of these two variables in our conclusions from the main text. The typical dynamics are summarized in Figure 4. In this figure it can be observed that the cycling remains with an alternation of hotspots and coldspots. In particular, when viability selection is weak ($f < \frac{1}{2}c$) and initially

one of the haplotypes is much more frequent than all the others, the frequency of the haplotypes fluctuates around the heteroclinic cycle ($\mathbf{x}^{*1} \rightarrow \mathbf{x}^{*2} \rightarrow \mathbf{x}^{*4} \rightarrow \mathbf{x}^{*3} \rightarrow \mathbf{x}^{*1}$) (Figure 6.b). This is intuitively consistent; selection and conversion favour the oscillation of haplotypic frequencies towards the heteroclinic cycle and genetic drift pushes some of them to extinction (Figure 6.b). Due to extinction, hotspots and coldspots alternate but how fast they alternate is determined by the mutation rates. To conclude, extinction slows down the oscillatory dynamics but does not put an end to the oscillations, recurrent mutations re-introduce the missing variability and the system is again in the initial conditions that favour the heteroclinic cycle (Figure 6.b). When viability selection is weak ($f < \frac{1}{2}c$) and initially all the haplotypes are abundant, the frequency of the haplotypes fluctuates around the polymorphic equilibrium (x^{*5}) (Figure 6.a). This is again consistent with ones intuition; selection and conversion favour the oscillation of haplotypic frequencies towards the internal equilibrium but genetic drift prevents them from settling (Figure 6.a). Because these oscillations remain close to the internal equilibrium the extinction of haplotypes is rarely observed (Figure 6.a). In the absence of extinction, hotspots and coldspots alternate rapidly. Genetic drift allows transition from oscillations around the heteroclinic cycle to oscillations around the equilibrium and back.

The insight gained from relaxing some of our assumptions in the main text suggests that in a finite population with multiple alleles and target locus and recurrent mutations we expect that our main results hold. Individual hotspots will die but they will resurrect later in evolutionary time thus precluding their extinction from the genome in the long term. It also suggests that these results apply to different details of the molecular architecture considered. In general, these results suggest that the solution to the recombination hotspot theory we propose here does extend to realistic conditions.

References

- Alves, I., Houle, A.A., Hussin, J.G., Awadalla, P., 2017. The impact of recombination on human mutation load and disease. *Phil. Trans. R. Soc. B* 372, 20160465.
- Baker, B.S., Carpenter, A.T., Esposito, M.S., Esposito, R.E., Sandler, L., 1976. The genetic control of meiosis. *Annual review of genetics* 10, 53–134.
- Baudat, F., Buard, J., Grey, C., Fledel-Alon, A., Ober, C., Przeworski, M., Coop, G.,

- De Massy, B., 2010. Prdm9 is a major determinant of meiotic recombination hotspots in humans and mice. *Science* 327, 836–840.
- Baudat, F., Imai, Y., De Massy, B., 2013. Meiotic recombination in mammals: localization and regulation. *Nature Reviews Genetics* 14, 794.
- Boulton, A., Myers, R.S., Redfield, R.J., 1997. The hotspot conversion paradox and the evolution of meiotic recombination. *Proceedings of the National Academy of Sciences* 94, 8058–8063.
- Brick, K., Smagulova, F., Khil, P., Camerini-Otero, R.D., Petukhova, G.V., 2012. Genetic recombination is directed away from functional genomic elements in mice. *Nature* 485, 642.
- Bürger, R., 2000. The mathematical theory of selection, recombination, and mutation. John Wiley & Sons.
- Calabrese, P., 2007. A population genetics model with recombination hotspots that are heterogeneous across the population. *Proceedings of the National Academy of Sciences* 104, 4748–4752.
- Coop, G., Myers, S.R., 2007. Live hot, die young: transmission distortion in recombination hotspots. *PLoS genetics* 3, e35.
- Coop, G., Wen, X., Ober, C., Pritchard, J.K., Przeworski, M., 2008. High-resolution mapping of crossovers reveals extensive variation in fine-scale recombination patterns among humans. *science* 319, 1395–1398.
- Haig, D., Grafen, A., 1991. Genetic scrambling as a defence against meiotic drive. *Journal of theoretical Biology* 153, 531–558.
- Hassold, T., Hunt, P., 2001. To err (meiotically) is human: the genesis of human aneuploidy. *Nature Reviews Genetics* 2, 280.
- Hassold, T., Sherman, S., Hunt, P., 2000. Counting cross-overs: characterizing meiotic recombination in mammals. *Human Molecular Genetics* 9, 2409–2419.
- Hey, J., 2004. What's so hot about recombination hotspots? *PLoS biology* 2, e190.
- Karlin, S., Feldman, M.W., et al., 1970. Linkage and selection: two locus symmetric viability model. *Theoretical population biology* 1, 39–71.

- Koehler, K.E., Hawley, R.S., Sherman, S., Hassold, T., 1996. Recombination and nondisjunction in humans and flies. *Human molecular genetics* 5, 1495–1504.
- Latrille, T., Duret, L., Lartillot, N., 2017. The red queen model of recombination hot-spot evolution: a theoretical investigation. *Phil. Trans. R. Soc. B* 372, 20160463.
- Lesecque, Y., Glémin, S., Lartillot, N., Mouchiroud, D., Duret, L., 2014. The red queen model of recombination hotspots evolution in the light of archaic and modern human genomes. *PLoS genetics* 10, e1004790.
- Lichten, M., Goldman, A.S., 1995. Meiotic recombination hotspots. *Annual review of genetics* 29, 423–444.
- Louis, E.J., Borts, R.H., 2003. Meiotic recombination: too much of a good thing? *Current Biology* 13, R953–R955.
- Myers, S., Bottolo, L., Freeman, C., McVean, G., Donnelly, P., 2005. A fine-scale map of recombination rates and hotspots across the human genome. *Science* 310, 321–324.
- Myers, S., Bowden, R., Tumian, A., Bontrop, R.E., Freeman, C., MacFie, T.S., McVean, G., Donnelly, P., 2010. Drive against hotspot motifs in primates implicates the *prdm9* gene in meiotic recombination. *Science* 327, 876–879.
- Paigen, K., Petkov, P., 2010. Mammalian recombination hot spots: properties, control and evolution. *Nature Reviews Genetics* 11, 221.
- Peters, A., 2008. A combination of cis and trans control can solve the hotspot conversion paradox. *Genetics* .
- Petes, T.D., 2001. Meiotic recombination hot spots and cold spots. *Nature Reviews Genetics* 2, 360.
- Pineda-Krch, M., Redfield, R., 2005. Persistence and loss of meiotic recombination hotspots. *Genetics* .
- Ptak, S.E., Hinds, D.A., Koehler, K., Nickel, B., Patil, N., Ballinger, D.G., Przeworski, M., Frazer, K.A., Pääbo, S., 2005. Fine-scale recombination patterns differ between chimpanzees and humans. *Nature genetics* 37, 429.
- Ptak, S.E., Roeder, A.D., Stephens, M., Gilad, Y., Pääbo, S., Przeworski, M., 2004. Absence of the *tap2* human recombination hotspot in chimpanzees. *PLoS biology* 2, e155.

- Rosenberg, N.A., Huang, L., Jewett, E.M., Szpiech, Z.A., Jankovic, I., Boehnke, M., 2010. Genome-wide association studies in diverse populations. *Nature Reviews Genetics* 11, 356.
- Ségurel, L., Leffler, E.M., Przeworski, M., 2011. The case of the fickle fingers: how the *prdm9* zinc finger protein specifies meiotic recombination hotspots in humans. *PLoS biology* 9, e1001211.
- Stevison, L.S., Woerner, A.E., Kidd, J.M., Kelley, J.L., Veeramah, K.R., McManus, K.F., Project, G.A.G., Bustamante, C.D., Hammer, M.F., Wall, J.D., 2015. The time scale of recombination rate evolution in great apes. *Molecular biology and evolution* 33, 928–945.
- Sun, H., Treco, D., Szostak, J.W., 1991. Extensive 3'-overhanging, single-stranded dna associated with the meiosis-specific double-strand breaks at the *arg4* recombination initiation site. *Cell* 64, 1155–1161.
- Szostak, J.W., Orr-Weaver, T.L., Rothstein, R.J., Stahl, F.W., 1983. The double-strand-break repair model for recombination. *Cell* 33, 25–35.
- Úbeda, F., Wilkins, J., 2011. The red queen theory of recombination hotspots. *Journal of evolutionary biology* 24, 541–553.
- Winckler, W., Myers, S.R., Richter, D.J., Onofrio, R.C., McDonald, G.J., Bontrop, R.E., McVean, G.A., Gabriel, S.B., Reich, D., Donnelly, P., et al., 2005. Comparison of fine-scale recombination rates in humans and chimpanzees. *Science* 308, 107–111.
- Wright, S., 1969. *Evolution and the genetics of populations: Vol. 2. The theory of gene frequencies.*
- Yahara, K., Fukuyo, M., Sasaki, A., Kobayashi, I., 2009. Evolutionary maintenance of selfish homing endonuclease genes in the absence of horizontal transfer. *Proceedings of The National Academy of Sciences* , pnas-0908404106.

Chapter 4

Stable yet distinct linkage disequilibria between sexes due to sexually-antagonistic recombination hotspot evolution

Author contributions

Myself and Francisco Úbeda formulated the model. I analysed the model including the numerical analysis. I wrote the paper.

Contents

4.1	Introduction	85
4.2	Methods	87
4.2.1	Two-locus n-alleles model	87
4.2.2	Cases of biological interest	88
4.2.3	Two-locus two-alleles model	90
4.2.4	Simplified model with sex-antagonistic viability	92
4.3	Results	93
4.3.1	Equilibria	93
4.3.2	Stability	98
4.4	Discussion	102

Stable sex-specific polymorphic equilibrium due to sexually antagonistic recombination hotspot evolution

Timothy W. Russell^{a,*}, Francisco Úbeda^a

^a*School of Biological Sciences, Royal Holloway University of London, Egham, Surrey, TW20 0EX, UK*

Abstract

Recent advances in molecular biology have shed light on the genetic control of recombination. Specifically, a gene (*PRDM9*) the protein it codes for (PRDM9) and its target site has been strongly associated with the initiation of recombination via double-strand breaks (DSBs). Some of the regions nearby these target sites have been identified as having much higher than average rates of recombination and have since been coined as *recombination hotspots*. Furthermore, the intensity of such hotspots differs between haplotypes of opposite sexes in many mammalian species. Given these recent empirical advances, we extend an existing model of the evolution of recombination hotspots modelling how haplotype frequencies change over generations. The novel aspect of the original model was the inclusion of the action of PRDM9 on the initiation of recombination. Here, we extend this model to allow two distinct sexes, aiming to shed light on differences between the sexes recent empirical observations have found. We carry out an extensive analytic and numerical analysis of the extended model, finding explicit stability conditions for the edge equilibria. Plus, we are able to find, using approximation techniques, a closed-form solution for the polymorphic (interior) equilibrium. We then assess the stability of the interior equilibrium numerically, finding extensive ranges of the biological parameters which admit stability for the polymorphic equilibrium, which has differing values for the male and female haplotype frequencies. Our model extension, which allows for sexual antagonism, includes a stable, yet distinct, polymorphic equilibrium. This implies that sexual antagonism may be the root cause for the observed sex differences in some of the attributes of recombination hotspot evolution.

*Corresponding author

Email address: Timothy.Russell.2015@rhul.ac.uk (Timothy W. Russell)

1. Introduction

Understanding meiotic recombination is vital to a vast number of fields of biology across a range of length scales. The specific control and action of recombination within the genome is of primary concern to molecular biologists (Myers et al., 2010); the maintenance of a recombination rate above a certain threshold within an organism is significant for the health of an individual, ensuring correct segregation of homologs (Brick et al., 2012; Alves et al., 2017); lastly, on a population scale, the ability of recombination to affect the relative gene frequencies has fascinated applied and theoretical population geneticists for decades (Barton, 1995; Otto and Michalakis, 1998). Great progress has been made understanding aspects of recombination — and therefore crossover events — across all of the aforementioned scales. Yet, there remain open questions about the evolutionary role of recombination. Some examples of such questions include: how does the molecular mechanisms which are known to be associated with the initiation of recombination persist over evolutionary time? And, why do the locations of recombination within a species genome — and for that matter, many other aspects of crossover events — differ so greatly between sexes of many mammals?

Meiotic recombination occurs at highly non-uniform rates across many genomes of many species (Lichten and Goldman, 1995; Petes, 2001). In fact, the rate of recombination has such peaks and troughs at different locations in mammalian genomes, it was necessary to coin a term for such peaks: *recombination hotspots* (Lichten and Goldman, 1995; Petes, 2001). Recombination hotspots have been discovered in humans, where it is known that the recombination rate can be up to a thousand times greater than the average (Myers et al., 2005, 2010; Paigen and Petkov, 2010) — where average is the mean of the rate is taken across the entire genome. The existence and control of such hotspots have provided many fascinating evolutionary research avenues. One such avenue is primarily concerned with the evolutionary maintenance of these hotspots. Coined by Boulton et al. (1997), the *recombination hotspot paradox* asks how recombination hotspots persist over evolutionary timescales, given that the gene initiating recombination has a high chance of recombining its own sequence away over short timescales? Many studies, both theoretical and applied, have provided plenty of insight into this question. Indeed, many believe the resolution of the paradox was the discovery of a gene known as *PRDM9* and continued molecular understanding of the action of its products, a protein known as PRDM9 (Myers et al., 2010; Baudat et al., 2010; Parvanov et al., 2010).

It is established that recombination is one of the repair pathways, repairing the DNA nearby a double-strand break (DSB) (Szostak et al., 1983). During the repair, the broken

strand of DNA is often involved in a crossover event (Lichten and Goldman, 1995; Petes, 2001). Alternatively, repairing the DNA using the homolog, some level of gene conversion can occur (Lichten and Goldman, 1995; Petes, 2001). It is the asymmetry between the results of crossover events and conversion events which led to the specifics of the recombination hotspot paradox (Boulton et al., 1997; Úbeda and Wilkins, 2011). Recent attempts to model this asymmetric interaction over evolutionary timescales include Úbeda and Wilkins (2011); Latrille et al. (2017); Úbeda et al. (2019). The first two provide plausible explanations reminiscent of the well-known Red Queen hypothesis of coevolution. Specifically, the connection to the Red Queen theory is made through the balance of the two opposing forces of gene conversion and viability selection. These studies modelled this process, showing that this balance of forces can produce stable evolutionary trajectories where hotspots, move around throughout the genome, but persist evolutionarily (Úbeda and Wilkins, 2011; Latrille et al., 2017). The final paper sought to develop a mechanistic model, rather than an IBM and in doing so found plausible solutions to the paradox which allowed for resurrection of hotspots, rather than constant birth and death. The dynamics of PRDM9 and its target sites in reality is almost certainly somewhere between the IBM models and the dynamical system model, where both birth and death and resurrection are possible. But these investigations, amongst others, certainly show that a balance between the two main forces of selection and conversion give rise to persistent cycling behaviour (Úbeda and Wilkins, 2011; Latrille et al., 2017; Russell et al., 2019).

Recent empirical advances of the molecular biology of PRDM9 and its target site, especially in mammalian genomes, have revealed differences between the sexes of the location and intensity of the recombination hotspots (de Boer et al., 2015; Halldorsson et al., 2016; Brick et al., 2018). Indeed, the last of these papers finds that most of the differences are produced at sex-biased hotspots (Brick et al., 2018), finding — contrary to previous findings — that most hotspots ($\sim 88 - 97\%$) can be found in both sexes (Brick et al., 2018). The high number of similar empirical findings of sex-specific attributes of recombination hotspots, in humans and other mammals, suggest that they are relatively evolutionarily stable.

We aim to address the seeming stability of these sex-specific attributes of recombination hotspots. To do so, we extend the model developed in (Úbeda et al., 2019) which mechanistically describes the aforementioned interplay between gene conversion and viability selection of PRDM9 and its target site(s). It does so by deriving a two-locus n -allele population genetic model including these forces, finding stable cycling behaviour between hotspot/target site combinations (Úbeda et al., 2019; Russell et al., 2019). The extension we derive here

includes separated systems, one for each sex — similar to that of the models in (Úbeda et al., 2010; Patten et al., 2010). Our model describes the frequencies of the genes at each loci are coupled together, similarly to the original model. However, as the extended model includes separate subsystems for each sex, it produces a dynamical system of twice the dimension of the original model (Úbeda et al., 2019). Using some simplifying parameter definitions, and the use of a coordinate transformation — from haplotypes frequencies, to allelic frequencies plus linkage disequilibria, we are able to analyse this system both analytically and numerically. Indeed, the use of symmetric (allelic) coordinates aids us in deriving an approximate closed-form expression for the unique polymorphic equilibrium. Furthermore, we find that the linkage disequilibria at this equilibrium differs between the sexes. A difference in linkage disequilibrium at a stable interior polymorphic equilibrium indicates that the mechanism modelled can indeed produce the observed differences in recombination hotspot attributes.

2. Methods

2.1. Two locus n-allele model

Following the framework from the original paper (Úbeda et al., 2019), we derive a Wright-Fisher model: the population is assumed to be infinite; the generations are non-overlapping and the individuals are assumed to be diploid. We track the changes of haplotypes between generations, where the (random) union of gametes occurs implicitly between the generations. More specifically, we follow how the frequencies of alleles at two loci change between generations. For the molecular biological details of the action of the protein produced at the first locus on its target site at the second locus, refer to Úbeda et al. (2019). It suffices to know that a protein produced by an allele at the first locus with a specific index, breaks a target site at the other locus if the allele at the target locus has the same index.

Let $x_{i,k}$ and $y_{i,k}$ be the frequency of haplotype $A_i B_k$ in eggs and sperm respectively. Random union of gametes results in an embryo with genotype $\frac{A_i A_j}{B_k B_l}$ (where the first haplotype has maternal origin and the second has paternal origin) with frequency $x_{i,k} y_{j,l}$. This embryo has a probability of reaching adulthood which is independent of its genotype. Its genotype, however, determines the outcome of meiosis in adult individuals during gametogenesis. In particular, the probability that, during meiosis, there is a DSB (due to either of the two allelic motifs, the maternally inherited M_k or the paternally inherited M_l) is

$$B_{i,j;k,l}^\xi = \frac{1}{2}(B_{i,j;k,\cdot}^\xi + B_{i,j;\cdot,l}^\xi) \quad (1)$$

in sex ξ where $B_{i,j;k,\cdot}^\xi = \frac{1}{2}b_{i,\cdot;k,\cdot}^\xi + b_{\cdot,j;k,\cdot}^\xi$ and $B_{i,j;\cdot,l}^\xi = \frac{1}{2}b_{i,\cdot;\cdot,l}^\xi + b_{\cdot,j;\cdot,l}^\xi$ are the probabilities that it is the maternally inherited motif M_k and the paternally inherited motif M_l the one that breaks respectively in sex ξ . N.B. For brevity we let $\xi \in \{\varphi, \sigma\}$ represent either sex, for parameters which are considered to be non sex-specific given a particular context. A DSB is followed by crossover between alleles at locus A and B with probability r^ξ , and conversion of the allelic motif that breaks into the allelic motif that does not break with probability c^ξ . Recombination is followed by Mendelian segregation of haplotypes into gametes that undergo fertility selection. The expected fitness of an individual $\frac{A_i, A_j}{B_k, B_l}$ of sex ξ is

$$F_{i,j;k,l}^\xi = B_{i,j;k}^\xi f_{b_1}^\xi + (1 - B_{i,j;k,l}^\xi) f_{b_2}^\xi. \quad (2)$$

For simplicity, we assume no parent-of-origin effects. Mathematically, this corresponds to: $b_{i,\cdot;k,\cdot}^\xi = b_{\cdot,j;k,\cdot}^\xi = b_{i,j;k}^\xi = b_{i,j;\cdot,l}^\xi = b_{i,j;k,l}^\xi$. Therefore, $B_{i,j;k,l}^\xi = B_{j,i;k,l}^\xi = B_{i,j;l,k}^\xi = B_{j,i;l,k}^\xi$.

The frequency of each haplotype in gametes in the next generation in eggs is:

$$x'_{i,k} = \frac{1}{\bar{w}^\varphi} \sum_{j,l}^n \left[\left(F_{i,j;k,l}^\varphi - f_{b_1}^\varphi \left(\frac{1}{4} c^\varphi B_{i,j;k}^\varphi + r^\varphi (1 - c^\varphi) B_{i,j;k,l}^\varphi \right) \right) \frac{1}{2} (x_{i,k} y_{j,l} + x_{j,l} y_{i,k}) \right. \\ \left. + f_{b_1}^\varphi \left(\frac{1}{4} c^\varphi B_{i,j;l}^\varphi + r^\varphi (1 - c^\varphi) B_{i,j;k,l}^\varphi \right) \frac{1}{2} (x_{i,l} y_{j,k} + x_{j,k} y_{i,l}) \right] \quad (3)$$

where $\bar{w}^\varphi = \frac{1}{2} \sum_{i,k} \sum_{j,l} F_{i,j;k,l}^\varphi (x_{i,k} y_{j,l} + x_{j,l} y_{i,k})$ is the expected fitness in females. The frequency of each haplotype in gametes in the next generation in sperm is:

$$y'_{i,k} = \frac{1}{\bar{w}^\sigma} \sum_{j,l}^n \left[\left(F_{i,j;k,l}^\sigma - f_{b_1}^\sigma \left(\frac{1}{4} c^\sigma B_{i,j;k}^\sigma + r^\sigma (1 - c^\sigma) B_{i,j;k,l}^\sigma \right) \right) \frac{1}{2} (x_{i,k} y_{j,l} + x_{j,l} y_{i,k}) \right. \\ \left. + f_{b_1}^\sigma \left(\frac{1}{4} c^\sigma B_{i,j;l}^\sigma + r^\sigma (1 - c^\sigma) B_{i,j;k,l}^\sigma \right) \frac{1}{2} (x_{i,l} y_{j,k} + x_{j,k} y_{i,l}) \right] \quad (4)$$

where $\bar{w}^\sigma = \frac{1}{2} \sum_{i,k} \sum_{j,l} F_{i,j;k,l}^\sigma (x_{i,k} y_{j,l} + x_{j,l} y_{i,k})$ is the expected fertility in males.

We henceforth assume no sex-specificity in crossover rate. Mathematically, this corresponds to the following relation on the parameters $r^\varphi = r^\sigma = r$.

2.2. Cases of biological interest

Henceforth, we present special cases of the model representing cases of distinct biological interest. Mathematically, each case of interest is given by a specific parameterisation. We consider no sex-antagonistic fertility and sex-antagonistic fertility benefits after a DSB occurs. From this point forwards we assume, for simplicity, no sex-specificity in the crossover

rate $r^{\ominus} = r^{\ominus} =: r$. However, we do consider sex-specific effects for the conversion rate $c^{\ominus} \neq c^{\ominus}$ in general. We include the resulting model only for the final subsection for sex-antagonistic fertility, as this is the focal model for the paper. The others are included to clarify how the parameterisations are formed from the biological assumptions. The first three cases are presented to show how correspondence between the biological assumption and its mathematical representation. It is the fourth case — that of sexually antagonistic viability selection — which is the linchpin of this paper.

2.2.1. No viability effects, no sex-antagonistic break

Here, there are no sex-specific effects and therefore the resulting model is the same as the version presented in the previous paper (Úbeda et al., 2019). To arrive at that model from within the framework of the sex-specific model, we define the parameters in the following way

$$\begin{aligned} f_b^{\ominus} &= f_b^{\ominus} = 1, \\ f_r^{\ominus} &= f_r^{\ominus} = 1 - f, \\ b^{\ominus} &= b^{\ominus} = b, \\ c^{\ominus} &= c^{\ominus} = c, \end{aligned} \tag{5}$$

recalling that the remaining parameter, the crossover rate r is considered to not have sex-specific effects throughout.

With this parameterisation, and not distinguishing between haplotypes within sperm and eggs, we arrive at the model from the previous paper.

2.2.2. No viability effects, sex-antagonistic break

There is a sex-antagonistic break when

$$b_{i,j}^{\ominus} = \begin{cases} b^{\ominus} & \text{if } i = j, \\ 0 & \text{if } i \neq j, \end{cases} \tag{6}$$

and

$$b_{i,j}^{\ominus} = \begin{cases} 0 & \text{if } i = j, \\ b^{\ominus} & \text{if } i \neq j. \end{cases} \tag{7}$$

This means matching alleles will be driven against in females but driven in favour of in males.

2.2.3. Sex-specific viability effects but not sexually antagonistic

Firstly, we define how the match and break dynamics work. For no sex-specific effects for DSB's, let

$$b_{i,j}^{\xi} = \begin{cases} b^{\xi} & \text{if } i = j, \\ 0 & \text{if } i \neq j. \end{cases} \quad (8)$$

I.e. matching alleles are driven against in females and males although the strength of the drive can differ between the sexes. Previously we studied the case where $b^{\varnothing} = b^{\sigma} =: b$. Similarly, viability selection is sex-specific but not antagonistic, meaning the strength of the effect can differ between the sexes but they are not necessarily driving against each other. Mathematically this corresponds to the following parameterisation

$$\begin{aligned} f_b^{\xi} &= 1 \\ f_r^{\xi} &= 1 - f^{\xi}. \end{aligned} \quad (9)$$

2.2.4. Sex-antagonistic viability

Here, we include sex-antagonistic viability selection, but simply sex-specific effects for the breakage and conversion terms. Mathematically, this corresponds to the following for the breakage rate

$$b_{i,j}^{\xi} = \begin{cases} b^{\xi} & \text{if } i = j, \\ 0 & \text{if } i \neq j, \end{cases} \quad (10)$$

and for the fertility benefit

$$\begin{aligned} f_b^{\varnothing} &= 1 & f_b^{\sigma} &= 1 - f^{\sigma}, \\ f_r^{\varnothing} &= 1 - f^{\varnothing} & f_r^{\sigma} &= 1. \end{aligned} \quad (11)$$

2.3. Two-locus two-alleles model

In this paper, we focus only on the case where we have two allelic variants possible at each locus.

The equations allowing for two allelic variants at each locus are unwieldy when fully expanded. Therefore, we omit the expanded equations in their original biological formulation and seek a simpler form. In a manner similar to the non sex-specific version of the model,

we define the following compound parameters

$$\begin{aligned}
 \alpha_1 &= b^{\varnothing}(f_b^{\varnothing} - f_r^{\varnothing}), & \alpha_2 &= b^{\sigma}(f_b^{\sigma} - f_r^{\sigma}), \\
 \beta_1 &= f_r^{\varnothing}, & \beta_2 &= f_r^{\sigma}, \\
 \gamma_1 &= \frac{1}{4}b^{\varnothing}c^{\varnothing}f_b^{\varnothing}, & \gamma_2 &= \frac{1}{4}b^{\sigma}c^{\sigma}f_b^{\sigma}, \\
 \delta_1 &= b^{\varnothing}(1 - c^{\varnothing})f_b^{\varnothing}, & \delta_2 &= b^{\sigma}(1 - c^{\sigma})f_b^{\sigma}.
 \end{aligned} \tag{12}$$

Using these definitions, the expanded system can be written as:

$$\begin{aligned}
 x'_1 &= \frac{1}{\bar{w}_1} \left[\alpha_1(x_1 + y_1 + 2x_1y_1) + 2\beta_1(x_1 + y_1) - 2\gamma_1(x_2y_1 + x_1y_2) - (\gamma_1 + \delta_1)D_t \right], \\
 x'_2 &= \frac{1}{\bar{w}_1} \left[\alpha_1(x_2 + y_2 - 2x_2y_2) + 2\beta_1(x_2 + y_2) + 2\gamma_1(x_2y_1 + x_1y_2) + (\gamma_1 + \delta_1)D_t \right], \\
 x'_3 &= \frac{1}{\bar{w}_1} \left[\alpha_1(x_3 + y_3 - 2x_3y_3) + 2\beta_1(x_3 + y_3) + 2\gamma_1(x_3y_4 + x_4y_3) + (\gamma_1 + \delta_1)D_t \right], \\
 x'_4 &= \frac{1}{\bar{w}_1} \left[\alpha_1(x_4 + y_4 + 2x_4y_4) + 2\beta_1(x_4 + y_4) - 2\gamma_1(x_3y_4 + x_4y_3) - (\gamma_1 + \delta_1)D_t \right], \\
 y'_1 &= \frac{1}{\bar{w}_2} \left[\alpha_2(x_1 + y_1 + 2x_1y_1) + 2\beta_2(x_1 + y_1) - 2\gamma_2(x_2y_1 + x_1y_2) - (\gamma_2 + \delta_2)D_t \right], \\
 y'_2 &= \frac{1}{\bar{w}_2} \left[\alpha_2(x_2 + y_2 - 2x_2y_2) + 2\beta_2(x_2 + y_2) + 2\gamma_2(x_2y_1 + x_1y_2) + (\gamma_2 + \delta_2)D_t \right], \\
 y'_3 &= \frac{1}{\bar{w}_2} \left[\alpha_2(x_3 + y_3 - 2x_3y_3) + 2\beta_2(x_3 + y_3) + 2\gamma_2(x_3y_4 + x_4y_3) + (\gamma_2 + \delta_2)D_t \right], \\
 y'_4 &= \frac{1}{\bar{w}_2} \left[\alpha_2(x_4 + y_4 + 2x_4y_4) + 2\beta_2(x_4 + y_4) - 2\gamma_2(x_3y_4 + x_4y_3) - (\gamma_2 + \delta_2)D_t \right],
 \end{aligned} \tag{13}$$

where use \bar{w}_1 and \bar{w}_2 to denote the population mean fitness of females and males respectively, x_i and y_i are the frequencies of haplotype i in females and males respectively. We move from double subscripts to single subscripts for both sexes in the following way: A_1B_1 becomes haplotype 1, A_1B_2 becomes haplotype 2, A_2B_1 becomes haplotype 3 and A_2B_2 becomes haplotype 4. Lastly, D_t is the linkage disequilibrium of the population.

Explicitly, the mean fitnesses are given by

$$\begin{aligned}
 \bar{w}_1 &= \alpha_1(x_1 + y_1 + 2x_1y_1 + x_2 + y_2 - 2x_2y_2 + x_3 + y_3 - 2x_3y_3 + x_4 + y_4 + 2x_4y_4) \\
 &\quad + 2\beta_1(x_1 + y_1 + x_2 + y_2 + x_3 + y_3 + x_4 + y_4), \\
 \bar{w}_2 &= \alpha_2(x_1 + y_1 + 2x_1y_1 + x_2 + y_2 - 2x_2y_2 + x_3 + y_3 - 2x_3y_3 + x_4 + y_4 + 2x_4y_4) \\
 &\quad + 2\beta_2(x_1 + y_1 + x_2 + y_2 + x_3 + y_3 + x_4 + y_4),
 \end{aligned} \tag{14}$$

and the total linkage disequilibrium of the population is

$$D_t = \frac{1}{2} \left(x_1 y_4 + x_4 y_1 - x_2 y_3 - x_3 y_2 \right). \quad (15)$$

2.4. Simplified model with sex-antagonistic fertility

The biological parameterisation for sex-antagonistic fertility given by (10) and (11) — along with the two for the crossover rate and the conversion rate discussed at the start of this section — produces the following set of compound parameters

$$\begin{aligned} \alpha_1 &= b^{\varnothing} f^{\varnothing}, & \alpha_2 &= -b^{\sigma} f^{\sigma}, \\ \beta_1 &= 1 - f^{\varnothing}, & \beta_2 &= 1, \\ \gamma_1 &= \frac{1}{4} b^{\varnothing} c^{\varnothing}, & \gamma_2 &= \frac{1}{4} b^{\sigma} c^{\sigma} (1 - f^{\sigma}), \\ \delta_1 &= b^{\varnothing} (1 - c^{\varnothing}) r, & \delta_2 &= b^{\sigma} (1 - c^{\sigma}) (1 - f^{\sigma}) r. \end{aligned} \quad (16)$$

With these compound parameters which now represent the system under the assumptions of sex-specific DSBs and sexually antagonistic fertility benefits, we arrive at the following system of equations

$$\begin{aligned} x'_1 &= \frac{1}{\bar{w}_1} \left[\alpha_1 (x_1 + y_1 + 2x_1 y_1) + 2\beta_1 (x_1 + y_1) - 2\gamma_1 (x_2 y_1 + x_1 y_2) - (\gamma_1 + \delta_1) D_t \right], \\ x'_2 &= \frac{1}{\bar{w}_1} \left[\alpha_1 (x_2 + y_2 - 2x_2 y_2) + 2\beta_1 (x_2 + y_2) + 2\gamma_1 (x_2 y_1 + x_1 y_2) + (\gamma_1 + \delta_1) D_t \right], \\ x'_3 &= \frac{1}{\bar{w}_1} \left[\alpha_1 (x_3 + y_3 - 2x_3 y_3) + 2\beta_1 (x_3 + y_3) + 2\gamma_1 (x_3 y_4 + x_4 y_3) + (\gamma_1 + \delta_1) D_t \right], \\ x'_4 &= \frac{1}{\bar{w}_1} \left[\alpha_1 (x_4 + y_4 + 2x_4 y_4) + 2\beta_1 (x_4 + y_4) - 2\gamma_1 (x_3 y_4 + x_4 y_3) - (\gamma_1 + \delta_1) D_t \right], \\ y'_1 &= \frac{1}{\bar{w}_2} \left[\alpha_2 (x_1 + y_1 + 2x_1 y_1) + 2(x_1 + y_1) - 2\gamma_2 (x_2 y_1 + x_1 y_2) - (\gamma_2 + \delta_2) D_t \right], \\ y'_2 &= \frac{1}{\bar{w}_2} \left[\alpha_2 (x_2 + y_2 - 2x_2 y_2) + 2(x_2 + y_2) + 2\gamma_2 (x_2 y_1 + x_1 y_2) + (\gamma_2 + \delta_2) D_t \right], \\ y'_3 &= \frac{1}{\bar{w}_2} \left[\alpha_2 (x_3 + y_3 - 2x_3 y_3) + 2(x_3 + y_3) + 2\gamma_2 (x_3 y_4 + x_4 y_3) + (\gamma_2 + \delta_2) D_t \right], \\ y'_4 &= \frac{1}{\bar{w}_2} \left[\alpha_2 (x_4 + y_4 + 2x_4 y_4) + 2(x_4 + y_4) - 2\gamma_2 (x_3 y_4 + x_4 y_3) - (\gamma_2 + \delta_2) D_t \right], \end{aligned} \quad (17)$$

where use \bar{w}_1 and \bar{w}_2 to denote the population mean fitness of females and males respectively and D_t is the linkage disequilibrium of the population. Explicitly, the two mean fitness

functions are given by

$$\begin{aligned}
 \bar{w}_1 &= \alpha_1(x_1 + y_1 + 2x_1y_1 + x_2 + y_2 - 2x_2y_2 + x_3 + y_3 - 2x_3y_3 + x_4 + y_4 + 2x_4y_4) \\
 &\quad + 2\beta_1(x_1 + y_1 + x_2 + y_2 + x_3 + y_3 + x_4 + y_4), \\
 \bar{w}_2 &= \alpha_2(x_1 + y_1 + 2x_1y_1 + x_2 + y_2 - 2x_2y_2 + x_3 + y_3 - 2x_3y_3 + x_4 + y_4 + 2x_4y_4) \\
 &\quad + 2\beta_2(x_1 + y_1 + x_2 + y_2 + x_3 + y_3 + x_4 + y_4).
 \end{aligned} \tag{18}$$

3. Results

We focus our results on the biologically interesting case of sex-antagonistic fertility (17). However, the simplifying parameterisation captures — relative to the full model — how restrictive this biological constraint is. Using this, it is easy to see how the results would easily generalise to the full model (13).

3.1. Equilibria

Attempting to directly solve the resulting system of polynomials after applying the equilibrium condition ($\mathbf{x}' = \mathbf{x}$ and $\mathbf{y}' = \mathbf{y}$) does not prove very successful as it is of high order. As we will see, even the much reduced system, constrained to the invariant lines the polymorphic equilibrium lies on is a nonlinear system of polynomials, which, when reduced to its fundamental dimension, is of order 4. As solutions to quartics are unwieldy to say the least, we use a combination of numerical and approximation techniques instead.

3.1.1. Edge equilibria

The edge equilibria, where one haplotype in both the female and male populations is at fixation, are easy to find both numerically and by inspection. The latter is clear after noticing, similarly to the replicator equations, the edges of the phase space are invariant for each population. It is easily verified that the following four points are equilibria with respect to (17)

$$\begin{aligned}
 \Phi_1 &= (1, 0, 0, 0, 1, 0, 0, 0), \\
 \Phi_2 &= (0, 1, 0, 0, 0, 1, 0, 0), \\
 \Phi_3 &= (0, 0, 1, 0, 0, 0, 1, 0), \\
 \Phi_4 &= (0, 0, 0, 1, 0, 0, 0, 1),
 \end{aligned} \tag{19}$$

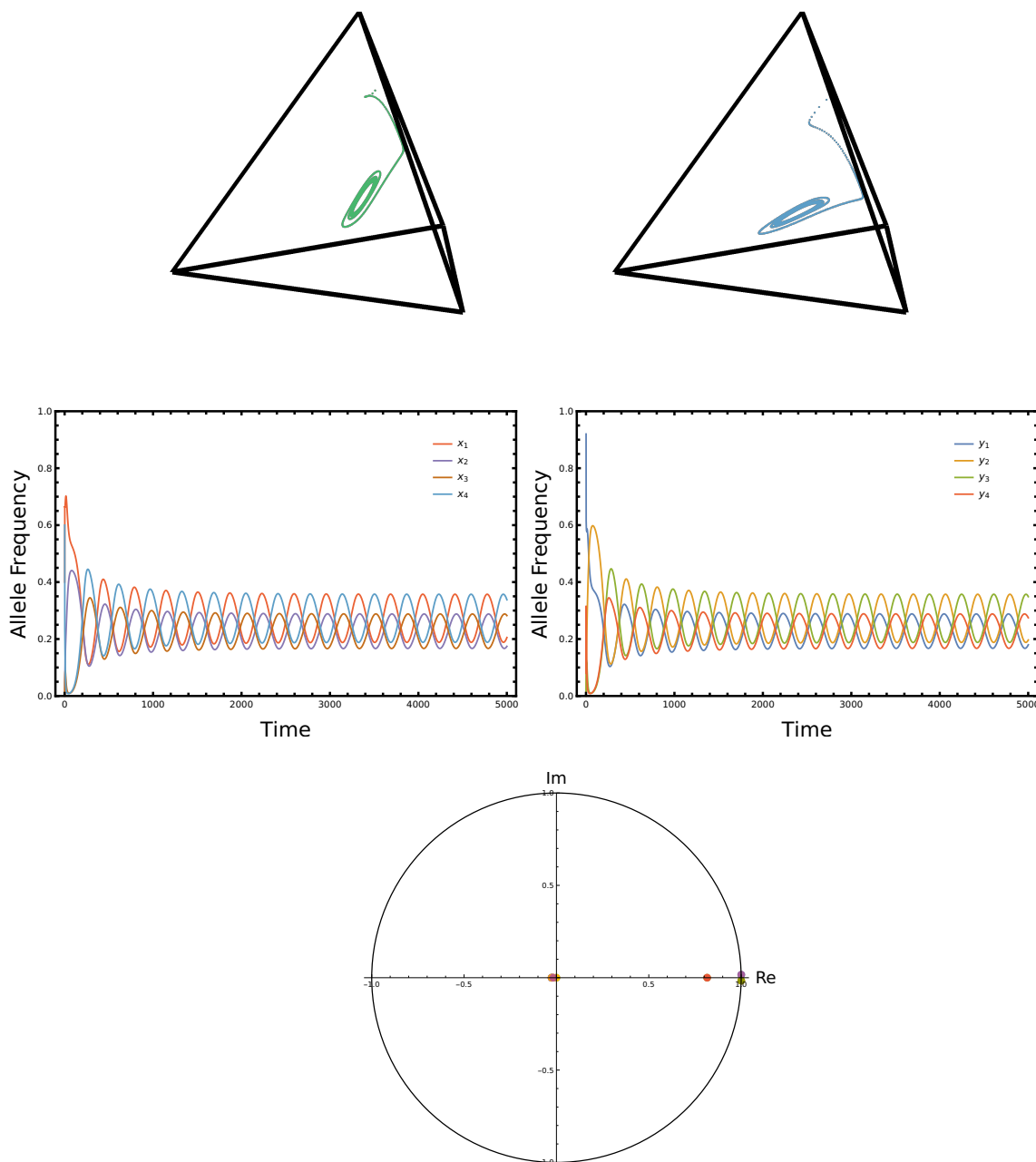


Figure 1: **The dynamics of the system: an attracting limit cycle.** We plot a trajectory of the system exhibiting cycling behaviour. The first row shows this trajectory in the tetrahedron — separately for each of the two sexes. The second row shows the same trajectory, but as time series. Lastly, in the third row, we plot the corresponding eigenvalues at the unique interior equilibrium. We find that there are two eigenvalues off the real axis implying the possibility of a Hopf bifurcation. The parameters used are: $f_b^{\varnothing} = 0.7$, $f_r^{\varnothing} = 0.08$, $b^{\varnothing} = 1$, $r^{\varnothing} = 0.5$, $c^{\varnothing} = 1$, $f_b^{\sigma} = 0.08$, $f_r^{\sigma} = 0.1$, $b^{\sigma} = 1$, $r^{\sigma} = 0.5$ and $c^{\sigma} = 1$. The initial conditions for the females were $x_1 = 0.4$, $x_2 = x_3 = 0$ and $x_4 = 0.6$. For the males $y_1 = 0.92$, $y_2 = y_3 = 0$ and $y_4 = 0.08$.

where we denote the i^{th} equilibria of the system (17) by

$$\Phi_i = (x_1^*, x_2^*, x_3^*, x_4^*, y_1^*, y_2^*, y_3^*, y_4^*). \quad (20)$$

3.1.2. Interior equilibria

Similarly to the non sex-specific hotspots model in [Úbeda et al. \(2019\)](#), the polymorphic equilibria lie on an invariant subspace within the phase space of the system. The invariant subspace, using haplotype coordinates, is described by

$$\begin{aligned} \xi_1 &= \xi_4, \\ \xi_2 &= \xi_3, \end{aligned} \quad (21)$$

where $\xi \in \{x, y\}$. It is relatively easy to show that the surface defined by these variable relations is invariant under the action of system (13). Let

$$\begin{aligned} x'_i &= g_i(\mathbf{x}, \mathbf{y}), \\ y'_i &= h_i(\mathbf{x}, \mathbf{y}), \end{aligned} \quad (22)$$

represent our system in compact notation. The system at equilibrium is therefore given by

$$\begin{aligned} x_i^* &= g_i(\mathbf{x}^*, \mathbf{y}^*), \\ y_i^* &= h_i(\mathbf{x}^*, \mathbf{y}^*), \end{aligned} \quad (23)$$

where superscript x^* and y^* represent the value of the haplotypes in eggs and sperm at equilibrium (respectively). Restricting the dynamics to this invariant surface reduces the number of polynomials which need to be solved to find the unique polymorphic (interior) equilibrium. To derive the resulting system of two second-order polynomials the equilibrium calculation reduces to, we establish that on this invariant surface, the variables can be re-written using the simplified versions of the conservation laws

$$\begin{aligned} x_1 + x_2 + x_3 + x_4 &= 1, \\ y_1 + y_2 + y_3 + y_4 &= 1, \end{aligned} \quad (24)$$

which, using the relations in (21) can be simplified to

$$\begin{aligned} x_1 + x_2 &= \frac{1}{2} \iff x_1 = \frac{1}{2} - x_2, \\ y_1 + y_2 &= \frac{1}{2} \iff y_1 = \frac{1}{2} - y_2. \end{aligned} \quad (25)$$

We are now able to constrain the dynamics to this two-dimensional subspace, on which the polymorphic equilibrium lives. Before we do so, we introduce a coordinate transformation which helps simplify the algebra and clarify the interpretation of the position of this invariant subspace.

Extending the haplotype frequency to allelic frequency coordinate transformation used in Russell et al. (2019) to allow for both female (A_x, B_x, D_x) and male (A_y, B_y, D_y) populations of haplotype gives the following forward transformation

$$\begin{aligned} A_x &= x_1 + x_2, & A_y &= y_1 + y_2, \\ B_x &= x_1 + x_3, & B_y &= y_1 + y_3, \\ D_x &= x_1 x_4 - x_2 x_3, & D_y &= y_1 y_4 - y_2 y_3. \end{aligned} \quad (26)$$

The transformed equations in their full form are given in the complementary Mathematica notebook (see the last section of the Introduction for instructions on how to find the notebook).

First of all we note that the original invariant surface on which the interior equilibrium is positioned becomes, under transformation (26)

$$\begin{aligned} A_x^* &= \frac{1}{2}, & A_y^* &= \frac{1}{2}, \\ B_x^* &= \frac{1}{2}, & B_y^* &= \frac{1}{2}. \end{aligned} \quad (27)$$

The expressions for D_x^* and D_y^* can be found implicitly by evaluating the D'_x and D'_y equations at the transformed equilibrium values given by (27). Explicitly, if we define the right-hand side of the D'_x and D'_y equations as

$$\begin{aligned} D'_x &= g_1(A_x, B_x, A_y, B_y, D_x, D_y), \\ D'_y &= g_2(A_x, B_x, A_y, B_y, D_x, D_y). \end{aligned} \quad (28)$$

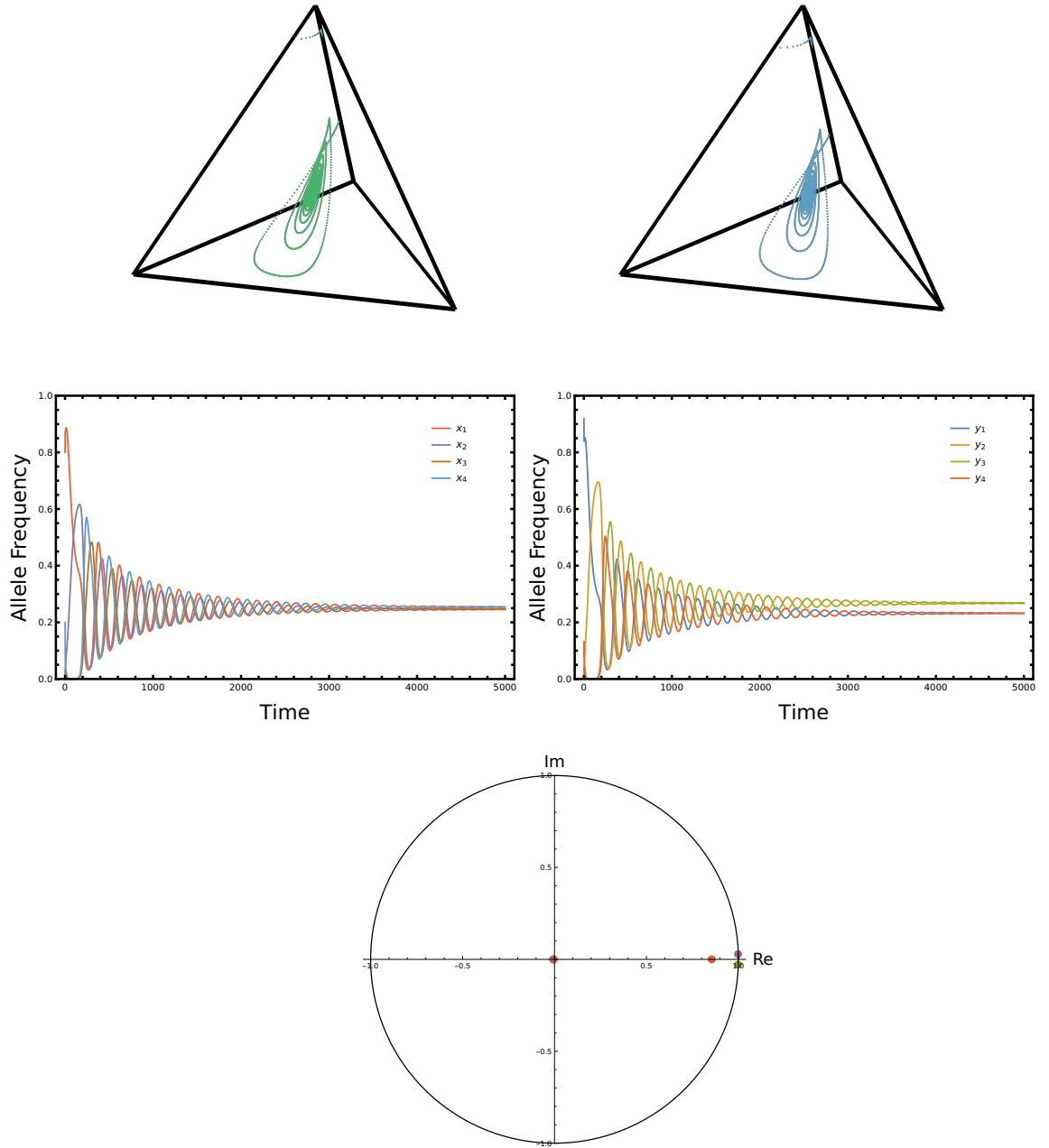


Figure 2: **The dynamics of the system: an attracting interior equilibrium.** The plot layout is similar to Figure 1. In this plot, the trajectory converges to the attracting interior equilibrium. All eigenvalues are within the unit circle in the complex plan. The parameters used are: $f_b^{\varnothing} = 0.25$, $f_r^{\varnothing} = 0.08$, $b^{\varnothing} = 0.8$, $c^{\varnothing} = 0.9$, $f_b^{\sigma} = 0.05$, $f_r^{\sigma} = 0.06$, $b^{\sigma} = 0.7$, $c^{\sigma} = 0.8$ and $r = 0.5$. The initial conditions for the females were $x_1 = 0.8$, $x_2 = x_3 = 0$ and $x_4 = 0.2$. For the males $y_1 = 0.92$, $y_2 = y_3 = 0$ and $y_4 = 0.08$.

Setting these equations to be at the polymorphic equilibrium (27) and evaluating them gives

$$\begin{aligned} D_x^* &= g_1(D_x^*, D_y^*)|_{A_x=\frac{1}{2}, B_x=\frac{1}{2}, A_y=\frac{1}{2}, B_y=\frac{1}{2}}, \\ D_y^* &= g_2(D_x^*, D_y^*)|_{A_x=\frac{1}{2}, B_x=\frac{1}{2}, A_y=\frac{1}{2}, B_y=\frac{1}{2}}. \end{aligned} \quad (29)$$

which, once g_1 and g_2 are expressed explicitly, these equations become

$$\begin{aligned} & -\alpha_1 D_x^2 + 2\gamma_1 D_x D_y + \frac{1}{2}\alpha_1(D_y - D_x) + \frac{1}{2}(\gamma_1 + \delta_1)(D_x + D_y) \\ & + D_x - D_y - \frac{1}{8}(\gamma_1 - \frac{1}{2}\alpha_1) = 0, \\ & -\alpha_2 D_y^2 + 2\gamma_2 D_x D_y + \frac{1}{2}\alpha_2(D_y - D_x) + \frac{1}{2}(\gamma_2 + \delta_2)(D_x + D_y) \\ & - D_x + D_y - \frac{1}{8}(\gamma_2 - \frac{1}{2}\alpha_2) = 0. \end{aligned} \quad (30)$$

This is a system of two second-order polynomials, which results in having to solve a quartic for each variable D_x and D_y . The solution can be found in Mathematica or a similar symbolic programming language. However, the solution includes thousands of terms and is far too unwieldy to state or work with. Therefore, to proceed, we use an approximation method. Namely, we Taylor expand around the point $(D_x, D_y) = (0, 0)$ which reduces the resulting order of each polynomial by one, we arrive at a system of far simpler polynomials to solve.

3.1.3. Approximating the interior equilibrium

The new coordinates representing linkage disequilibrium in female and male haplotypes respectively lie within the following region $(D_x, D_y) \in [-\frac{1}{4}, \frac{1}{4}]$ and solving the system representing the polymorphic equilibrium numerically reveals that most polymorphic equilibrium values are very close to the point $(D_x, D_y) = (0, 0)$. Therefore, we choose this point to Taylor expand around to arrive at an approximate but far more tractable system to solve for the polymorphic equilibrium. Taylor expanding around this point gives

$$\begin{aligned} & 2\gamma_1 D_x D_y + \frac{1}{2}\alpha_1(D_y - D_x) + \frac{1}{2}(\gamma_1 + \delta_1)(D_x + D_y) \\ & + D_x - D_y - \frac{1}{8}(\gamma_1 - \frac{1}{2}\alpha_1) = 0 \\ & 2\gamma_2 D_x D_y + \frac{1}{2}\alpha_2(D_y - D_x) + \frac{1}{2}(\gamma_2 + \delta_2)(D_x + D_y) \\ & - D_x + D_y - \frac{1}{8}(\gamma_2 - \frac{1}{2}\alpha_2) = 0. \end{aligned} \quad (31)$$

The system is identical to (30) except without the first term in each original equation, $-\alpha D_x^2$ and $-\alpha D_y^2$ respectively. As a result of the interval in which the variables D_x and D_y lie, these squared terms clearly contributed very little to the overall solution. They did, however,

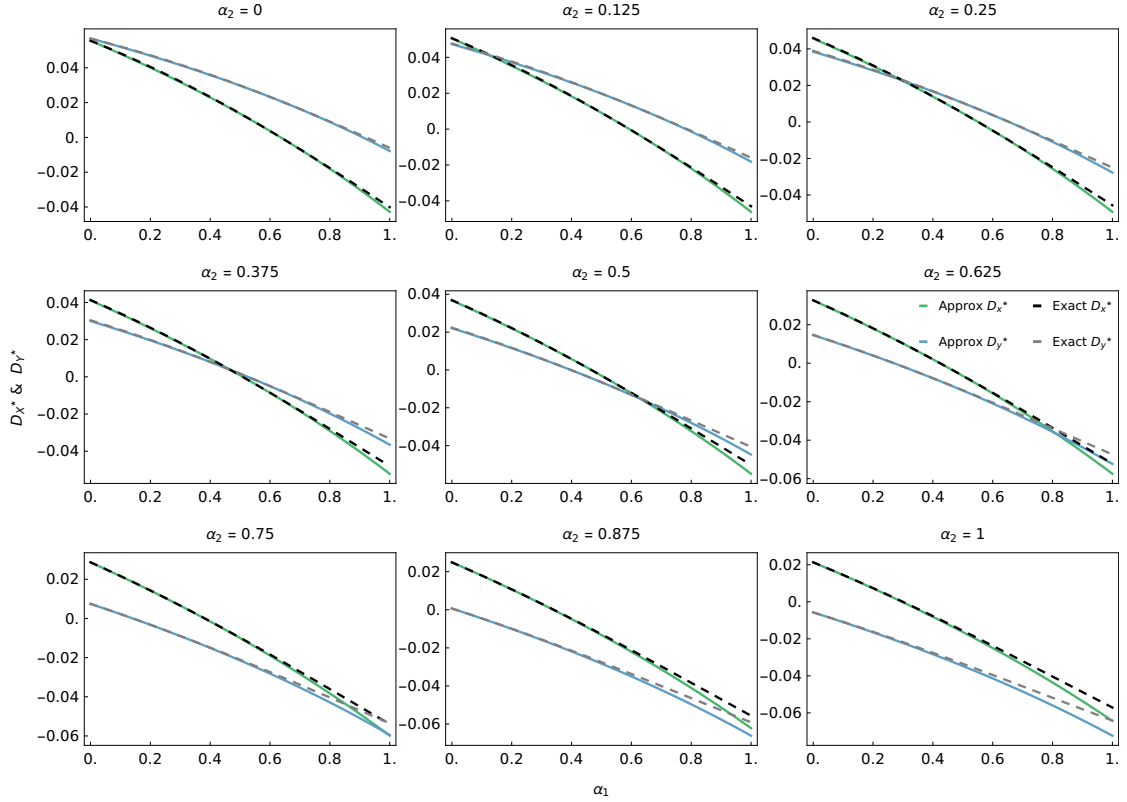


Figure 3: Numerically assessing the accuracy of the approximate polymorphic equilibrium. The closed-form expression for the approximate polymorphic equilibrium is plotted against α_1 for a range of biologically realistic values of α_2 along with numerical solutions to (30) — representing the exact value of the polymorphic equilibrium — in order to assess the accuracy of the approximation. Clearly, the two are in close agreement, apart from at the higher end for α_1 , where the influence of the second-order term (dropped in the approximate solution) proportional to α_1 or α_2 begins to have a greater affect. The other parameters were set to $\gamma_1 = 0.25$, $\gamma_2 = 0.2$, $\delta_1 = 0.3$ and $\delta_2 = 0.2$. Note that the values of d_ζ^* are not equivalent at the stable polymorphic equilibrium, for $\zeta \in (x, y)$. The intersection of the two solutions for d_ζ^* is the stable polymorphic equilibrium found in the non sex-specific model in [Úbeda et al. \(2019\)](#).

increase the algebraic complexity significantly. The solutions to the system without these terms (31) are still large, but are tractable. We give these solutions in full in the accompanying Mathematica notebook.

We numerically assess the accuracy of the equilibria across a range of the parameter's which influence its values the most, α_1 and α_2 . It is clear that, apart from in the extremely high regions of the parameter space, which are not particularly biologically realistic, the approximation is very accurate (see Figure 3).

3.2. Stability

Let $\mathbf{J}(\mathbf{z})$ denote the Jacobian of system (13) where $\mathbf{z} = (x_1, x_2, x_3, x_4, y_1, y_2, y_3, y_4)$. We determine the stability of the edge equilibria by directly evaluating \mathbf{J} at the first two Φ_1 and Φ_2 (19). We omit the multipliers of Φ_3 and Φ_4 as, similarly to the edge equilibria in [Úbeda et al. \(2019\)](#), they are equivalent to the multipliers of Φ_2 and Φ_1 respectively. Due to the complexity and dimension of the system, we study the eigenvalues of the polymorphic equilibrium numerically.

Recall, a fixed point in a discrete-time dynamical system is stable if and only if the modulus of all its multipliers — within the complex plane — lie inside, or on, the unit circle. If the modulus of its multipliers is identical to one, a higher-order analysis is required to determine stability.

Simulations suggest that, similarly to the analogous parameters in the non sex-specific model ([Úbeda et al., 2019](#)), the breakage rate parameters simply scale time (apart from when they are zero, at which most of the selection dynamics are prevented). With this in mind, for mathematical convenience, we assume throughout the rest of this section that $b^{\varphi} = b^{\sigma} = 1$. Plus, we switch between the original parameters and the simplified parameters, (10) and (11), at leisure, whichever is mathematically simpler for a given result.

3.2.1. Edge equilibria

The eigenvalues of the matrices $\mathbf{J}|_{\mathbf{z}=\Phi_1}$ and $\mathbf{J}|_{\mathbf{z}=\Phi_2}$ represent the multipliers of the fixed points Φ_1 and Φ_2 . Calculating these directly in Mathematica gives the following two sets of eigenvalues $\boldsymbol{\lambda}^1 = (0, 0, 0, 0, \lambda_6^1, \lambda_7^1, \lambda_8^1)$ and $\boldsymbol{\lambda}^2 = (0, 0, 0, 0, \lambda_6^2, \lambda_7^2, \lambda_8^2)$ where the non-trivial elements of $\boldsymbol{\lambda}^1$ are given by

$$\begin{aligned}\lambda_6^1 &= \frac{1}{4} \left(3 + \frac{1}{1 + \alpha_2} - \frac{\alpha_1}{\alpha_1 + \beta_1} \right), \\ \lambda_7^1 &= \frac{2\gamma_1(\alpha_2 + 1) + \alpha_1(2\alpha_2 + 2\gamma_2 + 3) + \beta_1(3\alpha_2 + 2\gamma_2 + 4)}{4(\alpha_2 + 1)(\alpha_1 + \beta_1)}, \\ \lambda_8^1 &= \frac{\alpha_1(2\alpha_2 - \gamma_2 - \delta_2 + 3) + \beta_1(3\alpha_2 - \gamma_2 - \delta_2 + 4) - (\alpha_2 + 1)(\gamma_1 + \delta_1)}{4(\alpha_2 + 1)(\alpha_1 + \beta_1)},\end{aligned}\tag{32}$$

and the non-trivial elements of λ^2 are given by

$$\begin{aligned}\lambda_6^2 &= 1 + \frac{1}{4}\alpha_2 + \frac{1}{4}\frac{\alpha_1}{\beta_1}, \\ \lambda_7^2 &= \frac{\alpha_1 - 2\gamma_1 + \beta_1(\alpha_2 - 2\gamma_2 + 4)}{4\beta_1}, \\ \lambda_8^2 &= \frac{\alpha_1 - \gamma_1 - \delta_1 + \beta_1(\alpha_2 - \gamma_2 - \delta_2 + 4)}{4\beta_1}.\end{aligned}\tag{33}$$

Moving back to the biological parameters, for mathematical convenience and to aid the interpretation the conditions, $\lambda_6^1 < 1$ is satisfied when

$$f^{\sigma} < \frac{f^{\varphi}}{1 + f^{\varphi}}.\tag{34}$$

Similarly, $\lambda_7^1 < 1$ is satisfied when

$$f^{\sigma} - \frac{1}{\frac{1}{2}c^{\varphi} + \frac{1}{2}c^{\sigma} - f^{\varphi} + 1} > 1.\tag{35}$$

Lastly, $\lambda_8^1 < 1$ is satisfied when

$$\frac{1}{f^{\varphi} + c^{\varphi}(\frac{1}{4} - r) + c^{\sigma}(\frac{1}{4} - r) + 2r + 1} + f^{\sigma} > 1.\tag{36}$$

Now, we present the conditions for stability for the second set of eigenvalues λ^2 . The first eigenvalue in this set, $\lambda_6^2 < 1$ is satisfied when the same condition as $\lambda_6^1 < 1$ is satisfied, given by condition (34). The second eigenvalue in this set is stable, i.e. $\lambda_7^2 < 1$ when

$$\frac{c^{\varphi} + c^{\sigma} + (c^{\sigma} - 2)(f^{\varphi} - 1)f^{\sigma}}{c^{\sigma} + 2} > f^{\varphi}.\tag{37}$$

Lastly, the stability condition for the third eigenvalue in this set, $\lambda_8^2 < 1$ is when

$$f^{\varphi} - \frac{\frac{1}{4}c^{\varphi} - f^{\varphi} - r - c^{\varphi}r}{\frac{1}{4}(1 - f^{\sigma}) + r(c^{\sigma} - 1)(f^{\sigma} - 1)} < 1\tag{38}$$

3.2.2. Polymorphic equilibrium

Even after using an approximation technique to derive a closed-form solution for the unique interior polymorphic equilibrium, its large functional form means an explicit stability anal-

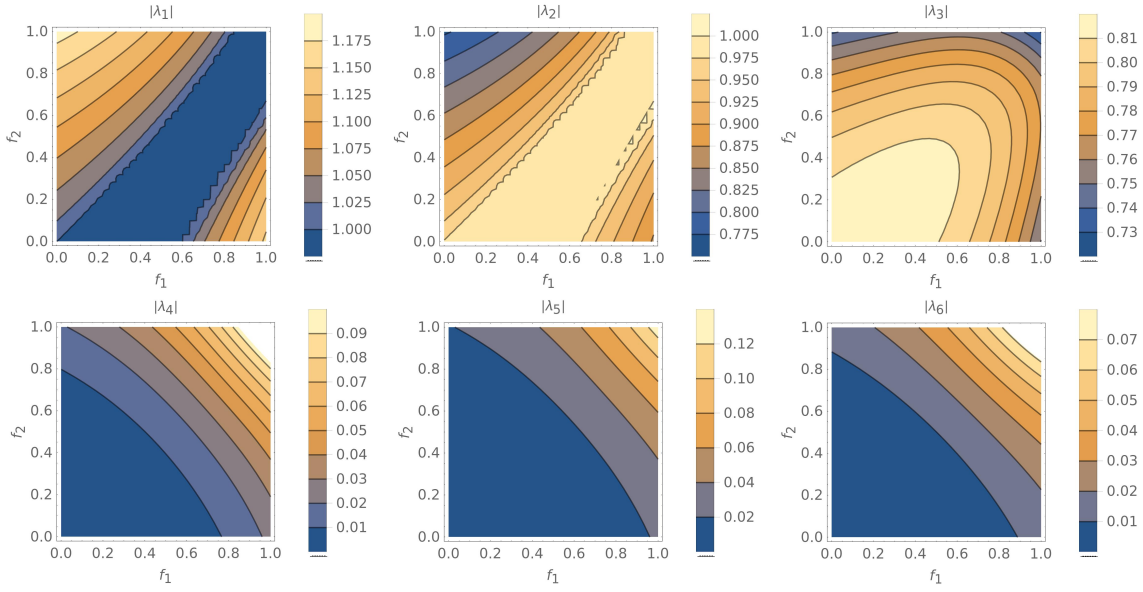


Figure 4: **Numerically assessing the stability of the unique polymorphic equilibrium.** We find the eigenvalues of the Jacobian matrix evaluated at the unique polymorphic equilibrium for a range of parameter values. The breakage parameters b and r are fixed (as described in the main text). However, f^\varnothing and f^σ are varied. The level sets of the modulus of each of the six (non-zero) eigenvalues are plotted against these two parameters, showing the interior equilibrium to be stable for almost the entire fitness parameter (f) range. The only eigenvalue whose modulus can be greater than one is the first. The others always attract the dynamics of the system (in the direction of the corresponding eigenvector). The conversion parameters were set to $c^\varnothing = 0.9$ and $c^\sigma = 0.5$. A total of 900 sets of eigenvalues were solved for and plotted in each subplot.

ysis is intractable. Therefore, we assess the stability of this equilibria numerically over a range of parameter values. Specifically, we find the value of the interior equilibrium for a given set of parameters; we then find the eigenvalues of the Jacobian at all of these equilibria; lastly, we plot them against the parameters being varied. We found that the parameters with the biggest influence on the qualitative dynamics — similarly to those which were most important for the non sex-specific models dynamics (Úbeda et al., 2019) — are f^\varnothing , f^σ , c^\varnothing and c^σ . Therefore, we fixed the remaining parameters: $b^\varnothing = b^\sigma = 1$ and $r = \frac{1}{2}$ and varied the others. We plot the level sets of the modulus of each of the six non-trivial eigenvalues — two out of the eight orthogonal directions of the linearised dynamics give eigenvalues identically equal to zero, due to the two conservation laws (24). Figure 4 shows these level sets plotted against the viability fitness parameters f^\varnothing and f^σ . The results show the interior equilibrium is attracting throughout most of the parameter space. The attached Mathematica notebook includes many more versions of the plot, over the whole range of biologically realistic parameter values.

4. Discussion

We present a model which is a direct extension of the model in [Úbeda et al. \(2019\)](#) that models the evolution of a specific gene *PRDM9*, the protein it produces, PRDM9, and its target site. The gene is involved in the initiation of recombination and has been strongly associated with locations in the genome where recombination occurs orders of magnitude higher than the chromosomal average: *recombination hotspots* ([Boulton et al., 1997](#); [Myers et al., 2005](#)). The original model found persistent cycling behaviour, caused by a balance of the following evolutionary forces: viability selection for matching protein and target site and gene conversion ([Úbeda et al., 2019](#)). However, there have been manifold recent discoveries describing sex-specific differences between location and intensity of hotspots in mammals ([de Boer et al., 2015](#); [Halldorsson et al., 2016](#); [Brick et al., 2018](#)). Motivated by these discoveries, we extend the original recombination hotspot evolution model to include sex-specificity.

To extend the model, we followed the modelling framework used in [Úbeda et al. \(2010\)](#). Specifically, we allow for one system of equations describing the evolution of *PRDM9* in female haplotypes and another system describing this evolution in male haplotypes (17). If two allelic variants are permitted at each locus, our extended model mathematically boils down to a system of eight coupled nonlinear difference equations. Given the already high level of complexity a nonlinear model of this dimension presents, we do not consider parent-of-origin effects in this paper. For these effects to be included, one would need different breakage functions, where a DSB would only be caused if both the protein and target came from the same parent. We conjecture that a model which included such effects would have complex dynamics, including novel heteroclinic cycles which did not necessarily move between the edge equilibria — as was the case for the heteroclinic cycle in the original paper ([Úbeda et al., 2019](#)).

We present the model which allows for n -alleles. However, due to the complexity of the model, we focus on the two-allele case. We also focus on the case where the viability selection effects are sex-antagonistic. Specifically, this means that a high level of viability selection for the haplotypes of one sex, carries precisely the inverse level of benefit (10) and (11), producing the effect of sexually-antagonistic viability ([Patten et al., 2010](#)).

To begin the analysis of the system, we first define new sets of compound parameters which allow for the system to be written in a much more mathematically concise form (13). The simplifying compound parameters chosen are analogous to those in [Úbeda et al. \(2019\)](#); [Russell et al. \(2019\)](#). We are then able to find all the edge equilibria. Furthermore, after

transforming to allelic with linkage disequilibrium coordinates, we find the system of two nonlinear polynomials whose solutions give the value of linkage disequilibrium at the interior equilibrium (30). We observe the system is equivalent to solving a quartic equation, meaning closed-form solutions exist, but are intractable. We therefore use an approximation method, where we Taylor expand around the point where the two solutions for the interior equilibrium — one for each sex — intersect (Figure 3). Truncating the Taylor expansion at one order lower than the original system reduces the complexity of the solution dramatically. Numerically, we show that the accuracy of the approximate solution is very high, especially close to the point of intersection.

We go on to show that the interior equilibrium is stable across most of the range of parameter space which is biologically relevant. We plot the modulus of the eigenvalues against the values of the most relevant parameters. We also attach a Mathematica notebook which can numerically compute the ranges of parameter values which allow for a stable polymorphic equilibrium. Only unrealistically high values of the viability selection parameters cause instability at the interior equilibrium. However, often a pair of eigenvalues at the interior equilibrium are complex, meaning that on approach toward the equilibrium, the trajectory exhibits damped oscillations. We used this to guide the search for a limit cycle. [Úbeda et al. \(2019\)](#) found that there was an unstable limit cycle acting as the separatrix between the interior equilibrium and the heteroclinic cycle. As we did not find an attracting heteroclinic cycle analogous to that found in the original model ([Úbeda et al., 2019](#)), we suspected there could now be a stable limit cycle in the interior. After searching numerically, we found trajectories that converged to a low amplitude limit cycle (Figure 1).

Our original question can be summarised as: if we extend the original model of recombination hotspot evolution ([Úbeda et al., 2019](#)) to allow for distinct sexes, will some sex-specific attributes of the hotspots — observed in abundance in the literature — be displayed by the model? The stable polymorphic equilibrium identified in the model with sexually antagonistic viability selection suggests that sexual antagonism at loci involved in the genetic control of recombination can produce evolutionary persistent behaviours. Furthermore, we found some sex-specific attributes of recombination hotspot evolution: both the polymorphic equilibrium and the stable limit cycle — a novel behaviour relative to the non sex-specific implementation of the model ([Úbeda et al., 2019](#)) — involve haplotype frequencies that differ (sometimes slightly, sometimes by a great deal) between the sexes.

Lastly, we hope the model presented in this paper can serve as a framework for other population genetic models for which sex-specific differences are being discovered. Even

though the process modelled here is particular to the evolution of *PRDM9* and recombination hotspots, the way in which the model was extended to allow for two distinct sexes is generic and can be used to extend most non sex-specific theoretical population genetic models.

References

- Alves, I., Houle, A.A., Hussin, J.G., Awadalla, P., 2017. The impact of recombination on human mutation load and disease. *Philosophical Transactions of the Royal Society B: Biological Sciences* 372, 20160465.
- Barton, N., 1995. A general model for the evolution of recombination. *Genetics Research* 65, 123–144.
- Baudat, F., Buard, J., Grey, C., Fledel-Alon, A., Ober, C., Przeworski, M., Coop, G., De Massy, B., 2010. *Prdm9* is a major determinant of meiotic recombination hotspots in humans and mice. *Science* 327, 836–840.
- de Boer, E., Jasin, M., Keeney, S., 2015. Local and sex-specific biases in crossover vs. noncrossover outcomes at meiotic recombination hot spots in mice. *Genes & Development* 29, 1721.
- Boulton, A., Myers, R.S., Redfield, R.J., 1997. The hotspot conversion paradox and the evolution of meiotic recombination. *Proceedings of the National Academy of Sciences* 94, 8058–8063.
- Brick, K., Smagulova, F., Khil, P., Camerini-Otero, R.D., Petukhova, G.V., 2012. Genetic recombination is directed away from functional genomic elements in mice. *Nature* 485, 642.
- Brick, K., Thibault-Sennett, S., Smagulova, F., Lam, K.W.G., Pu, Y., Pratto, F., Camerini-Otero, R.D., Petukhova, G.V., 2018. Extensive sex differences at the initiation of genetic recombination. *Nature* 561, 338.
- Halldorsson, B.V., Hardarson, M.T., Kehr, B., Styrkarsdottir, U., Gylfason, A., Thorleifsson, G., Zink, F., Jonasdottir, A., Jonasdottir, A., Sulem, P., et al., 2016. The rate of meiotic gene conversion varies by sex and age. *Nature genetics* 48, 1377.

- Latrille, T., Duret, L., Lartillot, N., 2017. The red queen model of recombination hot-spot evolution: a theoretical investigation. *Philosophical Transactions of the Royal Society B: Biological Sciences* 372, 20160463.
- Lichten, M., Goldman, A.S., 1995. Meiotic recombination hotspots. *Annual review of genetics* 29, 423–444.
- Myers, S., Bottolo, L., Freeman, C., McVean, G., Donnelly, P., 2005. A fine-scale map of recombination rates and hotspots across the human genome. *Science* 310, 321–324.
- Myers, S., Bowden, R., Tumian, A., Bontrop, R.E., Freeman, C., MacFie, T.S., McVean, G., Donnelly, P., 2010. Drive against hotspot motifs in primates implicates the *prdm9* gene in meiotic recombination. *Science* 327, 876–879.
- Otto, S.P., Michalakis, Y., 1998. The evolution of recombination in changing environments. *Trends in ecology & evolution* 13, 145–151.
- Paigen, K., Petkov, P., 2010. Mammalian recombination hot spots: properties, control and evolution. *Nature Reviews Genetics* 11, 221.
- Parvanov, E.D., Petkov, P.M., Paigen, K., 2010. *Prdm9* controls activation of mammalian recombination hotspots. *Science* 327, 835–835.
- Patten, M.M., Haig, D., Úbeda, F., 2010. Fitness variation due to sexual antagonism and linkage disequilibrium. *Evolution: International Journal of Organic Evolution* 64, 3638–3642.
- Petes, T.D., 2001. Meiotic recombination hot spots and cold spots. *Nature Reviews Genetics* 2, 360.
- Russell, T.W., Russell, M.J., Úbeda, F., Jansen, V.A., 2019. Stable cycling in quasi-linkage equilibrium: fluctuating dynamics under gene conversion and selection. *Journal of theoretical biology* 477, 84–85.
- Szostak, J.W., Orr-Weaver, T.L., Rothstein, R.J., Stahl, F.W., 1983. The double-strand-break repair model for recombination. *Cell* 33, 25–35.
- Úbeda, F., Haig, D., Patten, M.M., 2010. Stable linkage disequilibrium owing to sexual antagonism. *Proceedings of the Royal Society B: Biological Sciences* 278, 855–862.

- Úbeda, F., Russell, T.W., Jansen, V.A., 2019. Prdm9 and the evolution of recombination hotspots. *Theoretical population biology* 126, 19–32.
- Úbeda, F., Wilkins, J., 2011. The red queen theory of recombination hotspots. *Journal of evolutionary biology* 24, 541–553.

Chapter 5

Stable cycling in quasi-linkage equilibrium: Fluctuating dynamics under gene conversion and selection

Publication

This work has been published as

Stable cycling under quasi-linkage equilibrium: Fluctuating dynamics under gene conversion and selection (Russell et al., 2019)

Timothy W. Russell, Matthew J. Russell, Francisco Úbeda, Vincent A. A. Jansen

Journal of Theoretical Biology: 477, 84-95, (2019)

doi: <https://doi.org/10.1016/j.jtbi.2019.06.010>

Author contributions

Myself and Vincent A. A. Jansen conceived of the research and analysed the model. Myself and Matthew J. Russell carried out the numerical analysis. I wrote the initial draft of the manuscript and completed the paper with feedback from all three authors.

Contents

5.1	Introduction	111
5.2	The model	113
5.3	Analysis and results	115
5.4	Discussion	130

Stable cycling in quasi-linkage equilibrium: fluctuating dynamics under gene conversion and selection

Timothy W. Russell^{a,*}, Matthew J. Russell^b, Francisco Úbeda^a, Vincent A.A. Jansen^a

^a*School of Biological Sciences, Royal Holloway University of London, Egham, Surrey, TW20 0EX, UK*

^b*School of Mathematical Sciences, University of Nottingham, University Park, Nottingham, NG7 2RD, UK*

Abstract

Genetic systems with multiple loci can have complex dynamics. For example, mean fitness need not always increase and stable cycling is possible. Here, we study the dynamics of a genetic system inspired by the molecular biology of recognition-dependent double strand breaks and repair as it happens in recombination hotspots. The model shows slow-fast dynamics in which the system converges to the quasi-linkage equilibrium (QLE) manifold. On this manifold, sustained cycling is possible as the dynamics approach a heteroclinic cycle, in which allele frequencies alternate between near extinction and near fixation. We find a closed-form approximation for the QLE manifold and use it to simplify the model. For the simplified model, we can analytically calculate the stability of the heteroclinic cycle. In the discrete-time model the cycle is always stable; in a continuous-time approximation, the cycle is always unstable. This demonstrates that complex dynamics are possible under quasi-linkage equilibrium.

Keywords:

Slow manifold, Lyapunov function, Multiple time-scales, Heteroclinic cycle, Two-locus two-allele

*Corresponding author

Email address: timothy.russell.2015@rhul.ac.uk (Timothy W. Russell)

1. Introduction

Genetic equilibrium, the idea that gene frequencies are the same from one generation to the next, was the focus of early work in population genetics. The attention shifted when it was discovered that one-locus viability models can exhibit cycling behaviour and genetic equilibrium does not have to be achieved (Kimura, 1958; Haderler and Liberman, 1975; Asmussen and Feldman, 1977; Cressman, 1988). Further investigation showed that two-locus viability models with recombination can also exhibit cycling behaviour (Akin, 1979; Hastings, 1981; Akin, 1982, 1983, 1987).

The discrete-time selection-recombination equations (Lewontin and Kojima, 1960; Bürger, 2000) have provided a deterministic model for changes in the genetic make up of a population. Despite the fact that these equations are often used to study the properties of stable equilibria, they are inherently nonlinear, meaning even the most simple formulations of the equations can have complex dynamics. Examples include limit cycles (Akin, 1983) and heteroclinic cycles (Haig and Grafen, 1991; Úbeda et al., 2019). Whether the cycles are maintained indefinitely or eventually die out (i.e. their stability properties) is mathematically challenging and of significant biological importance. This is the focus of the research we present here.

Many genetic processes within an interacting population of individuals can be captured by the selection-recombination equations, as they allow for arbitrary selection regimes defined by model-specific fitness matrices. Here, we investigate the stability of cycles in two-locus genetic systems characterised by a specific interaction between selection, gene conversion and crossover. This interaction corresponds to a model of the evolution of recombination hotspots (Úbeda et al., 2019). However, we re-write this model in standard selection-recombination equations form by noticing that the effect of conversion in Úbeda et al. (2019) can be split into its effect on selection (and incorporated to the selection component of the standard selection-recombination equation) and its effect on formation of double heterozygotes (and incorporated into the recombination component of the standard selection-recombination equation). Furthermore, while the model in Úbeda et al. (2019) assumes that the values taken by the selection-recombination parameters are constrained by their biological interdependence, here we assume that the parameter values are independent and not limited by biological constraints. In doing so, we allow for multiple forms of interaction between selection, conversion and crossover, provided they produce the same equations. This formulation allow us to focus on the mathematical properties of the generalised model.

Biologically, the processes in our model are initiated by recognition between a protein

formed by a modifier gene and a target locus, whereby the protein interacts with the target, initiating conversion and potentially crossover (Úbeda and Wilkins, 2011; Úbeda et al., 2019). Other than the evolution of recombination hotspots (Úbeda and Wilkins, 2011; Úbeda et al., 2019), examples of similar recognition-initiated interactions producing sustained cycling include: the evolution of homing endonucleases (Yahara et al., 2009), the evolution of meiotic drive (Haig and Grafen, 1991), the evolution of host-parasite interactions (Sasaki et al., 2002) and the evolution of altruism via tag based recognition (Jansen and Van Baalen, 2006).

If selection is weak, stable cycling cannot occur within the two-locus selection-recombination equations if the equilibria are hyperbolic (Nagylaki et al., 1999; Pontz et al., 2018). These conditions produce dynamics which converge to a stable equilibrium. Under weak selection, the argument by Nagylaki et al. (1999) uses the existence of an invariant stable manifold which attracts the dynamics. On this attracting manifold, the dynamics are gradient-like and converge to equilibrium (Pugh et al., 1977). This manifold is known in genetics as the *quasi-linkage equilibrium* (QLE) manifold (Kimura, 1965). It is the set of states defined by the property that linkage disequilibrium changes an order of magnitude slower than the allele frequencies (Kimura, 1965).

In geometric terms, this means that the dynamics approach a manifold after a short initial time. If an approximate expression for such a manifold can be found, it can be exploited mathematically to simplify the system (Constable and McKane, 2017). This is usually done by assuming that selection in the model is weak (Barton, 1995; Nagylaki et al., 1999; Kirkpatrick et al., 2002; Lion, 2018). We identify the linkage disequilibrium as a fast variable in our model, isolate it using a coordinate transformation and find an approximation of the surface to which the dynamics converge. Here we show that the existence of a time-scale separation between variables and hence attraction to the QLE manifold is not exclusively associated with simple dynamics which are characterised by gradient-like convergence to an interior equilibrium.

The model presented here has complex dynamics, such as bistability and a global bifurcation. We show that, in such a system, it is still possible to find an approximate yet accurate explicit expression for the QLE manifold. For analytical tractability, following standard methods in population genetics, we derive a continuous-time approximation to our discrete-time model (Nagylaki et al., 1999; Bürger, 2000; Pontz et al., 2018). We use this continuous-time approximation to find an expression for the QLE manifold. We go on to use this to constrain the dynamics analytically to this surface, reducing the dimension of the sys-

tem. We are then able to calculate the stability of the now-planar heteroclinic cycle that exists in our model within certain parameter regimes. Constraining the dynamics is a powerful step as it allows for the use of the analytic heteroclinic stability condition for discrete-time planar heteroclinic cycles (Hofbauer and Schlag, 2000). In the vicinity of this heteroclinic cycle, strong fluctuations are possible on the QLE manifold.

Finally, we numerically assess the accuracy of our approximation of the QLE manifold against both sources of error: the *quasi steady-state assumption* and the use of the continuous-time derived manifold within the discrete-time system. We find that the manifold is a good approximation for the discrete-time system for both damped oscillations towards the unique interior equilibrium and the approach towards the heteroclinic cycle.

2. The model

We investigate the dynamics of haplotype frequencies of two alleles at two interacting loci, in an infinite population, undergoing a specific selection regime (uniquely defining the fitness matrix W), recombination and random union of gametes (panmixia). Once the fitness matrix and the parameter δ are defined, the system of equations in question is fully defined (A.1). First, we describe the biological processes which justify our selection regime, then we present the resulting fitness matrix (A.5).

Our model describes the evolution of recombination hotspots by following the dynamics between a modifier gene — producing a recombinogenic protein — and a target gene, on which the protein binds to, causing a double-strand break and initiating recombination (Úbeda et al., 2019). This model is here re-written as a system of selection-recombination equations. This system describes the following general processes: a fitness benefit derived from recognition between modifier and target (β), a fitness cost derived from gene conversion (γ) and the reshuffling of alleles in double heterozygotes caused by gene conversion and crossover (δ) (Úbeda et al., 2019). Our original formulation of the model included another parameter α , which we have normalised to one (without loss of generality).

The dynamics of the matching process between homozygotes and gene conversion leads to the following system of equations describing the frequency of each haplotype in the next

generation

$$\begin{aligned}x'_1 &= \frac{1}{\bar{w}} \left(x_1[1 + \beta x_1 - \gamma x_2] - \delta D \right), \\x'_2 &= \frac{1}{\bar{w}} \left(x_2[1 - \beta x_2 + \gamma x_1] + \delta D \right), \\x'_3 &= \frac{1}{\bar{w}} \left(x_3[1 - \beta x_3 + \gamma x_4] + \delta D \right), \\x'_4 &= \frac{1}{\bar{w}} \left(x_4[1 + \beta x_4 - \gamma x_3] - \delta D \right),\end{aligned}\tag{1}$$

where the linkage disequilibrium between alleles is

$$D = x_1 x_4 - x_2 x_3,\tag{2}$$

and the population mean fitness is

$$\bar{w} = x_1 + x_2 + x_3 + x_4 + \beta (x_1^2 - x_2^2 - x_3^2 + x_4^2).\tag{3}$$

Superscript primes indicate the value of the variable in the next generation. The population mean fitness, \bar{w} , ensures that the sum of the haplotype frequencies remains constant in time. To ensure the right hand side of the difference equations does not become negative, which would imply that the number of gametes produced is negative, we require that the parameters β, γ can only take values between 0 and 1. This can be justified by the fact parameters represent probabilities in the context of the selection-recombination equations. The parameter δ can only take values between 0 and $\frac{1}{2}$.

Our fitness matrix and therefore our model has similarities with that of (Karlin et al., 1970). They study symmetric viability, meaning they impose a symmetric fitness matrix. Ours is perhaps superficially similar but has a crucial difference; our matrix is not symmetric meaning mean fitness is no longer a Lyapunov function. Our matrix results in certain local symmetries within the resulting equations — symmetries which are a hallmark of heteroclinic cycles. In that sense, our model is closer to the ones of Haig and Grafen (1991) who also studied a process with a non-symmetric fitness matrix also finding a heteroclinic cycle. We choose a specific example to study for mathematical tractability and to link it to specific biological examples.

	A_1	A_2
B_1	x_1	x_3
B_2	x_2	x_4

Table 1: Relations between the haplotype frequencies, x_1, x_2, x_3, x_4 , the alleles controlling the recombinogenic protein type, A_1, A_2 , and the alleles controlling the target site sequence, B_1, B_2 . The table indicates that the allele frequencies are obtained by summing over the haplotype frequencies in the corresponding row or column. Explicitly, $A_1 = x_1 + x_2$, $A_2 = x_3 + x_4$, $B_1 = x_1 + x_3$ and $B_2 = x_2 + x_4$.

3. Analysis and results

The model has two different qualitative behaviours: convergence to equilibrium and sustained oscillations. In both cases, the rate-of-change of D tends towards zero on a faster time scale than the rate-of-change of the allele frequencies (see Figure 1). This suggests that the system has two separate time scales and that the dynamics converge towards the QLE manifold. We will find an approximate expression for this manifold.

For brevity, we introduce $A = A_1$ and $B = B_1$ to denote the frequency of the first recombinogenic protein and its matching target allele, respectively. The frequency of the second recombinogenic protein and its target allele can then be written as $A_2 = 1 - A$ and $B_2 = 1 - B$ (Table 1).

3.1. Change of variables

The first step towards finding an approximation of the QLE manifold is changing coordinates so that they describe the allele frequencies and linkage disequilibrium. We achieve this by transforming variables from haplotype frequencies to allele frequencies using

$$\begin{aligned} A &= x_1 + x_2, \\ B &= x_1 + x_3, \\ D &= x_1x_4 - x_2x_3, \end{aligned} \tag{4}$$

where A and B take values on the interval $[0, 1]$. D represents linkage disequilibrium between alleles and takes values on $[-\frac{1}{4}, \frac{1}{4}]$. If we consider (4) to be the forward transformation,

we arrive at the backward transformation

$$\begin{aligned}x_1 &= AB + D, \\x_2 &= A(1 - B) - D, \\x_3 &= (1 - A)B - D, \\x_4 &= (1 - A)(1 - B) + D.\end{aligned}\tag{5}$$

Transforming using (4), the discrete-time model becomes

$$\begin{aligned}A' &= \frac{1}{\bar{w}}\beta A(1 - A)(2B - 1) + A, \\B' &= \frac{1}{\bar{w}}\left[(\gamma - \beta)B(2A - 1)(B - 1) + \gamma(2B - 1)D\right] + B, \\D' &= \frac{1}{\bar{w}^2}\left[(A - 1)A(B - 1)B(\beta - \gamma) + \right. \\&\quad D\left(\beta[2A(A - 1)(B^2 - B)(\gamma + \beta) + \right. \\&\quad \left. A(A - 1)\gamma - (2A - 1)(\delta - 1)(2B - 1)] - \delta + 1\right) + \\&\quad D^2\left(\beta(\beta + \gamma)(2A - 1)(2B - 1) + \beta(-2\delta + 3) + \gamma\right) + \\&\quad \left. 2\beta D^3(\beta + \gamma)\right].\end{aligned}\tag{6}$$

Additionally, \bar{w} is transformed into

$$\bar{w} = 1 + \beta(2A - 1)(2B - 1) + 2\beta D.\tag{7}$$

As these coordinates include linkage disequilibrium (D) explicitly, they allow for a simple interpretation of the surface of total linkage equilibrium: the *Wright manifold*. This surface can now be written as the part of state space where $D = 0$ (Rice, 2004).

3.2. Equilibria and local stability

The system has a maximum of ten solutions when solving for potential equilibria. Five of these live within the positive state space of the model and are therefore biologically feasible. Four of the five biologically realistic equilibria are located at the four vertices of the tetrahedron that forms the 3-simplex (in haplotype coordinates). These corner equilibria, in allelic

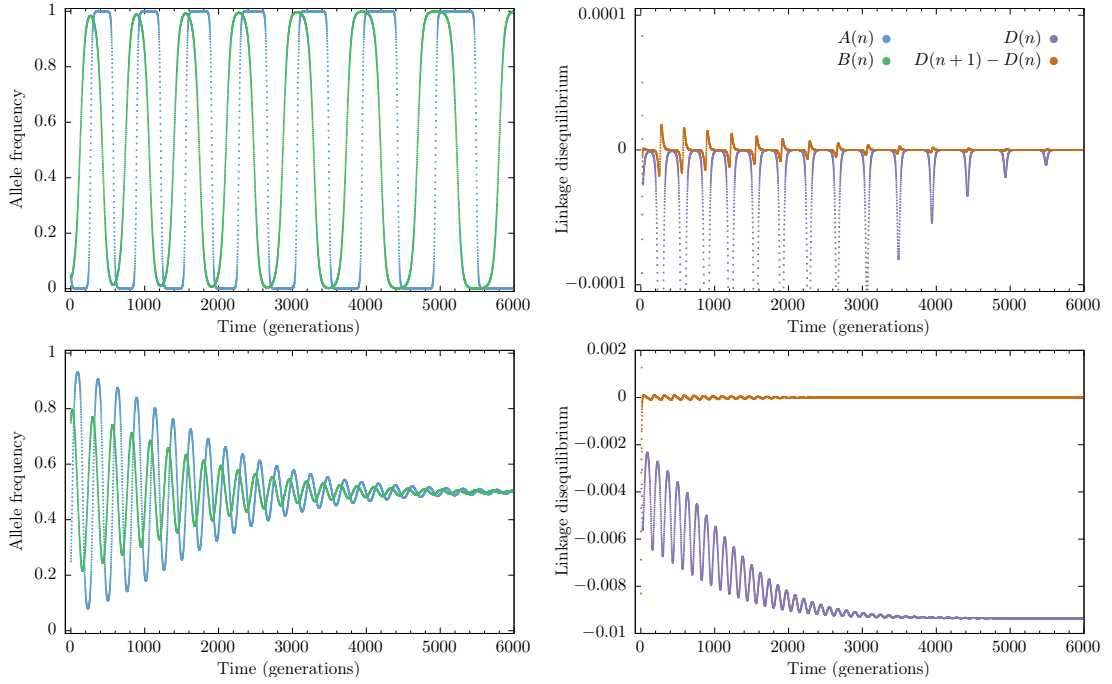


Figure 1: Time series showing examples of the two types of behaviour of the discrete-time model (6). The examples in the top row have initial conditions: $A(0) = 0.05$, $B(0) = 0.95$, $D(0) = 0.0005$ and those in the bottom row have initial conditions $A(0) = 0.25$, $B(0) = 0.75$, $D(0) = 0.0005$. Trajectories in both rows were solved with the same set of parameters: $\beta = 0.1$, $\gamma = 0.13$, $\delta = 0.2$. The top row shows a typical trajectory nearby the heteroclinic cycle. It also shows that after an initial period of rapid change, the linkage disequilibrium eventually changes relatively slowly (D' becomes approximately constant in time), indicating the convergence of the dynamics to QLE manifold. The bottom row shows a typical orbit exhibiting damped oscillations and convergence to the asymptotically stable interior equilibrium (9).

coordinates (A, B, D) , are

$$\begin{aligned}
 \Phi_1 &= (1, 1, 0), \\
 \Phi_2 &= (1, 0, 0), \\
 \Phi_3 &= (0, 1, 0), \\
 \Phi_4 &= (0, 0, 0).
 \end{aligned} \tag{8}$$

We analysed the linear stability of these equilibria in [Úbeda et al. \(2019\)](#) and we summarise the main results here. For our choice of parameters the equilibria Φ_2 and Φ_3 are always unstable. Moreover, if $\beta < \gamma$ these equilibria are saddles. The equilibria Φ_1 and Φ_4 are stable if $\beta > \gamma$ and are saddles, and thus unstable, if $\beta < \gamma$. Note that if A or B take values of either 0 or 1 then $D = 0$. Upon inspection of the transformed models, we find that the lines connecting the equilibria Φ_1 to Φ_2 ($A = 1, D = 0$), Φ_2 to Φ_4 ($B = 0, D = 0$), Φ_4 to Φ_3 ($A = 0, D = 0$) and Φ_3 to Φ_1 ($B = 1, D = 0$) are all invariant. When all these equilibria

are saddles (i.e. when $\beta < \gamma$) a heteroclinic cycle exists:

$$\cdots \rightarrow \Phi_1 \rightarrow \Phi_2 \rightarrow \Phi_4 \rightarrow \Phi_3 \rightarrow \Phi_1 \rightarrow \cdots .$$

The fifth equilibrium is positioned in the interior of the simplex. For this equilibrium it is easily verified that $\dot{A} = 0$ and $\dot{B} = 0$ for $A = B = \frac{1}{2}$. The interior equilibrium, in allelic coordinates, is

$$\Phi_5 = (\frac{1}{2}, \frac{1}{2}, D^*), \quad (9)$$

where D^* is the negative root of

$$(\gamma - \beta)D^{*2} - \delta D^* - \frac{1}{16}(\gamma - \beta) = 0, \quad (10)$$

given by

$$D^* = \frac{\delta - \sqrt{\delta^2 + \frac{1}{4}(\gamma - \beta)^2}}{2(\gamma - \beta)}. \quad (11)$$

The positive root is larger than $\frac{1}{4}$ for $\delta > 0$ and therefore the corresponding equilibrium has negative haplotype frequencies.

The multipliers of the discrete-time model (6) at the interior equilibrium Φ_5 are given by

$$\begin{aligned} \lambda_1 &= 1 + \frac{\gamma D^* + \sqrt{(\gamma D^*)^2 + \frac{1}{4}\beta(\beta - \gamma)}}{\bar{w}^*}, \\ \lambda_2 &= 1 + \frac{\gamma D^* - \sqrt{(\gamma D^*)^2 + \frac{1}{4}\beta(\beta - \gamma)}}{\bar{w}^*}, \\ \lambda_3 &= 1 - \frac{\delta + 2D^*(\beta - \gamma)}{\bar{w}^*}, \end{aligned} \quad (12)$$

where $\bar{w}^* = 1 + 2\beta D^*$ denotes the value of \bar{w} evaluated at the interior equilibrium (Úbeda et al., 2019). The eigenvalues $\hat{\lambda}_i$ of the interior equilibrium of the continuous-time approximation are given by $\hat{\lambda}_i = \lambda_i - 1$.

If $\beta > \gamma$ then $D^* > 0$ and $\bar{w}^* > 0$. Therefore, in this region of parameter space, it is relatively easy to see that the interior equilibrium is a saddle (both in the discrete and the continuous-time models). Specifically, λ_1 and λ_3 are always negative, and for $0 < \delta < \frac{1}{2}$, $\lambda_3 > -1$. λ_2 is always positive. If $\beta < \gamma$ then $D^* < 0$. Eigenvalues λ_1 and λ_2 can now form a conjugate pair of complex eigenvalues. For the equilibrium to be locally stable in the

discrete-time model we require $|\lambda_{1,2}| < 1$. This leads to the conditions for local stability

$$2\gamma\bar{w}^*D^* < \frac{1}{4}\beta(\beta - \gamma). \quad (13)$$

If $\delta < \frac{1}{2}$ this condition is always fulfilled (Úbeda et al., 2019). This stability condition (13) applies only to the discrete-time model as its continuous-time approximation (15) is always locally stable (for $\beta < \gamma$).

3.3. Global stability: A Lyapunov function and heteroclinic cycle

3.3.1. A continuous-time approximate model

These results on asymptotic local stability leave the question of what the global dynamics are and, in particular, if the heteroclinic cycle is an attractor, or whether orbits move away from it. While the focus of this paper is to analyse the global stability properties of the discrete-time model (1), we introduce the following continuous-time approximation of the discrete-time model (Nagylaki et al., 1999; Bürger, 2000) to aid us in this matter significantly

$$\begin{aligned} \dot{x}_1 &= \frac{1}{\bar{w}} \left(x_1[1 + \beta x_1 - \gamma x_2] - \delta D \right) - x_1, \\ \dot{x}_2 &= \frac{1}{\bar{w}} \left(x_2[1 - \beta x_2 + \gamma x_1] + \delta D \right) - x_2, \\ \dot{x}_3 &= \frac{1}{\bar{w}} \left(x_3[1 - \beta x_3 + \gamma x_4] + \delta D \right) - x_3, \\ \dot{x}_4 &= \frac{1}{\bar{w}} \left(x_4[1 + \beta x_4 - \gamma x_3] - \delta D \right) - x_4, \end{aligned} \quad (14)$$

where derivatives with respect to time t are denoted by a dot above a variable. The expressions for \bar{w} and D are given by (2) and (3), the same as in the discrete-time model. The continuous-time model written in the transformed variables is

$$\begin{aligned} \dot{A} &= \frac{1}{\bar{w}} \beta A(1 - A)(2B - 1), \\ \dot{B} &= \frac{1}{\bar{w}} \left[(\gamma - \beta)B(2A - 1)(B - 1) + \gamma(2B - 1)D \right], \\ \dot{D} &= \frac{1}{\bar{w}} \left[(\gamma - \beta) \left[D^2 - AB(1 - A)(1 - B) \right] - \beta D(2A - 1)(2B - 1) - \delta D \right]. \end{aligned} \quad (15)$$

It is easy to show that the equilibria for the discrete-time model and its continuous-time

approximation are the same (Bürger, 2000). Similarly, it is easy to show that the eigenvalues of the Jacobian at each equilibrium in the continuous-time model equal the discrete-time eigenvalues minus unity — a consequence of the fixed time-step in the discrete-time system. We use the continuous-time model in two ways: introducing a Lyapunov function for the interior equilibrium and to find an analytically tractable version of the approximate QLE manifold, as the expression is significantly simpler when derived from the continuous-time model.

3.3.2. Lyapunov function

For the continuous-time model it is relatively easy to show that the heteroclinic cycle repels orbits using a Lyapunov function. Before we show this, we first observe that for any solution of (15) as long as $D \leq 0$ at some point in time, $D \leq 0$ onwards if $\beta < \gamma$, and with equality only if the solution lives on the heteroclinic connection. This can easily be seen by inspecting the right hand side of the differential equation describing the change in D when $\beta < \gamma$, which is negative everywhere on the Wright manifold, apart from on the heteroclinic connection, where it is zero. Therefore, if $D(t_0) < 0$, then $D(t) < 0$ for all $t > t_0$. This means that trajectories can pass through the Wright manifold where $D = 0$ in only one direction, and are then confined to the region where $D \leq 0$ once they have done so.

With this established, we now consider the function

$$V(A, B) = [A(1 - A)]^{\gamma-\beta} [B(1 - B)]^\beta. \quad (16)$$

This function (16) serves as a natural candidate for a Lyapunov function of system (14) as it retains invariance of the system along the boundaries (where either $A = 0$, $A = 1$, $B = 0$ or $B = 1$). Indeed, for $\beta < \gamma$ this function takes the value $V = 0$ along the heteroclinic connection, and takes positive values anywhere else in or on the simplex. The continuous-time model with D set to zero (15) is equivalent to the replicator equations for 2×2 games and our Lyapunov function (16) is equivalent to that of this system, serving as its constant of motion (Hofbauer and Sigmund, 1998).

The candidate function V is a Lyapunov function if $\beta < \gamma$ for orbits which at some point pass through the Wright manifold. To show this, we inspect its time derivative along solutions of (15):

$$\dot{V} = -\beta\gamma \frac{D(1-2B)^2}{\bar{w}B(1-B)} V. \quad (17)$$

The right hand side of (17) is always less than or equal to zero if $D \leq 0$, meaning V is a Lyapunov function within this region. For orbits starting in the forward invariant part of

state space where $D < 0$ the value of V will thus increase or stay constant over time. The ω -limit of these orbits must therefore be invariant sets for which either $D = 0$ or $B = \frac{1}{2}$. If $\beta < \gamma$ the only invariant part of the Wright manifold $D = 0$ is the heteroclinic connection, where $V = 0$. As the value of V cannot decrease and is positive for all points in or on the simplex that are not part of the heteroclinic connection, the heteroclinic connection cannot be an ω -limit of these orbits, within which the only other candidates are the invariant sets contained with $B = \frac{1}{2}$, which is the interior equilibrium Φ_5 . Any orbits starting within the parts of the simplex where $D < 0$ will therefore move towards the interior equilibrium.

A corollary of this observation is that arbitrarily close to the heteroclinic connection, where $D = 0$, there will be points that are within the region of the simplex where $D < 0$. The Lyapunov function (16) shows that orbits starting at these points will move away from the heteroclinic connection, towards the interior equilibrium. The heteroclinic connection is therefore not stable. The interior equilibrium clearly is stable and must be the attractor for all initial points in the interior of the simplex for which initially $D < 0$. This shows that in the continuous-time model the heteroclinic cycle is unstable. Simulations suggest that the interior equilibrium is a global attractor within the simplex.

3.3.3. Discrete-time heteroclinic cycle

The Lyapunov argument does not carry over to the discrete-time model. In the discrete-time model, does the heteroclinic connection attract or repel? We analytically investigate this using the approximate QLE manifold in section 3.6. We also numerically investigate the regions of initial condition space in which the cycle is attracting, and the results are plotted in Figure 2. In the diagram we can distinguish two regions in parameter space with qualitatively different behaviour, and the boundary between them:

1. Within the first region, $\beta < \gamma$, the interior equilibrium is stable and attracts nearby orbits. Within this region the heteroclinic connection also attracts. Between the two attractors we find the boundary of the basins of attraction. The basin boundary moves towards the heteroclinic connection for small β .
2. Within the second region $\beta > \gamma$. All trajectories converge to one of the corner equilibria, Φ_1 or Φ_4 , apart from orbits starting exactly at the saddle interior equilibrium Φ_5 .
3. Between these two regions $\beta = \gamma$, all trajectories converge to the Wright manifold. On the Wright manifold there is a line of unstable equilibria for which $B = \frac{1}{2}$, $D = 0$.

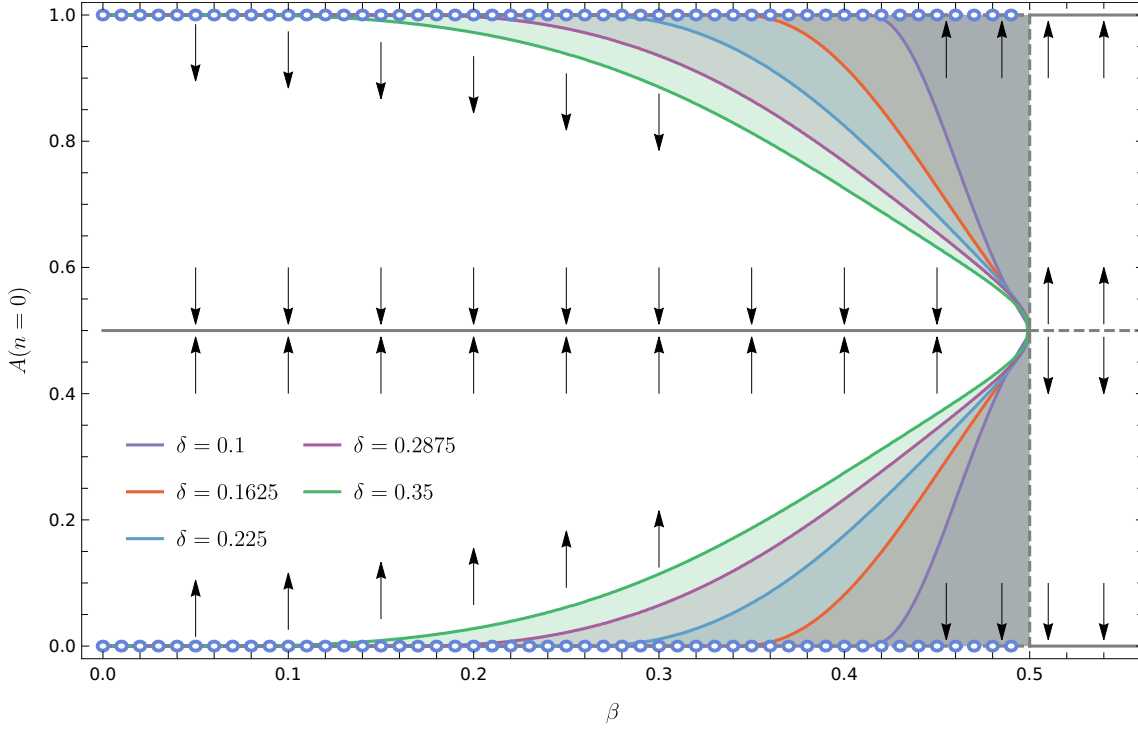


Figure 2: **The basin of attraction of the heteroclinic cycle against β for the discrete-time model.** The diagram shows the different qualitative behaviours of the model resulting from different initial conditions. The arrows point towards the different attractors. The shaded regions show the basins of attraction of heteroclinic cycle for varying values of δ (see legend). The diagram was constructed by starting orbits at different initial conditions, sampled at equally spaced intervals along the line connecting the equilibria Φ_1 and Φ_4 for which $A = B$ and $D = A(1 - A)$ in allelic coordinates, or $(x_1, 0, 0, 1 - x_1)$ in gametic coordinates. We determine whether a specific orbit reaches interior equilibrium or a heteroclinic cycle numerically: if an orbit reaches within $\epsilon = 10^{-12}$ distance from the equilibrium, it is assumed to be at equilibrium. The first trajectory moving along the line of initial conditions which does not tend towards equilibrium is taken to be on the basin boundary. The heteroclinic cycle exists on the left of the vertical dashed line at $\beta = \gamma = 0.5$. At this point both the interior equilibrium and heteroclinic cycle lose stability and all trajectories tend toward one of the corner equilibria, Φ_1 or Φ_4 . Parameters: $\gamma = 0.5$, δ as indicated in figure. Dashed lines represent unstable equilibria, drawn lines represent stable equilibria and small blue circles represent the heteroclinic cycles.

Orbits starting on the Wright manifold with $B < \frac{1}{2}$ converge to the line $A = 0, D = 0$, and those starting with $B > \frac{1}{2}$ converge to the line $A = 1, D = 0$.

These numerical results show that the heteroclinic connection in the discrete-time model can be stable. To find out how general this is we will next analytically determine the stability of the heteroclinic connection in the discrete-time model. First, we approximate the QLE manifold towards which the trajectories converge.

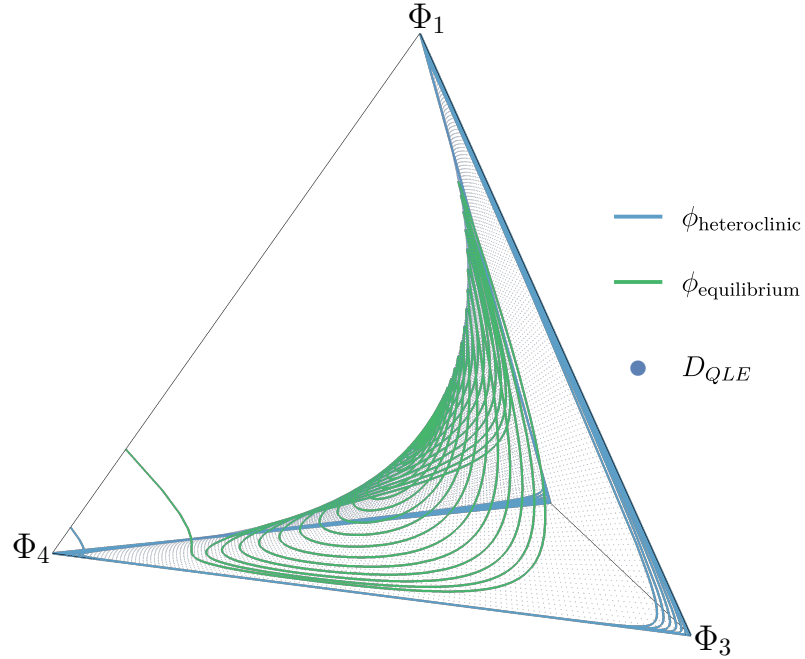


Figure 3: **The approximate quasi-linkage equilibrium manifold, and the approach to it by two typical trajectories of the discrete-time model.** Two trajectories, $\phi_{heteroclinic}$ and $\phi_{equilibrium}$, differing only in initial conditions, of the transformed discrete-time (1) system within the tetrahedron, both converging quickly to a slow manifold. Here, the small dots are points on the manifold D_{QLE} , given by (18). As can be seen, the trajectories converge quickly to this manifold. Parameters and initial conditions as in Figure 1.

3.4. The QLE manifold

If $\beta = \gamma$ the interior equilibrium is degenerate: in the discrete-time model the equilibrium has two real multipliers at unity (and the interior equilibrium of the continuous-time model has two eigenvalues at zero). Because there are two eigenvalues at unity (zero), the equilibrium will have a two dimensional center manifold. If $\beta = \gamma$ the center manifold is the Wright manifold, the part of state space where $D = 0$, and where the gamete frequencies are in linkage equilibrium. The third eigenvalue has a modulus smaller than one (smaller than zero for the continuous-time model) and the associated stable manifold is given by the line $A = B = \frac{1}{2}$. Orbits on this stable manifold move towards the center manifold.

If $\beta < \gamma$ these two multipliers become a complex pair with real part smaller than one (or negative real part for the continuous-time model). The equilibrium within this region is hyperbolic (for all $0 < \delta < \frac{1}{2}$) for the ODE (15). The same is true for the map (6) when there is not equality in the stability condition (13). The center manifold morphs into a two dimensional invariant manifold that is different from the Wright manifold and contains

the interior equilibrium (9). On this manifold, orbits cycle around the equilibrium. The invariant manifold containing the third eigenvector, the line on which $A = B = \frac{1}{2}$, remains in existence. Over this line, orbits quickly converge towards the equilibrium. On this approach, the linkage disequilibrium, D changes rapidly while the allele frequencies A and B remain unchanged. Other orbits show a similar behaviour (see Figure 3): orbits generally converge towards the two dimensional manifold. Once orbits are close to this manifold the orbits move slowly towards either the interior equilibrium or the heteroclinic cycle, depending on the initial conditions (see Figure 2).

To approximate the QLE manifold, we will use a quasi-steady state argument. Specifically, we say that the change in linkage disequilibrium $D(t)$ occurs on a much faster time scale than changes in the allele frequencies and will therefore settle on a quasi-equilibrium. This means that we can assume that the allele frequencies A and B are effectively constant, as D settles. With this assumption, we then solve the equilibrium equation for D (in continuous-time) as a function of the allele frequencies, $D_{QLE}(A, B)$. It turns out that this gives a good approximation for the QLE manifold for the discrete-time model as well as the continuous-time approximation.

Simulations suggest that the gamete frequencies are attracted towards the manifold where they are in quasi-linkage equilibrium (Fig. 4). We approximate the QLE manifold by

$$D_{QLE}(A, B) = \frac{\beta(2A - 1)(2B - 1) + \delta}{2(\gamma - \beta)} - \sqrt{\left(\frac{\beta(2A - 1)(2B - 1) + \delta}{2(\gamma - \beta)}\right)^2 + AB(1 - A)(1 - B)}. \quad (18)$$

As we show in [Appendix B](#) the relevant slow time-scale is proportional to $(\gamma - \beta)^{-\frac{1}{2}}$.

3.5. Simplification by reducing to allele frequencies

Given the tendency of haplotype frequencies to settle in QLE, one would expect that if $\gamma > \beta$, the dynamics proceed to the QLE manifold, and that the allele frequencies then change slowly, either towards, or away from the interior equilibrium. This is indeed what happens in the vicinity of the interior equilibrium. Further away from equilibrium, and in particular in the vicinity of the heteroclinic cycle, this is not necessarily true. It is possible that the manifold $D = D_{QLE}(A, B)$ is situated outside the simplex in which all gamete frequencies are positive. If that is the case, the dynamics will be constrained by the edges of the simplex.

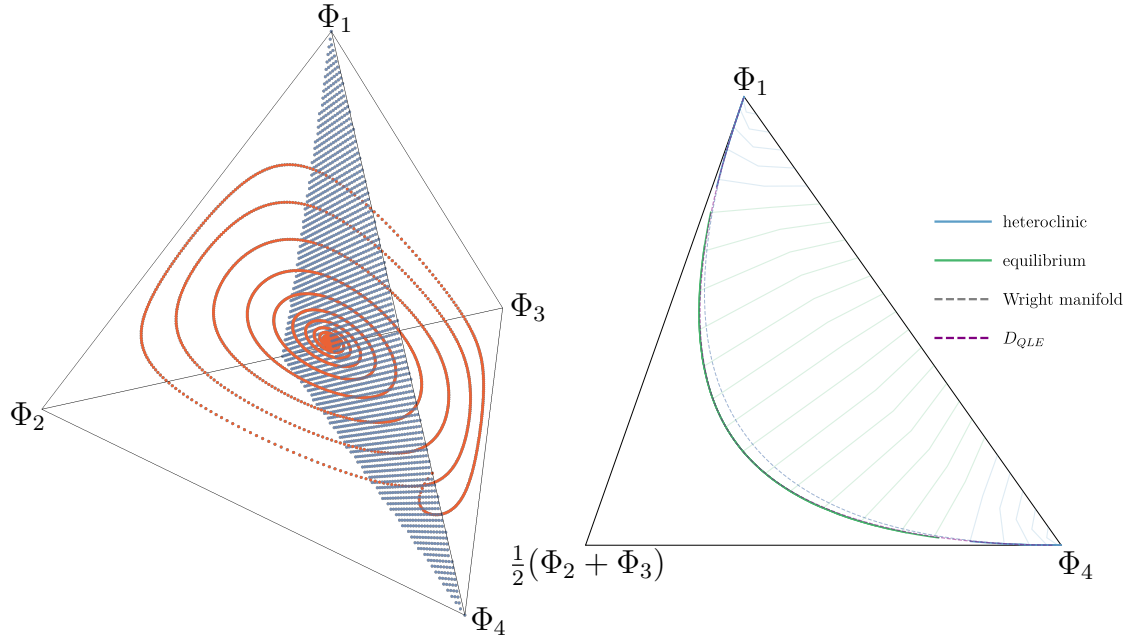


Figure 4: **The fast approach to the QLE manifold shown using a Poincaré section.** The dynamics of our model has two different times scales and shows slow-fast dynamics. (a) A typical trajectory of the model (1), simulated using $\beta = 0.1, \gamma = 0.13$ and $\delta = 0.11$ and initial conditions $(x_1(0), x_2(0), x_3(0), x_4(0)) = (0.24, 0, 0, 0.76)$. To visualise the slow-fast dynamics we following the Poincaré section $x_2 = x_3$ ($=A = B$) and record every instance where the orbit (shown in red) cuts through this section. (b) The intersection points for a orbit plotted on the Poincaré section. The points of intersection of 22 trajectories are shown. The trajectories have initial conditions equally spaced on the line connecting Φ_1 to Φ_4 . The parameters used are $\beta = 0.3, \gamma = 0.35$ and $\delta = 0.2$. The figure shows the fast approach towards the slow manifold (the thin, drawn lines connect the points of intersection from the same initial condition). The slow manifold is visible as the accumulation of points forming a curve. Although the true slow manifold (blue and green filled lines) and our approximation, D_{QLE} , (purple dashed line) are distinct from the Wright manifold (dashed grey line) apart from at the corners, where they intersect, they are very close and the purple curve is covered by the blue and green line in most of the figure. Green dots are from orbits that end up in the interior equilibrium, Φ_5 , blue dots from orbits going towards the heteroclinic cycle. The gap on the slow manifold between the blue and green points contains the basin boundary. There will be an invariant closed curve located on the slow manifold in the middle of this gap.

Inside the simplex, $D_{QLE} \leq 0$ if $\gamma > \beta$. If the manifold, D_{QLE} , cuts through the sides of the simplex, it can only be on the faces where $D \leq 0$, which is when $x_1 \leq 0$ or $x_4 \leq 0$. In terms of allele frequencies (A, B, D) , that is when $D = -AB$ or when $D = -(1 - A)(1 - B)$. The approximate manifold to which the dynamics are drawn is thus given by $D = D_S(A, B)$, where

$$D_S(A, B) = \max \left[D_{QLE}(A, B), -AB, -(1 - A)(1 - B) \right], \quad (19)$$

and we will use this to simplify the dynamics; in particular we will use it to determine the stability of the heteroclinic cycle.

The system constrained to the attracting manifold is given by just two equations, describing the frequencies of A and B on the slow manifold,

$$\begin{aligned} A' &= \frac{1}{\bar{w}} \beta A(1 - A)(2B - 1) + A, \\ B' &= \frac{1}{\bar{w}} \left[(\gamma - \beta)B(2A - 1)(B - 1) + \gamma(2B - 1)D_S(A, B) \right] + B, \end{aligned} \quad (20)$$

where

$$\bar{w} = \beta(2A - 1)(2B - 1) + 2\beta D_S(A, B) + 1. \quad (21)$$

The dimensionality is now reduced and the system is significantly simplified. We can now study and depict our model as a two dimensional system (Figure 5). The stability of the heteroclinic cycle is governed by the magnitude of the eigenvalues in the connected saddles that make up the cycle. In the planar system this is relatively simple to do.

3.6. Stability of heteroclinic cycle in the discrete-time model

To study the stability of our heteroclinic cycle, we use the condition derived in Hofbauer and Schlag (2000) which determines whether a planar discrete-time heteroclinic cycle is attracting or not. The condition involves the product of the ratio of the logarithm of the expanding (e_i) eigenvalues and the absolute value of the logarithm of the contracting eigenvalues (c_i) at the saddle equilibria (Φ_i where $i = 1, \dots, 4$) the heteroclinic cycle travels between. We follow their notation and use ρ_i to denote each individual ratio and ρ to denote the product

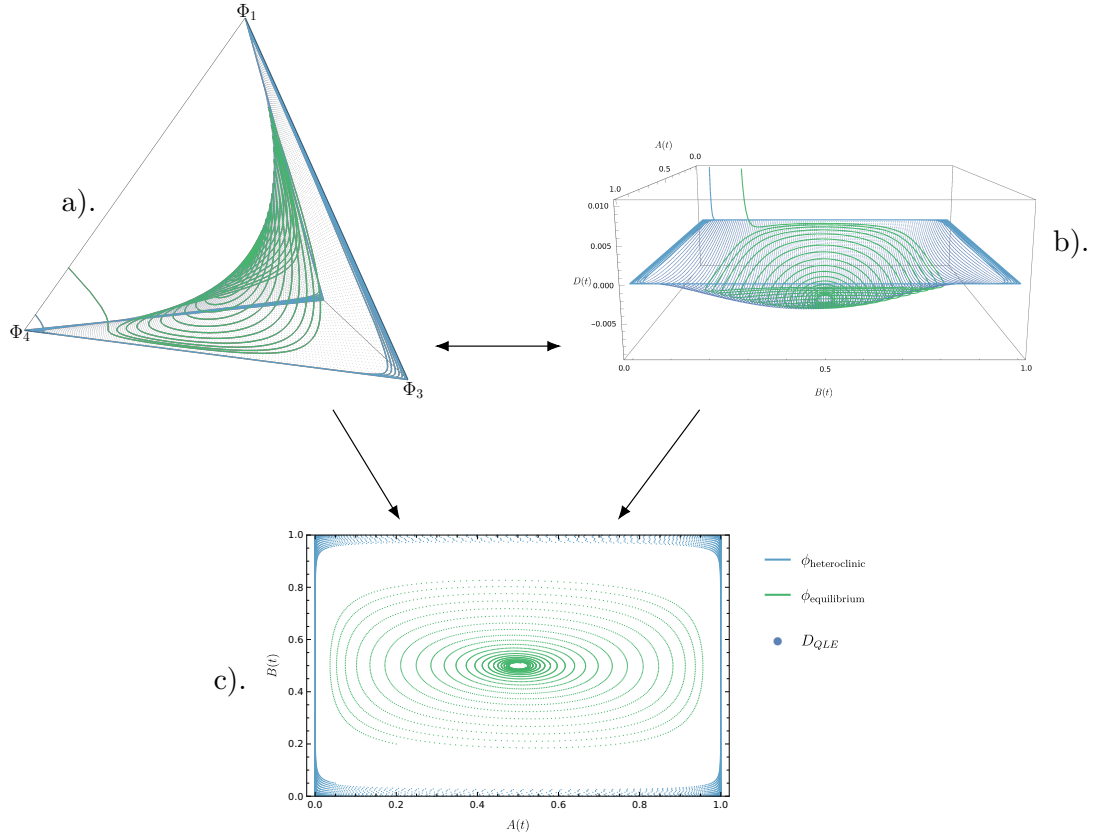


Figure 5: **The simplification of the system by using the approximate slow manifold, D_{QLE} .** (a) The trajectories of our model represented gamete frequencies as given by eqns (1), plotted on the 3-simplex. The QLE manifold, $D = D_{QLE}$, is also plotted with a grid of equally spaced points. (b) The same trajectories and the attracting manifold plotted for the transformed model (20); in both panels (a) and (b) the fast approach to the slow manifold is visible. (c) The same trajectories but plotted on the QLE manifold. The system is reduced to a planar system in the allele coordinates. Parameters and initial conditions as in Figures 1 and 3. Panel (a) is a re-use of Figure 3.

of the ρ_i ,

$$\rho = \prod_{i=1}^n \rho_i, \quad (22)$$

$$\rho_i = \frac{\log e_i}{|\log c_i|}, \quad i = 1, \dots, n.$$

For our model, $n = 4$ and therefore $\rho = \rho_1 \rho_2 \rho_3 \rho_4$. We are then able to state the stability condition: a planar discrete-time heteroclinic cycle is asymptotically stable if $\rho < 1$ and is unstable if $\rho > 1$ (Hofbauer and Schlag, 2000). The specific eigenvalues for the equilibria and their type are given in Table 2. Their derivation can be found in Appendix C.

Calculating ρ using the eigenvalues in Table 2, we arrive at the condition for stability of

Eigenvalue	$\frac{1}{1+\beta}$	$\frac{1+\gamma}{1+\beta}$	$\frac{1}{1-\beta}$	$\frac{1-\gamma}{1-\beta}$
Type	c_1, c_4	e_1, e_4	e_2, e_3	c_2, c_3
Equilibria	Φ_1 & Φ_4		Φ_2 & Φ_3	

Table 2: The eigenvalues of the saddle equilibria between which the heteroclinic cycle travels, used to determine the asymptotic stability of the heteroclinic cycle in discrete-time. Eigenvalues of type c are contracting (incoming), ones of type e are expanding (outgoing). Due to the symmetries in our system, the eigenvalues at Φ_1 and at Φ_4 are equal and the eigenvalues at Φ_2 and at Φ_3 are equal.

the heteroclinic cycle

$$\left(\frac{\log \frac{1+\gamma}{1+\beta}}{\left| \log \frac{1}{1+\beta} \right|} \frac{\log \frac{1}{1-\beta}}{\left| \log \frac{1-\gamma}{1-\beta} \right|} \right)^2 < 1, \quad (23)$$

which, if $\beta < \gamma$, can be rewritten as

$$\frac{\log(1+\beta)}{\log(1-\beta)} < \frac{\log(1+\gamma)}{\log(1-\gamma)}. \quad (24)$$

In this form, it is readily seen that (23) is always satisfied if $\beta < \gamma$. Therefore, in our discrete-time model constrained to the QLE manifold (20), the heteroclinic cycle is always asymptotically stable if it exists.

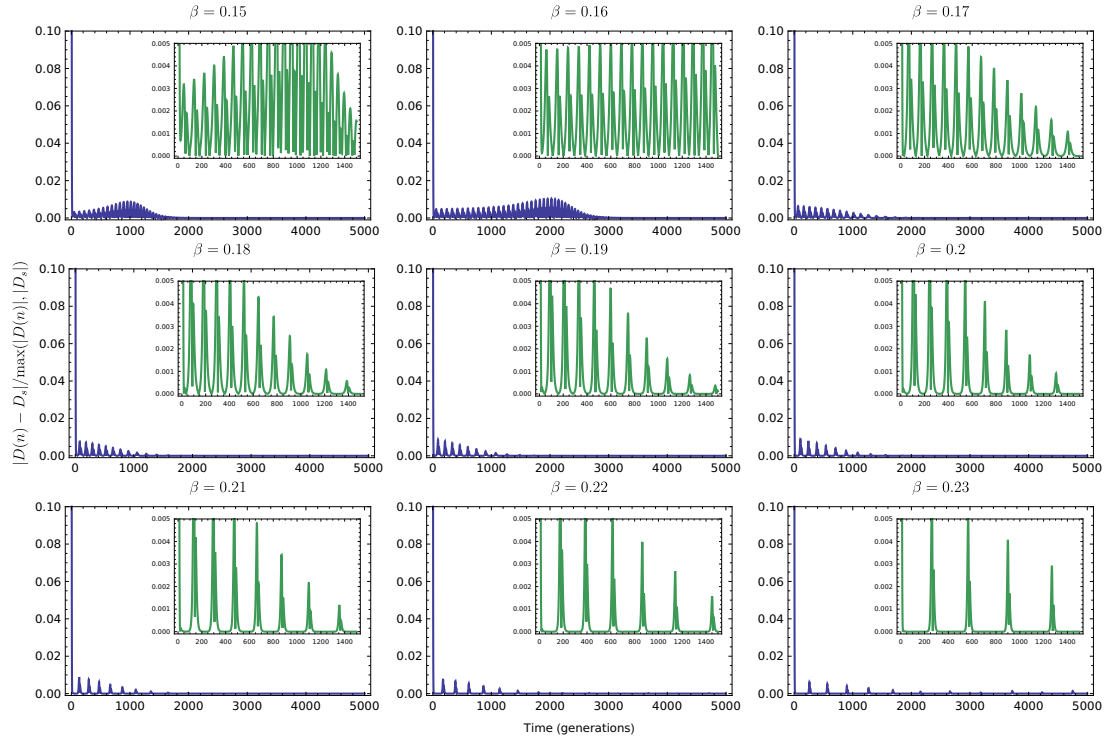


Figure 6: **Relative error of our approximate manifold D_S .** To justify the use of the manifold derived from the continuous-time system, D_S , we numerically compute the relative error between the manifold and the D component of an orbit of the discrete time system close to heteroclinic cycle. We compute both the manifold expression and the orbit at the generation times of the discrete-time model, n and plot the following error expressions $|D(n) - D_S| / \max(|D(n)|, |D_S|)$. Parameters were set to: $\gamma = 0.25$, $\delta = 0.3$, $A(0) = 0.9$, $B(0) = 0.9$, $D(0) = 0.05$ and the values of β are indicated in the plot titles. The insets show the same curves but with finer grain x-axis and y-axis scales allowing the bursts to be seen in more detail. The magnitude of error is always very low.

3.7. Justifying the use of D_S derived from the continuous-time model

In Figure 6, we show the relative error between the value of $D(n)$, the linkage disequilibrium within the discrete-time model (1), and $D_S(t)$, the approximate slow manifold derived using the continuous-time approximation of the discrete-time system, finding the difference to be small. The error is computed using

$$E = \frac{|D(n) - D_S|}{\max(|D(n)|, |D_S|)}, \quad (25)$$

a modified form of the relative error between the approximate manifold D_S , and the D -component of a trajectory of the discrete-time system, which aims to avoid division by zero when one of the quantities is very small. The standard relative error expression could be problematic in this case, since the orbits are close to the manifold. We produce a time se-

ries of the distance between the D -component of the discrete-time orbit and the value of D_S evaluated at the values of the other variables along the orbit. This indicates that the continuous-time manifold, D_S , provides a good approximation for the discrete-time dynamics.

4. Discussion

We studied a genetic system with viability selection and gene conversion that encompasses a wide range of variants where selection can be derived from different aspects of the re-combinational process (Úbeda and Wilkins, 2011; Úbeda et al., 2019). We show that the selection regime associated with a fitness benefit derived from a sequence recognition (β), a fitness cost derived from a gene conversion (γ) altogether with the reshuffling of alleles in double heterozygotes induced by gene conversion and crossover (δ), can lead to stable cycling dynamics in the two-locus, two-alleles model. Our model is most similar to that of Haig and Grafen (1991), because in both models the often assumed symmetry of the fitness matrix (Karlin et al., 1970) is broken. The fluctuations that feature in the model are caused by selection for one allele burning out a target sequence followed by selection for an alternative allele that can burn out the sequence that replaced the old one. This pattern can repeat indefinitely and the resulting dynamics form a heteroclinic cycle (Úbeda et al., 2019). To find out if sustained fluctuations are possible in either of our model variants we investigated whether the heteroclinic cycle attracts or repels (Hofbauer and Schlag, 2000).

We found that haplotype frequencies settle quickly on a state depending on the allele frequencies in the population, and the allele frequencies change on a slower time scale than the linkage disequilibrium (Kimura, 1965). After identifying the linkage disequilibrium D as a good candidate for the fast variable, we performed the nonlinear change of variables from haplotype to allele frequencies, which introduces $D(t)$ as an explicit variable. We then apply a quasi-steady state assumption to $D(t)$ and solve the resulting algebraic equation for D , which we use to reduce the dimension of our system by removing dependency on D altogether (Figure 5) (Kuehn, 2015). We find that the dynamics don't necessarily converge to a single stable interior (polymorphic) equilibrium. We thus provide a biological example of a doubly degenerate system that admits cycling.

After reducing the dimensionality, we found explicit conditions for stability of the heteroclinic cycles. Namely, the discrete-time model allows a heteroclinic cycle that is stable if $\beta < \gamma$; on the other hand, its continuous-time approximation has a heteroclinic cycle

that is always unstable and the dynamics eventually settle on an equilibrium. Furthermore, we established numerically the basin of attraction for the heteroclinic cycle and studied the accuracy of the closed-form approximation D_S of the QLE manifold used to constrain the dynamics (Figure 6).

The equilibria of the discrete and continuous-time models are the same (Bürger, 2000). However, the stability of the heteroclinic cycle differs between the two models: the discrete-time model can have an attracting heteroclinic cycle and a stable equilibrium, and thus has a region of bistability in parameter space; however, its continuous-time approximation has, in the same region of parameter space, $\beta < \gamma$, a globally attracting interior equilibrium point. From a dynamical systems point of view this is not a surprise: it is well known that similar nonlinear discrete and continuous-time models can differ in various ways (May, 1976).

However, preliminary results show that if the population in the model is finite and multinomial sampling is used to pick the individuals who mate and are replaced (Wright, 1984; Úbeda et al., 2019) — producing a stochastic and more biologically realistic version of our model — we see the gap between the discrete-time model and continuous-time approximation bridged. Indeed, similar oscillatory behaviour is now observed in both models. In fact, we see the two models behaving almost identically when the population is finite, just differing in time scale. We also observe that the deterministic slow manifold, D_{QLE} , is a good approximation for the dynamics of the stochastic model, as shown to be possible in some systems by (Constable and McKane, 2017). An in depth analysis of the stochastic model however, is beyond the scope of this paper. Further work could use D_{QLE} to simplify the dynamics of the stochastic implementation of the model. Globally attracting invariant QLE manifolds have recently been found to exist under certain parameter regimes in the continuous-time two locus-two allele selection-recombination equations by Baigent and Seymenoglu (2018).

Similar analyses using quasi-equilibria involving variables other than linkage disequilibrium have been conducted (Van Baalen and Rand, 1998; Day et al., 2011; Lion and Gandon, 2016; Lion, 2018). These models are evolutionary-ecological rather than population genetic models, and rely on the weak selection approximation, but they still observe a rapid convergence to quasi-linkage equilibrium. Our approach to studying the QLE manifold is very general, applicable to any system showing a significant separation of time-scales. Any genetic system of this sort converges to quasi-linkage equilibrium and therefore under an appropriate transformation of variables — one which isolates the fast subsystem — can be analysed in a similar fashion. Therefore, treating the QLE manifold as an slow manifold

and using linkage disequilibrium as a coordinate to approximate this surface explicitly, is a powerful technique for other genetic systems and even evolutionary ecological models.

Multi-locus models can have complex dynamics (Hastings, 1981; Hofbauer and Iooss, 1984; Haig and Grafen, 1991; Úbeda et al., 2019). It appears that most analyses of multi-locus models have been carried out under weak selection assumptions, in which case the dynamics are relatively simple: stable cycling is generally not possible and the dynamics go to an equilibrium (Nagylaki et al., 1999). The weak selection assumption allows for general analytic results (Akin, 1982; Hofbauer, 1985; Barton, 1995; Nagylaki et al., 1999; Kirkpatrick et al., 2002), often invoking the use of the QLE. Under weak selection, stable cycling and complex dynamics do not occur if the equilibria are not degenerate and therefore complex dynamics are not observed under QLE. This association of QLE with weak selection and stability might have led to the impression that complex dynamics are not compatible with quasi-linkage equilibrium (Pomiankowski and Bridle, 2004). What we have shown here is that complex dynamics are possible and, furthermore, are played out in a state of *quasi-linkage equilibrium* showing the association between QLE and convergence to equilibrium to not be true in general: it is possible to find continued fluctuations and sudden changes in the genetic make up in a population at quasi-linkage equilibrium.

References

- Akin, E., 1979. The geometry of population genetics. lect. Notes Biomath 31.
- Akin, E., 1982. Cycling in simple genetic systems. Journal of Mathematical Biology 13, 305–324.
- Akin, E., 1983. Hopf bifurcation in the two locus genetic model. volume 284. American Mathematical Soc.
- Akin, E., 1987. Cycling in simple genetic systems: Ii. the symmetric cases, in: Dynamical Systems. Springer, pp. 139–153.
- Asmussen, M.A., Feldman, M.W., 1977. Density dependent selection 1: A stable feasible equilibrium may not be attainable. Journal of Theoretical Biology 64, 603–618.
- Baigent, S., Seymenoglu, B., 2018. Competitive selection-recombination dynamics: A new approach to studying the quasilinkage equilibrium manifold. URL: <https://www.ucl.ac.uk/~zcahge7/files/SRpaper.pdf>.

- Barton, N.H., 1995. A general model for the evolution of recombination. *Genetics Research* 65, 123–144.
- Bürger, R., 2000. The mathematical theory of selection, recombination, and mutation. John Wiley & Sons.
- Constable, G.W.A., McKane, A.J., 2017. Exploiting fast-variables to understand population dynamics and evolution. *Journal of Statistical Physics* , 1–41.
- Cressman, R., 1988. Frequency-dependent viability selection (a single-locus, multi-phenotype model). *Journal of theoretical biology* 130, 147–165.
- Day, T., Alizon, S., Mideo, N., 2011. Bridging scales in the evolution of infectious disease life histories: theory. *Evolution: International Journal of Organic Evolution* 65, 3448–3461.
- Hadeler, K.P., Liberman, U., 1975. Selection models with fertility differences. *Journal of Mathematical Biology* 2, 19–32.
- Haig, D., Grafen, A., 1991. Genetic scrambling as a defence against meiotic drive. *Journal of theoretical Biology* 153, 531–558.
- Hastings, A., 1981. Stable cycling in discrete-time genetic models. *Proceedings of the National Academy of Sciences* 78, 7224–7225.
- Hofbauer, J., 1985. The selection mutation equation. *Journal of mathematical biology* 23, 41–53.
- Hofbauer, J., Iooss, G., 1984. A Hopf bifurcation theorem for difference equations approximating a differential equation. *Monatshefte für Mathematik* 98, 99–113.
- Hofbauer, J., Schlag, K.H., 2000. Sophisticated imitation in cyclic games. *Journal of Evolutionary Economics* 10, 523–543.
- Hofbauer, J., Sigmund, K., 1998. *Evolutionary games and population dynamics*. Cambridge university press.
- Jansen, V.A.A., Van Baalen, M., 2006. Altruism through beard chromodynamics. *Nature* 440, 663.

- Karlin, S., Feldman, M.W., et al., 1970. Linkage and selection: two locus symmetric viability model. *Theoretical population biology* 1, 39–71.
- Kimura, M., 1958. On the change of population fitness by natural selection 2 3. *Heredity* 12, 145.
- Kimura, M., 1965. Attainment of quasi linkage equilibrium when gene frequencies are changing by natural selection. *Genetics* 52, 875–890.
- Kirkpatrick, M., Johnson, T., Barton, N., 2002. General models of multilocus evolution. *Genetics* 161, 1727–1750.
- Kuehn, C., 2015. Multiple time scale dynamics. volume 191. Springer.
- Lewontin, R.C., Kojima, K.i., 1960. The evolutionary dynamics of complex polymorphisms. *Evolution* 14, 458–472.
- Lion, S., 2018. From the Price equation to the selection gradient in class-structured populations: a quasi-equilibrium route. *Journal of theoretical biology* 447, 178–189.
- Lion, S., Gandon, S., 2016. Spatial evolutionary epidemiology of spreading epidemics. *Proc. R. Soc. B* 283, 20161170.
- May, R.M., 1976. Simple mathematical models with very complicated dynamics. *Nature* 261, 459.
- Nagylaki, T., Hofbauer, J., Brunovský, P., 1999. Convergence of multilocus systems under weak epistasis or weak selection. *Journal of mathematical biology* 38, 103–133.
- Pomiankowski, A., Bridle, J., 2004. Evolutionary genetics: no sex please we're at QLE (Quasi-Linkage Equilibrium).
- Pontz, M., Hofbauer, J., Bürger, R., 2018. Evolutionary dynamics in the two-locus two-allele model with weak selection. *Journal of mathematical biology* 76, 151–203.
- Pugh, C.C., Shub, M., Hirsch, M.W., 1977. Invariant manifolds. *Lecture Notes in Mathematics*, Springer, New York .
- Rice, S.H., 2004. Evolutionary theory: mathematical and conceptual foundations. Sinauer Associates Sunderland, MA.

- Sasaki, A., Hamilton, W.D., Ubeda, F., 2002. Clone mixtures and a pacemaker: new facets of red-queen theory and ecology. *Proceedings of the Royal Society of London. Series B: Biological Sciences* 269, 761–772.
- Ubeda, F., Haig, D., 2005. On the evolutionary stability of mendelian segregation. *Genetics* 170, 1345–1357.
- Úbeda, F., Russell, T.W., Jansen, V.A.A., 2019. PRDM9 and the evolution of recombination hotspots. *Theoretical population biology* 126, 19–32.
- Úbeda, F., Wilkins, J.F., 2011. The Red Queen theory of recombination hotspots. *Journal of evolutionary biology* 24, 541–553.
- Van Baalen, M., Rand, D.A., 1998. The unit of selection in viscous populations and the evolution of altruism. *Journal of theoretical biology* 193, 631–648.
- Wright, S., 1984. *Evolution and the genetics of populations: Vol. 2. The theory of gene frequencies*. University of Chicago Press.
- Yahara, K., Fukuyo, M., Sasaki, A., Kobayashi, I., 2009. Evolutionary maintenance of selfish homing endonuclease genes in the absence of horizontal transfer. *Proceedings of The National Academy of Sciences*, pnas-0908404106.

Appendix A. Deriving the discrete-time model

Our model (Úbeda et al., 2019) can be written as a particular case of the model known as the selection-recombination equations presented in (Lewontin and Kojima, 1960; Nagylaki et al., 1999; Bürger, 2000; Ubeda and Haig, 2005) and many other papers (Nagylaki et al., 1999). In the general model, haplotype frequencies evolve according to

$$\bar{w}x'_i(n) = \sum_{j=1}^m w_{i,j}x_ix_j + \epsilon_i\delta(w_{1,4}x_1x_4 - w_{2,3}x_2x_3), \quad (\text{A.1})$$

where x_i denotes the frequency of haplotype i , m is the number of alleles and $n \in \mathbb{N}_+$ represents the discrete time step. The recombination terms $\delta(w_{1,4}x_1x_4 - w_{2,3}x_2x_3)$ have different signs depending on the haplotype, provided by ϵ_i for haplotype i . Specifically, for

a two-locus two-allele implementation of the model, e_i is defined as

$$\epsilon_i = \begin{cases} -1 & \text{for } i = 1, 4 \\ 1 & \text{for } i = 2, 3. \end{cases} \quad (\text{A.2})$$

The marginal mean fitness of a haplotype whose frequency is x_i is given by

$$w_i = \sum_{j=1}^n w_{i,j} x_j, \quad (\text{A.3})$$

and the mean fitness of the population is given by

$$\bar{w} = \sum_{j=1}^n w_j x_j. \quad (\text{A.4})$$

Due to the normalisation of the right hand side of the governing equations of the model by the mean fitness of the population, the sum of the haplotype frequencies is always one. This means the state space of the model is the simplex of dimension $n^m - 1$, where n is the number of alleles and m is the number of loci.

Fitnesses for the two-locus two-allele version of our model are derived by computing all of the frequencies of offspring given by each possible mating combination. Due to the symmetries on the allele types determining when recombination occurs, the linkage disequilibrium D is the same for each haplotype and therefore can be taken out of the fitness matrix. This is clearly true in the more general versions of the model, meaning the linkage terms are separate in the statement of the general model equations (A.1). After this, and other simplifications which are possible due to symmetries in the gene conversion process and the viability benefits derived from crossover, we arrive at the following fitness matrix for the two allele two loci version of the model

$$W = \begin{pmatrix} 1 + \beta & 1 - \gamma & 1 & 1 \\ 1 + \gamma & 1 - \beta & 1 & 1 \\ 1 & 1 & 1 - \beta & 1 + \gamma \\ 1 & 1 & 1 - \gamma & 1 + \beta \end{pmatrix}. \quad (\text{A.5})$$

Applying our specific fitness matrix to the general model given gives the following system

of equations

$$\begin{aligned}
 \bar{w}x_1(n+1) &= (1+\beta)x_1^2 + (1-\gamma)x_1x_2 + x_1x_3 + x_1x_4 - \delta D, \\
 \bar{w}x_2(n+1) &= (1-\beta)x_2^2 + (1+\gamma)x_2x_1 + x_2x_3 + x_2x_4 + \delta D, \\
 \bar{w}x_3(n+1) &= (1-\beta)x_3^2 + (1+\gamma)x_3x_4 + x_3x_1 + x_3x_2 + \delta D, \\
 \bar{w}x_4(n+1) &= (1+\beta)x_4^2 + (1-\gamma)x_4x_3 + x_4x_1 + x_4x_2 - \delta D.
 \end{aligned} \tag{A.6}$$

Expanding the brackets in system (A.6) and applying the conservation law for the total population, $\sum_{i=1}^4 x_i = 1$, we can simplify the system to

$$\begin{aligned}
 \bar{w}x_1(n+1) &= x_1(n)[1 + \beta x_1(n) - \gamma x_2(n)] - \delta D, \\
 \bar{w}x_2(n+1) &= x_2(n)[1 - \beta x_2(n) + \gamma x_1(n)] + \delta D, \\
 \bar{w}x_3(n+1) &= x_3(n)[1 - \beta x_3(n) + \gamma x_4(n)] + \delta D, \\
 \bar{w}x_4(n+1) &= x_4(n)[1 + \beta x_4(n) - \gamma x_3(n)] - \delta D,
 \end{aligned} \tag{A.7}$$

where $\bar{w}\mathbf{x}(n+1) = \mathbf{f}(\mathbf{x})$ and $n \in \mathbb{N}_+$ and the population mean fitness is

$$\bar{w} = \sum_{i=1}^4 f_i(\mathbf{x}) = x_1 + x_2 + x_3 + x_4 + \beta(x_1^2 + x_4^2 - x_2^2 - x_3^2). \tag{A.8}$$

Appendix B. Isolation of the multiple time-scales

The region of parameter space for which the following arguments hold is where the heteroclinic cycle exists and is attracting in the discrete-time model, i.e. $\beta < \gamma$.

Appendix B.1. Time-scale separation nearby the interior equilibrium

We find three distinct time-scales in the dynamics of the linearised system nearby the interior equilibrium. Recall that the eigenvalues of the interior equilibrium of the continuous-time model are given by

$$\begin{aligned}
 \lambda_1 &= \frac{\gamma D^* + \sqrt{(\gamma D^*)^2 + \frac{1}{4}\beta(\beta - \gamma)}}{\bar{w}^*}, \\
 \lambda_2 &= \frac{\gamma D^* - \sqrt{(\gamma D^*)^2 + \frac{1}{4}\beta(\beta - \gamma)}}{\bar{w}^*}, \\
 \lambda_3 &= -\frac{\delta + 2D^*(\beta - \gamma)}{\bar{w}^*},
 \end{aligned} \tag{B.1}$$

where $\bar{w}^* = 1 + 2\beta D^*$. If $\beta > \gamma$ then $D^* > 0$. The interior equilibrium in that case is a saddle. If $\beta < \gamma$ then $D^* < 0$. Eigenvalues λ_1 and λ_2 then are complex with negative real parts and the interior equilibrium is always locally stable.

We introduce the parameter

$$\epsilon = \sqrt{\gamma - \beta}, \quad (\text{B.2})$$

which is small near the boundary of the region of parameter space in which we observe time-scale separation, $\beta < \gamma$. We substitute this definition into the equations and compute the eigenvalues at the interior equilibrium (9). For $0 < \epsilon \ll 1$, the eigenvalues satisfy the identities

$$\begin{aligned} \bar{w}^* \lambda_1 &= -\epsilon^2 \frac{\gamma}{8\delta} + i\epsilon \frac{\sqrt{\gamma}}{2} + O(\epsilon^3), \\ \bar{w}^* \lambda_2 &= -\epsilon^2 \frac{\gamma}{8\delta} - i\epsilon \frac{\sqrt{\gamma}}{2} + O(\epsilon^3), \\ \bar{w}^* \lambda_3 &= -\delta + O(\epsilon^3). \end{aligned} \quad (\text{B.3})$$

The dynamics of the system linearised around the interior equilibrium (9) operate on three distinct time-scales: $\bar{w}\delta^{-1}$, $2\bar{w}\epsilon^{-1}\gamma^{-\frac{1}{2}}$ and $8\delta\bar{w}\epsilon^{-2}\gamma^{-1}$. If $0 < \epsilon\sqrt{\gamma} \ll 2\delta < 1$ the time scales separate as $\delta^{-1} \ll 2\epsilon^{-1}\gamma^{-\frac{1}{2}} \ll 2\delta \left(2\epsilon^{-1}\gamma^{-\frac{1}{2}}\right)^2$. The second and third time-scales are associated with the motion within the QLE manifold, while the first relates to the approach towards the QLE manifold. Under this condition, the approach is very fast compared to the dynamics on the manifold, which justifies making a quasi-steady state assumption. This behaviour can be observed in Figure 3 where the approach to QLE is very fast with associated time-scale $\bar{w}\delta^{-1}$, and much faster than the cyclic behaviour on the manifold, which acts on time-scale $2\bar{w}\epsilon^{-1}\gamma^{-\frac{1}{2}}$, which in turn is faster than the approach to equilibrium which acts on time-scale $8\delta\bar{w}\epsilon^{-2}\gamma^{-1}$.

Note that the separation of time-scales is a direct consequence of the double degeneracy of the interior equilibrium (9). Specifically, when $\beta = \gamma$, and hence $\epsilon = 0$, two eigenvalues are zero. If the third eigenvalue is much smaller than zero, for small ϵ and continuous dependence of the eigenvalues on ϵ , the separation of time scales follows. This implies that the existence of a two-dimensional slow manifold is a generic result in the proximity of a double degeneracy and independent of the details of the model.

Appendix B.2. Time-scale separation in the full system

We introduce the new variables

$$\begin{aligned} X &= \sqrt{\gamma - \beta} \ln\left(\frac{A}{1-A}\right) + \sqrt{\beta} \ln\left(\frac{B}{1-B}\right), \\ Y &= (\gamma - \beta) \ln(A(1-A)) + \beta \ln(B(1-B)), \\ Z &= \frac{D}{\gamma - \beta}. \end{aligned} \tag{B.4}$$

If $\gamma \neq \beta$, these definitions implicitly define A and B locally as functions of X and Y and therefore the inverse transformation exists.

Rewriting the continuous-time model (15) in the new variables (B.4),

$$\begin{aligned} \frac{dX}{dt} &= \frac{\sqrt{\beta(\gamma - \beta)}}{\bar{w}} \left(\sqrt{\beta}(2B - 1) + \sqrt{\gamma - \beta}(2A - 1) + \frac{\gamma\sqrt{\gamma - \beta}(2B - 1)Z}{B(1 - B)} \right), \\ \frac{dY}{dt} &= -\frac{\beta(\gamma - \beta)}{\bar{w}} \gamma \frac{(1 - 2B)^2}{B(1 - B)} Z, \\ \frac{dZ}{dt} &= \frac{(\gamma - \beta)^{-1}}{\bar{w}} \left[(\gamma - \beta) \left[(\gamma - \beta)^2 Z^2 - AB(1 - A)(1 - B) \right] \right. \\ &\quad \left. - (\gamma - \beta)Z(\beta(2A - 1)(2B - 1) + \delta) \right]. \end{aligned} \tag{B.5}$$

Using (B.2), this can be written as

$$\begin{aligned} \frac{1}{\epsilon} \frac{dX}{dt} &= \frac{\sqrt{\beta}}{\bar{w}} \left(\sqrt{\beta}(2B - 1) + \epsilon(2A - 1) + \frac{\gamma\epsilon(2B - 1)}{B(1 - B)} Z \right), \\ \frac{1}{\epsilon^2} \frac{dY}{dt} &= -\frac{\beta\gamma}{\bar{w}} \frac{(1 - 2B)^2}{B(1 - B)} Z, \\ \frac{dZ}{dt} &= \frac{1}{\bar{w}} \left[\epsilon^4 Z^2 - AB(1 - A)(1 - B) - Z(\beta(2A - 1)(2B - 1) + \delta) \right]. \end{aligned} \tag{B.6}$$

When ϵ is small, the form of (B.6) isolates three distinct time-scales. The variable Z is changing at the fastest time-scale, and for Z small the variables X and Y (and A and B) are effectively constant. If A and B are constant, the variable Z has an equilibrium at

$$\begin{aligned} Z^* &= \epsilon^{-2} \frac{\beta(2A - 1)(2B - 1) + \delta}{2\epsilon^2} \\ &\quad - \epsilon^{-2} \sqrt{\left(\frac{\beta(2A - 1)(2B - 1) + \delta}{2\epsilon^2} \right)^2 + AB(1 - A)(1 - B)}. \end{aligned} \tag{B.7}$$

The linearised dynamics around Z^* are given by

$$\frac{d(Z - Z^*)}{dt} = -\frac{1}{w}(Z - Z^*)\sqrt{\left(\beta(2A - 1)(2B - 1) + \delta\right)^2 + 4\epsilon^4 AB(1 - A)(1 - B)} \quad (\text{B.8})$$

which always converges to the equilibrium $Z = Z^*$. Based on this we choose $D_{QLE} = \epsilon^2 Z^*$. If D_{QLE} is situated outside the simplex this argument is not relevant but a similar argument can be applied for attraction to the state $Z = \epsilon^{-2} D_S$.

Appendix C. Determining the contracting and expanding eigenvalues of the corner equilibria

Eigenvalue	$1 - \frac{\beta}{1+\beta}$	$1 + \frac{\gamma-\beta}{1+\beta}$	$1 - \frac{\beta}{1+\beta}$	$1 + \frac{\gamma-\beta}{1+\beta}$
Type	c_j	e_j	c_j	e_j
Condition	$\delta \leq \gamma - 2\beta$		$\delta > \gamma - 2\beta$	

Table C.3: The eigenvalues of the equilibria Φ_1 and Φ_4 . The eigenvalues do not depend on the condition.

In the vicinity of the origin (Φ_4), we find by Taylor expanding to second order that the QLE manifold is approximately defined by $D_{QLE}(0, 0) \approx -\frac{\gamma-\beta}{\beta+\delta} AB$. The attracting manifold $D = D_S(A, B)$ in the vicinity of the origin is approximately

$$D_S(A, B) \approx \begin{cases} -AB & \text{if } \delta \leq \gamma - 2\beta, \\ D_{QLE}(A, B) & \text{if } \delta > \gamma - 2\beta. \end{cases} \quad (\text{C.1})$$

The eigenvalues are therefore those given in table C.3.

Likewise, in the vicinity of the equilibrium Φ_2 and Φ_3 the QLE manifold is approximately

$$D_{QLE}(A, B) \approx \begin{cases} -\frac{\beta-\delta}{\gamma-\beta} + \frac{2\beta}{\gamma-\beta} A + \frac{2\beta}{\gamma-\beta} (1 - B) + (\frac{\gamma-\beta}{\beta-\delta} + \frac{4\beta}{\gamma-\beta}) A(B - 1) & \text{if } \delta < \beta, \\ -\frac{\gamma-\beta}{\delta-\beta} A(1 - B) & \text{if } \delta > \beta, \end{cases} \quad (\text{C.2})$$

Eigenvalue	$1 - \frac{\gamma-\beta}{1-\beta}$	$1 + \frac{\beta}{1-\beta}$	$1 - \frac{\gamma-\beta}{1-\beta}$	$1 + \frac{\beta}{1-\beta}$
Type	c_j	e_j	c_j	e_j
Condition	$\delta \leq \beta$		$\delta > \beta$	

Table C.4: The eigenvalues of the equilibria Φ_2 and Φ_3 . The eigenvalues do not depend on the condition

and hence

$$D_S(A, B) \approx \begin{cases} \max(-AB, -(1-A)(1-B)) & \text{if } \delta \leq \beta, \\ D_{QLE}(A, B) & \text{if } \delta > \beta, \end{cases} \quad (\text{C.3})$$

The eigenvalues are therefore those given in table [C.4](#).

Chapter 6

Chaotic evolutionary dynamics predict faster-than-drift divergence

Author contributions

Myself and Vincent A. A. Jansen conceived of the research, formulated the model and analysed it. Myself and Matthew J. Russell carried out the numerical analysis. Vincent A. A. Jansen and myself wrote the first draft of the manuscript.

Contents

6.1	Main text	145
6.2	Methods	153
6.2.1	The in-patch dynamics	153
6.2.2	The spatial model	156
6.3	Supplementary material	156
6.3.1	Model description and motivatoin	156
6.3.2	The models	157
6.3.3	The two-allele model explicitly	157
6.3.4	The three-allele model explicitly	158
6.3.5	Some analysis of the two-allele model	160
6.3.6	Projection function	164

Chaotic evolutionary dynamics predict faster-than-drift divergence

Timothy W. Russell^{a,*}, Matthew J. Russell^b, Vincent A.A. Jansen^a

^a*School of Biological Sciences, Royal Holloway University of London, Egham, Surrey, TW20 0EX, UK*

^b*School of Mathematical Sciences, University of Nottingham, University Park, Nottingham, NG7 2RD, UK*

Abstract

Selfish genetic elements are genes that seek to enhance their own frequency, at no benefit or even a cost to the individual [Lindholm et al. \(2016\)](#). Theoretical models of evolutionary dynamics tend to focus on populations near or at equilibrial gene frequencies, typically limiting their analyses to linear stability and seeking models that lend themselves to this procedure, i.e. focusing on models which do not exhibit sufficiently complex dynamics to warrant a different approach. Given the evolutionarily complex behaviour of SGEs, for example selective sweeps followed by stasis ([Lindholm et al., 2016](#); [Núñez et al., 2018](#)), we ask whether the interaction between selfish driver and target loci, interacting with specificity, exhibit complex behaviour. We show that genetic systems, with high enough biodiversity, can have chaotic dynamics arising from the linking of many heteroclinic cycles producing a heteroclinic network. We show, using symbolic dynamics, that this leads to a horseshoe map and positive Lyapunov exponents. The dependence on initial conditions means that nearby populations are driven apart. Populations diverge quickly, showcasing how chaotic dynamics can isolate populations. We believe this provides a plausible explanation for some observed chaotic genetic patterns, for example chaotic genetic patchiness.

Keywords:

Heteroclinic network, Chaos, Population genetics, Multi-locus, Three alleles

*Corresponding author

Email address: timothy.russell.2015@rhul.ac.uk (Timothy W. Russell)

1. Main text

The dynamics of biological populations are often erratic and unpredictable. Chaos theory has given us the insight that such dynamics come about even if the biological rules governing the system are simple (May, 1976). Gene frequencies, on the other hand, tend to have less complex dynamics and convergence to an equilibrium state is seen as the prevailing mode. Although genetic systems can theoretically have non-equilibrium behaviour and show, for instance, sustained oscillations (Akin, 1982; Hastings, 1981; Russell et al., 2019), such dynamics have not been widely supported by empirical results.

A notable exception are selfish genetics elements (SGEs). SGEs are genes, or sets of genes, that enhance their own transmission at the expense of the fitness of the organism they reside in (Werren, 2011). This results in rapid evolutionary change and genetic sweeps, punctuated by periods of relative stasis (Le Rouzic and Deceliere, 2005; Camacho et al., 1997; Goddard and Burt, 1999). Due to the fitness advantage they gain through overtransmission, populations can be invaded by SGEs. However, once established, they are prone to invasion themselves by genotypes that are resistant to overtransmission by the SGE. This can result in periods of rapid evolution including cyclic and recurrent replacement, as has been reported for meiotic drivers (Lindholm et al., 2016), a broad class of SGE's.

Meiotic drive systems typically involve a number of genes: the driver locus and a tightly linked target locus, on which the products of the driver locus act. Specific genes for drivers and targets have been identified in many cases, but the mechanism by which drive is achieved mostly remains elusive. Over transmission can be achieved through selective disruption or harm caused by a mismatch between driver and target, so that if the drivers in the gametes are matched to a different degree a departure from normal Mendelian segregation is achieved (Werren, 2011). It is further recognized to be likely that functional drivers impose a fitness cost; without such a cost, drivers would go to fixation (Núñez et al., 2018).

Meiotic drives often do not go to permanent fixation: drivers coexist in a population at relatively low frequencies, or show repeated invasion and degeneration, followed by re invasion (Lindholm et al., 2016). This is also supported by theoretical models which show that the dynamics of meiotic drivers can proceed to equilibrium, or have a sequence of cyclical connections between unstable (saddle) equilibria, known in mathematical terms as a heteroclinic cycle (Haig and Grafen, 1991; Stadler, 1996). This results in dynamics in which the population shows periods of stasis, interspersed with rapid sweeps (Figure 1). In models with two driver variants this results in dynamics in which the population shows an alternation of drivers sweeping through the population (Haig and Grafen, 1991; Stadler, 1996). Furthermore, the same patterns have been observed in models of homing endonuclease dynamics, another class of SGE (Yahara et al., 2009).

But what if there are more than two driver alleles? Will there be a stable equilibrium, will there be cycles of invasion in which the drivers take turns, or will the dynamics show an irregular sequence of invasions and become complex? Theoretically, if there are more than two driver alleles, multiple heteroclinic cycles can coexist and link together to form a heteroclinic network (Figure 2). In the vicinity of such heteroclinic networks complex dynamics are common and chaotic dynamics often ensue (Kirk et al., 2010). Here, we will explore if the heteroclinic networks that are associated with three allele systems for SGEs can give rise to chaotic dynamics.

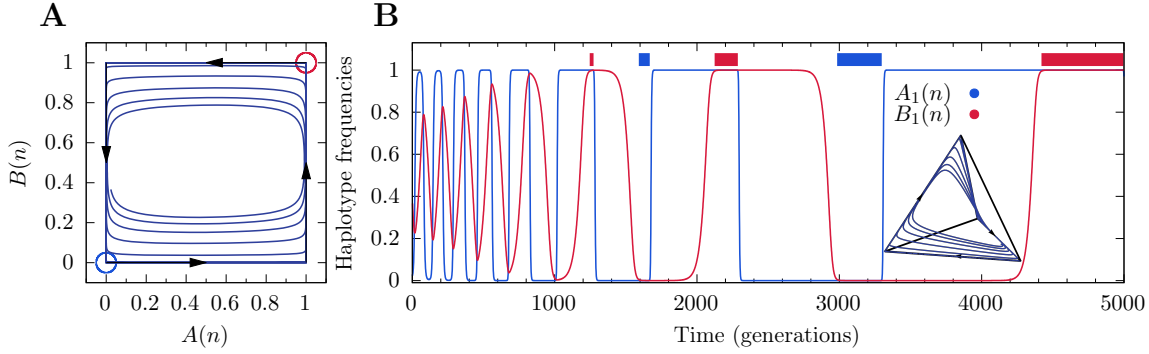


Figure 1: The dynamics of the two-allele model. We plot a solution of the two-allele model undergoing a heteroclinic cycle. When just two-alleles at each locus are present in our model, the allele frequencies proceed either towards the interior equilibrium or a heteroclinic cycle — where the system moves from one saddle equilibrium to another around the edges of the state space. During the approach to the heteroclinic cycle, the system stays in the vicinity of the unstable equilibria for longer and longer and dominant driver-target pairs in the population alternate. Panel A shows a phase space plot of a trajectory of the two-allele model using allele frequencies as coordinates. The environments in which a driver-target pair dominates are indicated by coloured spheres. Panel B shows a time series of the same trajectory, but in haplotype coordinates, with an inset of the phase space in haplotype coordinates — the tetrahedron. The bars above the time series indicate the times for which a matching driver-target pair dominates the population (i.e. when $p_{i,i}^2 - \phi_{i,i}^2 < \epsilon_{\text{ball}}^2$ for $i = 1, 2$ where $\phi_{i,i}$ is the saddle equilibria with haplotype $p_{i,i}$ at fixation and $\epsilon = 1 \times 10^{-2}$).

We formulated a simple model for a meiotic driver. Our model is a special case of the standard selection-recombination model (Bürger, 2000) that simplifies and generalizes a model for segregation distortion including drive, the reduction it causes in fitness, and recombination (Charlesworth and Hartl, 1978). We assume that there are m -alleles present in the population for both the driver and the target loci. Gametes that contain an unmatched driver allele are under transmitted relative to gametes that have a matched allele. The matching between the driver and target allele bears a fertility cost for the diploid: the more matches possible, the greater the cost. Therefore, a homozygous individual bearing matching driver and target has a reduction in fertility. Our model thus captures the essential feature of SGEs: they can invade when rare despite imposing a fitness cost on the individuals that bear them, thus capturing the complex dynamic interaction within a diverse population of SGEs.

For two-alleles we found the model to show oscillatory dynamics, which converged either to an equilibrium or to a heteroclinic cycle. This pattern can then repeat itself in a cyclic manner where the population alternates over time between the two different morphs of the distorters. The heteroclinic cycle can be characterized as follows: in a population in which a matching distorter-recognition pair dominates, a different recognition allele can invade, as it conveys a fitness benefit. Once this recognition allele has established itself in the population the matching distorter allele can invade (Figure 1).

The two-allele model exhibits regular dynamics, including stable cycling. Whereas, the dynamics of the three-allele model are much richer. Indeed, they can be irregular and highly complex. Figure 2 shows an example of the possible dynamics, suggesting the genetic system of three variant meiotic drivers can be chaotic. The irregular dynamics are easiest understood with reference to the heteroclinic cycles that the model allows. The three-allele model clearly has three heteroclinic cycles analogous to the one we encountered in the two-allele

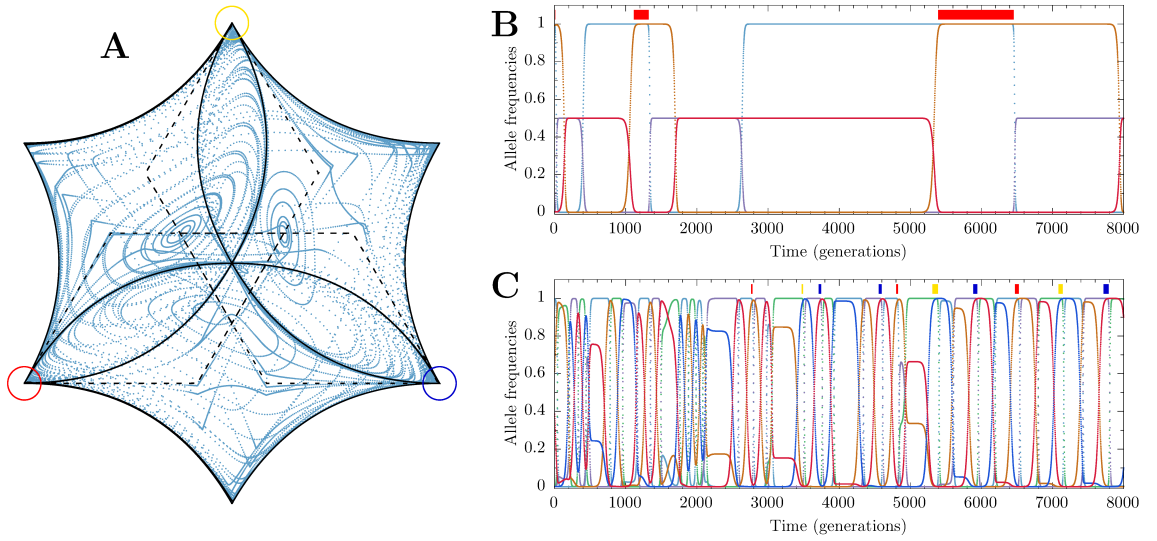


Figure 2: The dynamics of the three allele model. In the vicinity of heteroclinic networks, chaos is commonly found (Rodrigues et al., 2011). If three allelic variants are permitted in our model, we find a heteroclinic network with neighbouring chaotic dynamics in large regions of parameter space. More specifically, the population fluctuates, with one of the driver-target pairs dominating most of the time. This succession can be irregular and unpredictable. The left panel shows the state space projected into 2D using the projection function given by (39). Here, we see that the dynamics follow the heteroclinic network (heteroclinic connections are in solid and dashed black lines) with oscillatory behaviour in between connections. The dynamics occasionally get very close to nodes in the network, then to move away from it again. Panel B shows a time series of one of the same trajectories which is plotted using dashed lines in the projection (Panel A). There are three of these cycles in total. Panel C shows a time series of a chaotic solution which starts close but not on any of the cycles. Bars above both of the time series (Panel B and C) indicate which driver-target pair is dominating at that time in a similar fashion to Figure 1.

model. They occur in the three-allele model when one of the driver-target pairs is absent (Figure 2, Panel A, solid black lines). In addition, a further set of three heteroclinic cycles can exist if one driver competes against a coalition of two drivers that are present at equal frequencies (Figure 2, Panel A, dashed black lines). Starting from a population dominated by one type, say type 1, this state is then invaded by a coalition of equal frequencies of resistance alleles 2 and 3. This in turn leads to a population in which type 1 is absent and types 2 and 3 are at equilibrium. This polymorphic equilibrium can then be invaded by resistance gene 1, which in turn can be invaded by killer gene, which completes the cycle.

These six heteroclinic cycles link together form a heteroclinic network, and this heteroclinic network structure the dynamics of the three-allele model (Figure 2). When plotted in state space spanned up by the allele frequencies we see that the dynamics loosely follow the heteroclinic networks (Figure 2, Panel A, solid and dashed black lines). In the process we can see the population being close to a state where a single driver-target pair dominates the population, then to move away from it again.

Chaotic-like dynamics are commonly found in the vicinity of heteroclinic networks (Kirk et al., 2010). The three-allele system is an example of such a model. The population fluctuates and is being dominated by a succession of alleles. This succession can be irregular and unpredictable (Figure 2). The dynamics occasionally get very close to nodes in the network,

then move away again; a behaviour known as *switching* where a trajectory moving close to one heteroclinic cycle can abruptly switch and start following another cycle on the nearby network.

In natural populations, meiotic drivers vary over space and time; the dynamics often showing episodes of rapid turnover and sweeps, leading to a succession of different dominant drivers (Lindholm et al., 2016). This succession of different drivers provides a natural way to characterize the dynamics, both in empirical and model systems. In mathematics, the following concept is known as symbolic dynamics. Within the context of our model, the idea is to describe the dynamics as a sequence of states — which driver-target is dominating at a given time — rather than looking at the change in gene frequencies. To do so, we look at the sequence of bars that are depicted in Figures 1 and 2. If we assign the numbers $1, 2, 3, \dots, n$ to the distinct balls corresponding to the haplotypes with matching driver and target alleles, the succession of dominant types translates into a sequence of numbers. This sequence suffices to describe the dynamics. For instance, in the approach to the heteroclinic cycle in the two allele model the symbolic dynamics can be $1, 2, 1, 2, 1$ etc. (see Figure 1).

Which driver is the first one to become dominant depends on the initial conditions. Figure 3 shows a map of which driver is the first to become dominant in the three allele model, starting from different combinations of the 3 matching driver-allele pairs and using the same colours as Figure 2. The dependence on initial conditions is complicated, but note that the heteroclinic cycles that we have outlined (black dashed and solid lines in Figure 2, left panel) can be identified in this map. Concentrating on the corners of the triangular map we can see that starting from an initial condition dominated by one driver, we see that the next driver can be any of three (Figure 3b). If we then look at the state after that, we see that the domains leading to next state are split in 3: from one driver to the next anything is possible. This argument is similar to the of the Smale horseshoe map that is used in chaos theory to show that any sequence of types is possible: if from one dominant driver type to the next any driver can be picked there exist any sequence of symbols is possible and this shows the existence of irregular, and non-cyclic sequences – a hallmark of chaos (Smale, 1967).

Figure 3 also shows the sensitivity to initial conditions in the three-allele model. Solutions that start from nearby initial conditions will eventually diverge and lead to a very different sequence of states, therefore the map of the possible sequences becomes finer grained as the sequence gets longer (Figure 3b and 3c). This is further confirmed by the observation that the solutions can have a positive Lyapunov exponent.

A positive Lyapunov exponent means that two populations — with slightly different initial conditions — will eventually become very different (Arnold and Wihstutz, 1986). In a spatial setting of this model this means that spatial differences will increase over time if the coupling between two populations is less than the Lyapunov exponent (Jansen and Lloyd, 2000). To demonstrate this, we implement a finite population spatial version of the chaotic three allele model. We achieve this by first formulating the model for the subpopulation dynamics: a version of the model with demographic stochasticity, in the form of multinomial sampling of haplotypes between each generation, and mutation between alleles at both loci. Then, to produce the model representing the metapopulation dynamics, we couple n^2 subpopulations together on a square n -by- n lattice. The coupling represents migration between patches, causing gene flow between neighbouring subpopulations (see Subsection 2.2 in the Methods section).

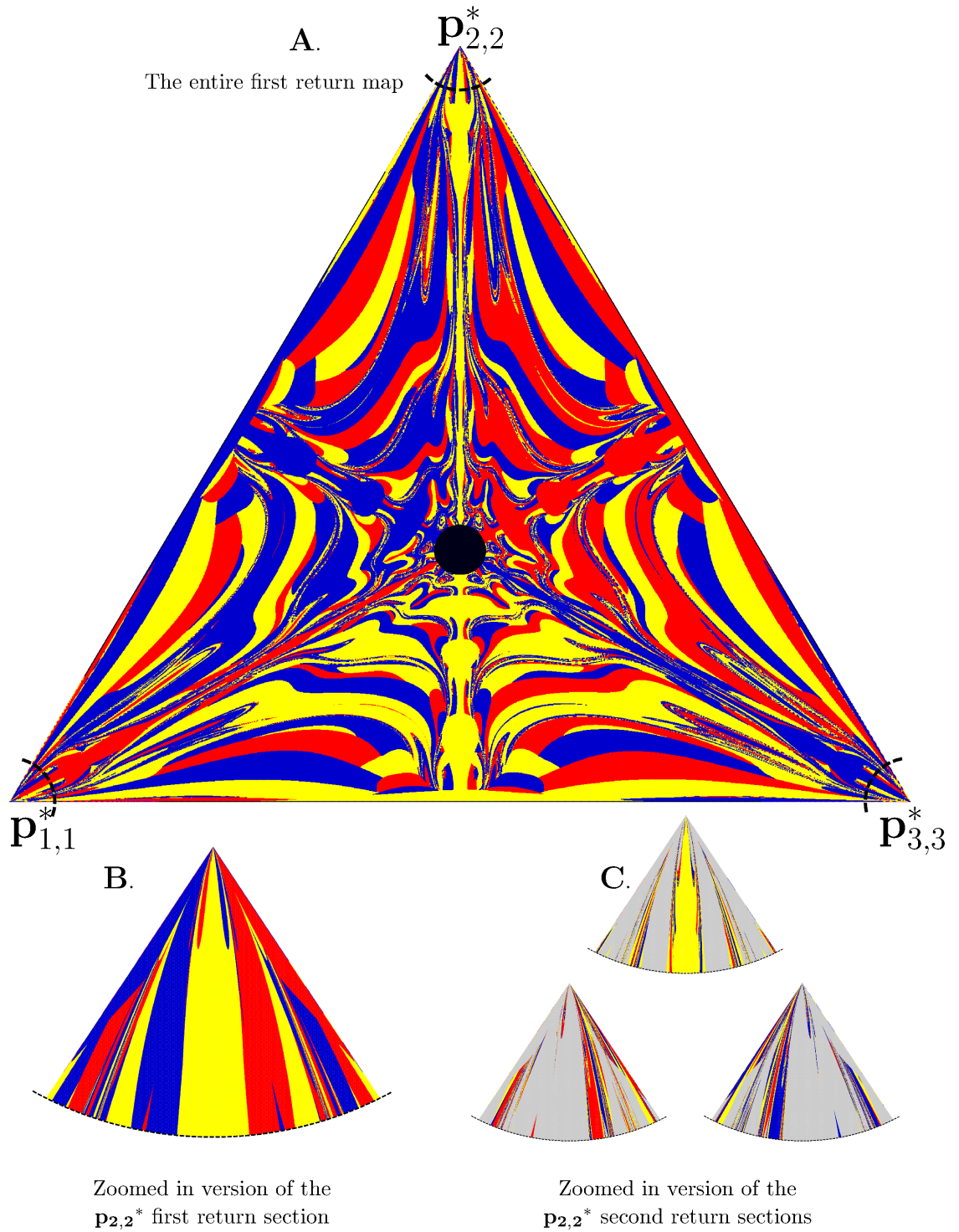


Figure 3 (previous page): **The next driver map.** We visualize the symbolic dynamics by constructing a map of the next driver for different starting frequencies. The map is constructed by computing trajectories which begin with a mixture of matching driver-target pairs (and all other haplotypes absent initially) — we depict the results as a barycentric map. More specifically, we linearly divide the space in which all three driver-target pairs are initially present in the population (and the other haplotypes are not present). We then iterate the system and determine which of the three driver-target pairs dominate next — determined by whether the trajectory has entered one of the three spheres depicted on the projection on the phase space with the same colours in Figure 3. The position of the map indicates the driver-target pair ($p_{1,1}$, $p_{2,2}$ or $p_{3,3}$), initial frequency and the colour indicates which sphere that trajectory entered first after simulating the dynamics.

Within the finite population metapopulation model, spatial patterning develops and the gene frequencies differ between locations if the local solutions are chaotic. The chaotic dynamics drive populations apart and the divergence in populations is faster than what one would obtain than through genetic drift causing classical isolation by distance (Figure 4).

Our results show that the specific features of SGEs can lead to complex, non-equilibrial dynamics in the gene frequencies. The dynamics are dominated by selective sweeps and repeated invasions which can lead to the unstable coexistence of multiple types of an SGE. If there are more than three driver and target genes possible in the population, chaotic dynamics are possible. In a spatial context this can lead to the divergence of local populations and a shifting mosaic type pattern. All these observations have parallels in the observed dynamics of SGEs. For example, selective sweeps and repeated invasions are commonplace for SGEs (Camacho et al., 1997; Goddard and Burt, 1999; Le Rouzic and Deceliere, 2005; Lindholm et al., 2016; Núñez et al., 2018). Diversity in types has been observed for meiotic drivers in the fungi *Neurospora* (Hammond et al., 2012) and *Podospora* (van der Gaag et al., 2000; Vogan et al., 2019): in the latter as many as seven types have been found to co-occur, as well as considerable spatial heterogeneity (Lindholm et al., 2016).

Our results show that chaotic dynamics can easily emerge in some simple genetic models, provided diversity is sufficiently high, suggesting that chaotic genetic dynamics could be more prevalent than hitherto assumed. Furthermore, the dynamics of our metapopulation model sheds new light on the potential speed and cause of genetic divergence of local populations. Specifically, chaotic in-patch dynamics can cause local populations to diverge faster than they would via genetic drift alone (Figure 4). The novelty of this pattern explains why few data exist supporting this statement. However, empirical phenomena this pattern might explain do exist. The clearest example comes from the genetics of marine ecosystems and is known as chaotic genetic patchiness. It sees genetic diversity at a small scale — in the order of a kilometer — appearing as large as would be expected through isolation by distance, over distances of hundreds of kilometers (Eldon et al., 2016).

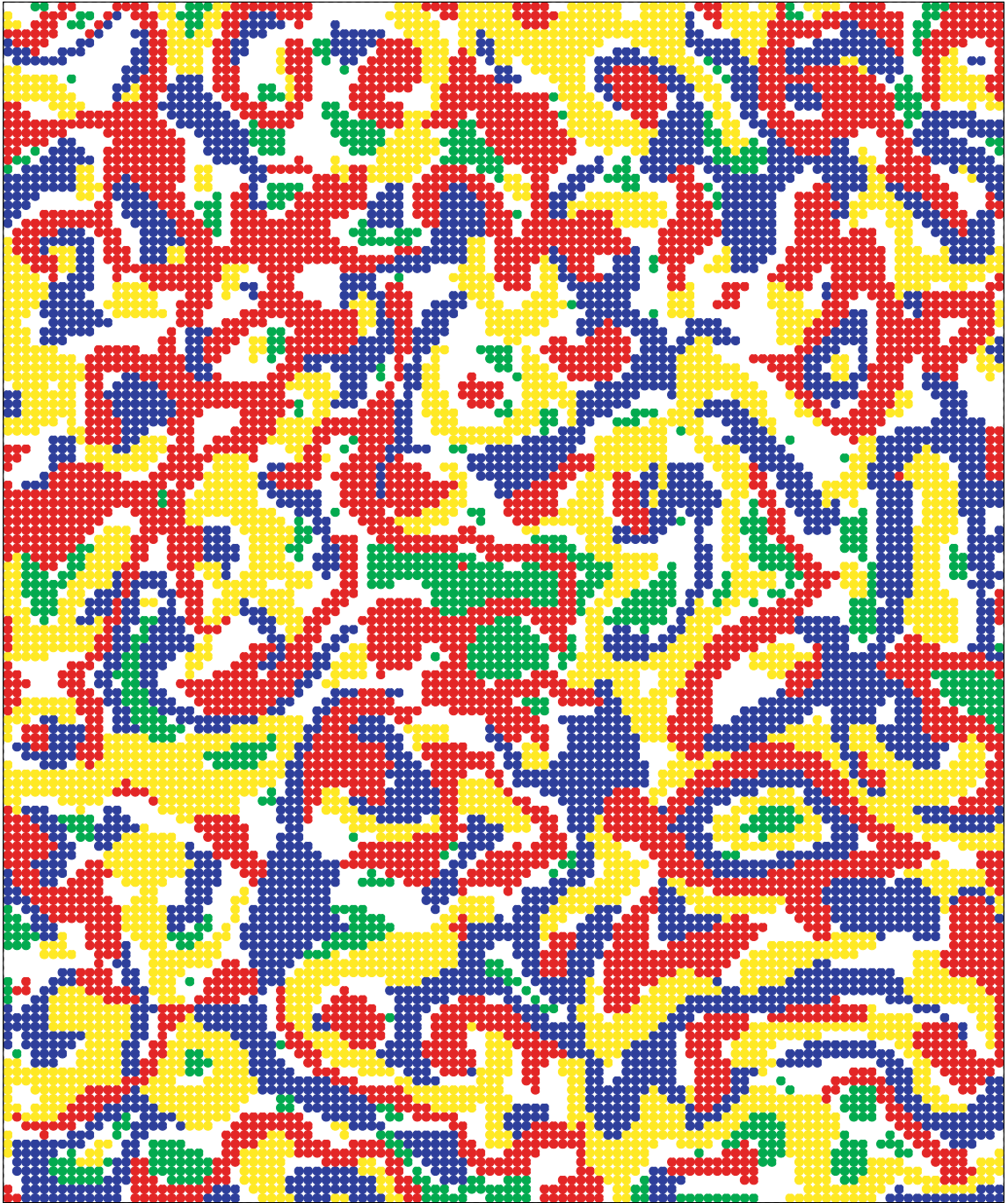


Figure 4: **A snapshot of the spatial three-allele model.** Snapshot taken at $t = 2,050$ of the spatial model (see Subsection 2.2 in the Methods section), with four neighbours per site and periodic boundary conditions. The same three colours as Figures 2 and 3 represent symbolically which of the homozygote haplotypes are dominant in the subpopulation. The parameters used were the same as those in Figure 2. Green represents non-matching driver-target haplotypes are dominating the subpopulation.

2. Methods

2.1. The in-patch dynamics

The mathematical model describing the dynamics within each patch is a special case of the selection-recombination equation for two interacting loci and m -alleles. The general selection-recombination equations are given by

$$p'_{i,j} = \bar{w}^{-1} \left(p_{i,j} \sum_{k,l=1}^m a_{i,j;k,l} p_{k,l} - r \sum_{k,l=1}^m (p_{i,j} p_{k,l} - p_{i,l} p_{k,j}) \right), \quad (1)$$

where

$$\bar{w} = \sum_{i,j,k,l=1}^m a_{i,j;k,l} p_{i,j} p_{k,l} \quad (2)$$

and $p_{i,j}$ is the frequency of gametes that have distorter allele i and recognition allele j . There are m^2 different haplotypes. We focus on the models with two or three variants of the driver and target loci, i.e. where $m = 2$ or $m = 3$.

We generalise the model for segregation distorters — by allowing for m alleles — originally formulated by [Charlesworth and Hartl \(1978\)](#). We also simplify their model by combining the effects of over transmission and fitness reduction, resulting in a far simpler formulation of the process. Their model describes distortion, the reduction in fitness distortion causes and recombination between two loci. The interaction of a driver and target loci is modelled by assuming the following: if a diploid contains one unmatched distorter allele, the gametes containing this allele are under transmitted and the other allele is over transmitted both by a factor of k_i ; if the distorter and recognition allele match (i.e. the subscripts at the two loci are equal), this bears a fitness cost to the resulting gamete by a factor of s_i . Therefore, homozygous individuals bearing matching distorter and recognition alleles have a drastic reduction in fertility. The effect of recombination follows the standard selection-recombination equation and remains unchanged from the general model (1).

Putting the over/under transmission and the fertility cost together, we arrive at the following rules for the fitness parameters $a_{i,j;k,l}$ for each haplotype

$$a_{i,j;k,l} = \begin{cases} s_{b(i;j,l)+b(k;j,l)} & \text{if } b(i;j,l) > 0 \vee b(k;j,l) > 0, \\ s_{b(k;j,l)} - k_{b(k;j,l)} & \text{if } b(i;j,l) = 0 \vee b(k;j,l) > 0, \\ s_{b(i;j,l)} + k_{b(i;j,l)} & \text{if } b(i;j,l) > 0 \vee b(k;j,l) = 0, \\ s_0 & \text{if } b(i;j,l) = 0 \vee b(k;j,l) = 0. \end{cases} \quad (3)$$

where — using $\delta(i,j)$, the Kronecker delta function — we define the function

$$b(i;j,l) = \delta_{i,j} + \delta_{i,l} \quad (4)$$

to count the total number of matches for distorter allele i that are possible in a diploid. The total number of matches in the diploid is $b(i;j,l) + b(k;j,l)$. For the explicit model in full, for both two and three-alleles, see Sections 3.3 and 3.4 respectively.

Note that the figures showing the in-patch dynamics (Figures 1 and 2) were of the allelic

frequencies, not the haplotype frequencies. The transformation, from haplotype frequencies to allelic frequencies (+ linkage disequilibrium) is known as symmetric coordinates and is standard in theoretical population genetics [Karlin et al. \(1970\)](#). We use it as our model has a lot of intrinsic symmetry, which is the cause of the many heteroclinic cycles connected, forming a heteroclinic network. Therefore the symmetric coordinates are a natural choice.

To aid some of the analysis, especially in the invariant subspaces subsection, we occasionally use single subscript notation via the following relation

$$x_{i+m(j-1)} = p_{i,j}. \quad (5)$$

2.1.1. Equilibria

We were able to determine the form of the unique polymorphic equilibrium of the m -allele model, using the form of the lower dimensional equilibria and the internal symmetries within the equations. The most concise way to write it is using vector notation. Let $\mathbf{1}$ denote a vector of ones of dimension m^2 . We use Φ to denote the equilibrium, D^* to denote the value of the linkage disequilibrium at the polymorphic equilibrium. Lastly, \mathbf{v} represents an eigenvector of the equilibrium. Using these definitions, it is possible to write the polymorphic equilibrium as

$$\Phi = \frac{1}{n}\mathbf{1} + D^*\mathbf{v}. \quad (6)$$

All three vectors in the equilibrium equation above, Φ , $\mathbf{1}$ and \mathbf{v} , are of dimension m^2 . The eigenvector \mathbf{v} is, using the single subscript notation, given by

$$v_{i+n(j-1)} = \begin{cases} m-1 & \text{if } i = j, \\ -1 & \text{if } i \neq j. \end{cases} \quad (7)$$

The equilibrium equation is derived in full for the two-allele model in the supplementary material (22). It is a cubic, therefore its solution is omitted for brevity.

2.1.2. Invariant subspaces and heteroclinic connections

To illustrate the existence of the heteroclinic connections within the three-allele model, we parameterise one of the three heteroclinic cycles for both the solid and the dashed cycles (see Figure 2, Panel A). The other two cycles for both types can be easily deduced by using the equivariance of the equations.

The cycles move on heteroclinic connection between equilibria (saddles): the solid cycles between equilibria that lie on the edges of the state space; the dashed cycles between a mixture of edge and interior equilibria. To explicitly state one cycle of each type, let l_i^p denote the i^{th} heteroclinic connection of p^{th} solid cycle where $i \in \{1, \dots, 4\}$ and $p \in \{1, 2, 3\}$. Furthermore, let \bar{l}_i^p similarly denote the i^{th} connection on the p^{th} dashed cycle. We present parameterised versions of all four connections, using haplotype coordinates, for l_i^1 and \bar{l}_i^1 .

The solid cycle is comprised of the following four heteroclinic connections

$$\begin{aligned}
 l_1^1 &= \left(x_1, 1 - x_1, 0, 0, 0, 0, 0, 0 \right), \\
 l_2^1 &= \left(0, x_2, 0, 0, 1 - x_2, 0, 0, 0 \right), \\
 l_3^1 &= \left(0, 0, 0, 1 - x_5, x_5, 0, 0, 0 \right), \\
 l_4^1 &= \left(1 - x_4, 0, 0, x_4, 0, 0, 0, 0 \right),
 \end{aligned} \tag{8}$$

where all variables are between zero and one and all lines are oriented positively (the variables increase as time increases).

Now for the dashed cycle

$$\begin{aligned}
 \bar{l}_1^1 &= \left(x_1, 0, 0, \frac{1}{2}(1 - x_1), 0, 0, \frac{1}{2}(1 - x_1), 0, 0 \right), \\
 \bar{l}_2^1 &= \left(0, 0, 0, x_4, x_5, x_6, x_4, x_6, x_5 \right), \\
 \bar{l}_3^1 &= \left(0, x_2, x_2, 0, x_5, x_6, 0, x_6, x_5 \right), \\
 \bar{l}_4^1 &= \left(x_1, \frac{1}{2}(1 - x_1), \frac{1}{2}(1 - x_1), 0, 0, 0, 0, 0, 0 \right).
 \end{aligned} \tag{9}$$

We evaluate the invariance of these subspaces by seeing A parameterised subset of the state space, \mathbf{y} , is invariant (with respect to the dynamics of our map) if

$$\mathbf{x} = \mathbf{y} \implies \mathbf{x}' = \mathbf{y}'. \tag{10}$$

This condition, for the lines presented above (and the other four heteroclinic cycles), is verified for our system in the attached Mathematica notebook (see Subsection 3.7 for details). The other cycles of both types are produced by the three-fold equivariance of our equations. The connections which make up those cycles can be found by permuting the connections given explicitly in this section. Alternatively, we provide their explicit form in the attached Mathematica notebook before verifying their invariance with respect to the dynamics of the system.

2.2. The spatial model

To extend the in-patch dynamics to a spatial model, we develop a well-known type of dynamical system known as a *coupled map lattice*. It is named so as we are coupling many maps — aka discrete-time dynamical systems — together in a lattice formation. The coupling biologically represents migration.

To ensure the spatial model was as biologically realistic as possible, we changed from

an infinite population (deterministic) model, for the in-patch dynamics, to a finite population (stochastic) model. We did this by multinomially sampling from the gamete pool at the end of each generation, representing classical genetic drift (Ewens, 2012). For individuals in a given patch, migration is possible to the patches four nearest neighbour patches, at a constant rate given by a parameter μ . Lastly, the boundaries are periodic, meaning that the surface is topologically equivalent to the torus.

3. Supplementary material

3.1. Model description and motivation

Selfish genetic elements enhance their own transmission at the expense of the fitness of the organism they reside in. One way in which selfish genetic elements achieve over-transmission is through segregation distortion: a manipulation of the genetic process so that one allele is passed on more than another to the next generation. This can be achieved through causing allele causing differential harm or mortality to the gametes. This can be achieved through linked loci coding for a distortion and recognition. The distortion allele produces a protein matches the recognition allele (or its product), and if so there is a reduction in the bearer's fitness. If the distorter allele isn't matched, then the part of the gametes containing such alleles fail to develop or function properly. If the distortion alleles in the gametes are matched to a different degree a departure from normal Mendelian segregation is achieved (Werren, 2011).

We formulate a simple model for such a segregation distorter. Our model is a simplified and generalised version of an earlier model for segregation distortion that describes distortion, the reduction its causes in fitness and recombination (Charlesworth and Hartl, 1978). We assume that there are many different alleles for the distorter and recognition alleles. If a diploid contains one unmatched distorter allele, the gametes containing this allele are under transmitted and the other allele is over transmitted. We assume that matching between the distorter and recognition allele bears a fitness cost for the individual in the form of reduced fertility. The more matches that are possible, the greater the cost and the stronger the over transmission. Therefore, a homozygous individuals bearing matching distorter and recognition alleles have a drastic reduction in fertility.

3.2. The models

Although the model simplifies many of the features found in other models for genetic elements, it does include the essential features of a selfish genetic element in that it imposes a cost on the individual that bears it, and that the selfish element can over-transmit.

3.3. The two-allele model explicitly

For two-alleles, the model reads

$$\begin{aligned}
 p'_{1,1} &= \frac{1}{\bar{w}} [p_{1,1}(s_4 p_{1,1} + s_2 p_{1,2} + (s_2 + k)p_{2,1} + s_2 p_{2,2}) - rD], \\
 p'_{1,2} &= \frac{1}{\bar{w}} [p_{1,2}(s_2 p_{1,1} + s_0 p_{1,2} + s_2 p_{2,1} + (s_2 - k)p_{2,2}) + rD], \\
 p'_{2,1} &= \frac{1}{\bar{w}} [p_{2,1}((s_2 - k)p_{1,1} + s_2 p_{1,2} + s_0 p_{2,1} + s_2 p_{2,2}) + rD], \\
 p'_{2,2} &= \frac{1}{\bar{w}} [p_{2,2}(s_2 p_{1,1} + s_2 p_{1,2} + (s_2 + k)p_{2,1} + s_4 p_{2,2}) - rD],
 \end{aligned} \tag{11}$$

where $D = p_{1,1}p_{2,2} - p_{1,2}p_{2,1}$ and the population mean fitness is given by

$$\begin{aligned}
 \bar{w} &= -kp_{1,2}p_{2,2} + kp_{2,1}p_{2,2} + s_4 p_{1,1}^2 + 2s_2 p_{2,1}p_{1,1} + 2s_2 p_{2,2}p_{1,1} \\
 &\quad + s_0 p_{1,2}^2 - 2s_2 p_{1,2}^2 + s_0 p_{2,1}^2 + s_4 p_{2,2}^2 + 2s_2 p_{1,2} + 2s_2 p_{2,1}p_{2,2}.
 \end{aligned} \tag{12}$$

For compactness of notation, similarly to the methods section of the main text, we denote the frequencies of the gametic genotypes through the variable x , which has a single subscript such that $x_{i+n(j-1)} = p_{i,j}$. By introducing the new variables $\beta = \frac{s_0 - s_4}{2s_2}$, $\epsilon = \frac{2s_2 - s_0 - s_4}{2s_2}$, $\delta = \frac{r}{s_2}$, $\gamma = \frac{k_2}{s_2}$, the system becomes

$$\begin{aligned}
 x'_1 &= \frac{1}{\bar{w}} [x_1(1 - (\beta + \epsilon)x_1 + \gamma x_2) - \delta D], \\
 x'_2 &= \frac{1}{\bar{w}} [x_2(1 + (\beta - \epsilon)x_2 - \gamma x_1) + \delta D], \\
 x'_3 &= \frac{1}{\bar{w}} [x_3(1 + (\beta - \epsilon)x_3 - \gamma x_4) + \delta D], \\
 x'_4 &= \frac{1}{\bar{w}} [x_4(1 - (\beta + \epsilon)x_4 + \gamma x_3) - \delta D],
 \end{aligned} \tag{13}$$

with

$$\bar{w} = 1 - \beta(x_1^2 - x_2^2 - x_3^2 + x_4^2) - \epsilon(x_1^2 + x_2^2 + x_3^2 + x_4^2) \tag{14}$$

and where we used $p_{11} + p_{12} + p_{21} + p_{22} = 1$.

3.4. The three-allele model explicitly

For the three-allele model written out explicitly, we begin with the version after the same parameter simplifications as used for the two-allele model have been used as the original parameterisation produces a very large system. After expanding, transforming the parameters

and some simplification, the three-allele system reads

$$\begin{aligned}
 p'_{1,1} &= \frac{1}{\bar{w}} \left[p_{1,1}(1 - (\beta + \epsilon)p_{1,1} + \phi(p_{2,3} + p_{3,2}) + \gamma(p_{1,2} + p_{1,3} + p_{2,3} + p_{3,2}) + \delta D_1 \right], \\
 p'_{1,2} &= \frac{1}{\bar{w}} \left[p_{1,2}(1 + (p_{1,2} + p_{1,3} + p_{3,2})(\beta - \epsilon) + \phi(p_{2,3} + p_{3,1} + p_{3,3}) \right. \\
 &\quad \left. - \gamma(p_{1,1} - p_{2,3} + p_{3,1} + p_{3,3}) + \delta D_2 \right], \\
 p'_{1,3} &= \frac{1}{\bar{w}} \left[p_{1,3}(1 + (p_{1,2} + p_{1,3} + p_{2,3})(\beta - \epsilon) + \phi(p_{2,1} + p_{2,2} + p_{3,2}) \right. \\
 &\quad \left. - \gamma(p_{1,1} + p_{2,1} + p_{2,2} - p_{3,2}) + \delta D_3 \right], \\
 p'_{2,1} &= \frac{1}{\bar{w}} \left[p_{2,1}(1 + (p_{2,1} + p_{2,3} + p_{3,1})(\beta - \epsilon) + \phi(p_{1,3} + p_{3,2} + p_{3,3}) \right. \\
 &\quad \left. - \gamma(-p_{1,3} + p_{2,2} + p_{3,2} + p_{3,3}) + \delta D_4 \right], \\
 p'_{2,2} &= \frac{1}{\bar{w}} \left[p_{2,2}(1 - (\beta + \epsilon)p_{2,2} + \phi(p_{1,3} + p_{3,1}) + \gamma(p_{1,3} + p_{2,1} + p_{2,3} + p_{3,1}) + \delta D_5 \right], \\
 p'_{2,3} &= \frac{1}{\bar{w}} \left[p_{2,3}(1 + (p_{1,3} + p_{2,1} + p_{2,3})(\beta - \epsilon) + \phi(p_{1,1} + p_{1,2} + p_{3,1}) \right. \\
 &\quad \left. - \gamma(p_{1,1} + p_{1,2} + p_{2,2} - p_{3,1}) + \delta D_6 \right], \\
 p'_{3,1} &= \frac{1}{\bar{w}} \left[p_{3,1}(1 + (p_{2,1} + p_{3,1} + p_{3,2})(\beta - \epsilon) + \phi(p_{1,2} + p_{2,2} + p_{2,3}) \right. \\
 &\quad \left. - \gamma(-p_{1,2} + p_{2,2} + p_{2,3} + p_{3,3}) + \delta D_7 \right], \\
 p'_{3,2} &= \frac{1}{\bar{w}} \left[p_{3,2}(1 + (p_{1,2} + p_{3,1} + p_{3,2})(\beta - \epsilon) + \phi(p_{1,1} + p_{1,3} + p_{2,1}) \right. \\
 &\quad \left. - \gamma(p_{1,1} + p_{1,3} - p_{2,1} + p_{3,3}) + \delta D_8 \right], \\
 p'_{3,3} &= \frac{1}{\bar{w}} \left[p_{3,3}(1 - (\beta + \epsilon)p_{3,3} + \phi(p_{1,2} + p_{2,1}) + \gamma(p_{1,2} + p_{2,1} + p_{3,1} + p_{3,2}) + \delta D_9 \right],
 \end{aligned} \tag{15}$$

where the population mean fitness is given by

$$\bar{w} = \sum_{i,j;k,l}^n a_{i,j;k,l} p_{i,j} p_{k,l}, \tag{16}$$

or alternatively, it can be thought of as the sum of the right-hand side of the entire system. The expanded version of the population mean fitness can be found in the accompanying

Mathematica notebook as its size makes it very difficult to present here. The D_k terms are given by (18).

3.4.1. Matrix notation

Matrix and vector notation allows us to write the general model (1) as follows. We collect the elements x_i in a row vector \mathbf{x} . The model then reads

$$\mathbf{x}' = \bar{w}^{-1}(\mathbf{x} + \mathbf{diag}(\mathbf{x}) \cdot \mathbf{F} \cdot \mathbf{x} - \delta \mathbf{D}), \quad (17)$$

where $\bar{w} = 1 + \mathbf{x}^T \cdot \mathbf{F} \cdot \mathbf{x}$ and the vector \mathbf{D} has elements

$$D_{i+n(j-1)} = \sum_{k,l=1}^n p_{i,j}p_{k,l} - p_{i,l}p_{k,j}. \quad (18)$$

The elements of \mathbf{F} are defined as

$$F_{i+n(j-1),k+n(l-1)} = \frac{a_{i,j;k,l} - s_2}{s_2}. \quad (19)$$

3.5. Some analysis of the two-allele model

We give a brief analysis including explicit equilibria and stability calculations for the two-allele model only. An analytic analysis of the three-allele model is beyond the scope of this paper.

If at any point $x_1 = x_4$ and $x_2 = x_3$, then this remains so in the future. If this is the case the difference equations become:

$$\begin{aligned} \bar{w}x'_1 &= \bar{w}x'_4, \\ \bar{w}x'_2 &= \bar{w}x'_3 \end{aligned}$$

and thus the increments of x_1 are the same as for x_4 and for x_2 they are the same as for x_3 . If this is the case we also have that $2x_1 + 2x_2 = 1$ and thus $x_2 = \frac{1}{2} - x_1$. The difference equation for x_1 then is

$$\bar{w}x'_1 = x_1 \left(1 - (\beta + \epsilon)x_1 + \gamma \left[\frac{1}{2} - x_1 \right] \right) - \delta \left(x_1 - \frac{1}{4} \right), \quad (20)$$

with

$$\bar{w} = 1 - \beta(2x_1 - \frac{1}{2}) - 2\epsilon(2x_1^2 + \frac{1}{4} - x_1) = 1 - 2\beta D^* - \epsilon(4D^{*2} + \frac{1}{4}). \quad (21)$$

On this manifold there is an equilibrium. On this manifold the linkage disequilibrium is $D = x_1 - \frac{1}{4}$. At equilibrium the linkage disequilibrium D^* can be found from as the root of the cubic

$$(\beta - \gamma + 4\epsilon D^*) \left(\frac{1}{16} - D^{*2} \right) + \delta D^* = 0, \quad (22)$$

for which $-\frac{1}{4} \leq D^* \leq \frac{1}{4}$ and the equilibrium is given by $\mathbf{x}^* = \frac{1}{4}\mathbf{1} + D^*(1, -1, -, 1, 1)^T$.

Note that if $\beta = \gamma$ then there is a solution $D^* = 0$. In the vicinity of $\beta - \gamma$, D^* is approximately $-(\beta - \gamma) \frac{1}{4(\epsilon + 4\delta)}$. If $\delta = 0$, $D^* = -\frac{\beta - \gamma}{4\epsilon}$.

The Jacobian takes the form:

$$\begin{aligned} \mathbf{J}|_{\mathbf{x}=\mathbf{x}^*} &= \frac{1}{\bar{w}^*} \left(\mathbf{I} - \mathbf{x}^* \mathbf{1}^T \right) D(\mathbf{x} + \text{diag}(\mathbf{x}) \cdot \mathbf{F} \cdot \mathbf{x} - \delta \mathbf{D})|_{\mathbf{x}=\mathbf{x}^*} \\ &= \frac{1}{\bar{w}^*} \left(\mathbf{I} - \mathbf{x}^* \mathbf{1}^T \right) (\mathbf{I} + \text{diag}(\mathbf{F} \cdot \mathbf{x}^*) + \text{diag}(\mathbf{x}^*) \cdot \mathbf{F} - \delta D \mathbf{D}|_{\mathbf{x}=\mathbf{x}^*}). \end{aligned}$$

where, for $m = 2$

$$D \mathbf{D}|_{\mathbf{x}=\mathbf{x}^*} = \begin{bmatrix} \frac{1}{4} + D^* & -\frac{1}{4} + D^* & -\frac{1}{4} + D^* & \frac{1}{4} + D^* \\ -\frac{1}{4} - D^* & \frac{1}{4} - D^* & \frac{1}{4} - D^* & -\frac{1}{4} - D^* \\ -\frac{1}{4} - D^* & \frac{1}{4} - D^* & \frac{1}{4} - D^* & -\frac{1}{4} - D^* \\ \frac{1}{4} + D^* & -\frac{1}{4} + D^* & -\frac{1}{4} + D^* & \frac{1}{4} + D^* \end{bmatrix}. \quad (23)$$

Direct analysis of the Jacobian is cumbersome. Following the analysis in [Úbeda et al. \(2019\)](#), which involves a similar model to this two-alleles model, we define the following matrix

$$\mathbf{M} = \begin{bmatrix} 1 & 1 & 1 & 1 \\ 1 & -1 & -1 & 1 \\ 1 & 1 & 0 & 0 \\ 1 & 0 & 1 & 0 \end{bmatrix}. \quad (24)$$

The matrix $\mathbf{M} \cdot (\mathbf{J} - \mathbf{I}) \cdot \mathbf{M}^{-1}$ is given by

$$\begin{pmatrix} -1 & 0 & 0 & 0 \\ \frac{1}{2} (16\beta D^{*2} - 8(\delta + 1)D^* - \beta + \gamma) & 8\epsilon D^{*2} - 2\gamma D^* - \delta - \frac{\epsilon}{2} & 0 & 0 \\ \frac{1}{4} (4D^* \beta + \beta + 4D^* \epsilon + \epsilon - 2) & 0 & -2D^* \beta - \frac{\epsilon}{2} & -\frac{\beta}{2} - 2D^* \epsilon \\ \frac{1}{4} ((\beta + \epsilon + \gamma)(4D^* + 1) - 2\gamma - 2) & 0 & \frac{1}{2} (-\beta + \gamma - 4D^* \epsilon) & -2D^* (\beta + \gamma) - \frac{\epsilon}{2} \end{pmatrix}.$$

and with eigenvalues

$$\begin{aligned} \lambda_1 &= 0, \\ \lambda_2 &= -\delta + 8D^{*2}\epsilon - 2\gamma D^* - \frac{\epsilon}{2}, \\ \lambda_{3,4} &= \frac{1}{2} \left(-2D^* (2\beta + \gamma) - \epsilon \pm \sqrt{\beta^2 - \beta(\gamma - 8D^* \epsilon) + 4D^* (-\gamma\epsilon + \gamma^2 D^* + 4D^* \epsilon^2)} \right). \end{aligned} \quad (25)$$

3.5.1. Corner and side equilibria

The corner and side equilibria all have the property that one of the allele frequencies is zero, so either $x_1 + x_2 = 0$, $x_1 + x_3 = 0$, $x_3 + x_4 = 0$ or $x_2 + x_4 = 0$. Whichever it is, as will only consider non-negative frequencies, for all these equilibria both terms in the sum have to be

zero and $D = 0$. So the equilibria are the solutions of

$$\begin{aligned}\bar{w}x_1 &= x_1 \left[1 - (\beta + \epsilon)x_1 + \gamma x_2 \right], \\ \bar{w}x_2 &= x_2 \left[1 + (\beta - \epsilon)x_2 - \gamma x_1 \right], \\ \bar{w}x_3 &= x_3 \left[1 + (\beta - \epsilon)x_3 - \gamma x_4 \right], \\ \bar{w}x_4 &= x_4 \left[1 - (\beta + \epsilon)x_4 + \gamma x_3 \right].\end{aligned}\tag{26}$$

The four possibilities are:

The side $x_1 = 0, x_2 = 0$

The dynamics are given by

$$\begin{aligned}\bar{w}(x'_3 - x_3) &= x_3 \left[1 + (\beta - \epsilon)x_3 - \gamma x_4 - \bar{w} \right], \\ \bar{w}(x'_4 - x_4) &= x_4 \left[1 - (\beta + \epsilon)x_4 + \gamma x_3 - \bar{w} \right],\end{aligned}\tag{27}$$

with

$$\bar{w} = x_3 + x_4 - \beta(-x_3^2 + x_4^2) - \epsilon(x_3^2 + x_4^2).\tag{28}$$

It is easy to work out that $x_3 + x_4$ is constant, and we choose this sum equal to 1. The dynamics for x_4 simplify to

$$\begin{aligned}\bar{w}(x'_4 - x_4) &= x_4 \left[-(\beta + \epsilon)x_4 + \gamma(1 - x_4) + \beta(2x_4 - 1) + \epsilon(1 - 2x_4 + 2x_4^2) \right], \\ \bar{w}(x'_4 - x_4) &= x_4 \left[\gamma + \epsilon - \beta + (-\gamma + \beta - 3\epsilon)x_4 + 2\epsilon x_4^2 \right], \\ \bar{w}(x'_4 - x_4) &= x_4(1 - x_4) \left[(\gamma + \epsilon - \beta) - 2\epsilon x_4 \right].\end{aligned}\tag{29}$$

The side equilibrium is given by

$$\begin{aligned}\frac{1}{2} \left(1 - \frac{\beta - \gamma}{\epsilon} \right) &= x_4, \\ \frac{1}{2} \left(1 + \frac{\beta - \gamma}{\epsilon} \right) &= x_3,\end{aligned}$$

with bifurcations at $\epsilon = \gamma - \beta$ and $\epsilon = \beta - \gamma$ and it has no negative elements if $\epsilon \leq \beta - \gamma \leq -\epsilon$ and $\epsilon = \beta - \gamma$.

The side $x_1 = 0, x_3 = 0$

The equilibria of the system are solutions of

$$\begin{aligned}\bar{w}x_2 &= x_2 \left(1 + (\beta - \epsilon)x_2 \right), \\ \bar{w}x_4 &= x_4 \left(1 - (\beta + \epsilon)x_4 \right),\end{aligned}\tag{30}$$

with

$$\bar{w} = 1 - \beta(-x_2^2 + x_4^2) - \epsilon(x_2^2 + x_4^2),\tag{31}$$

hence

$$\begin{aligned}-(\beta + \epsilon)x_4 &= (\beta - \epsilon)x_2, \\ \bar{w}(x_2 + x_4) &= \bar{w}\end{aligned}\tag{32}$$

$$\begin{aligned}-\beta &= \epsilon(x_4 - x_2), \\ 1 &= x_2 + x_4,\end{aligned}\tag{33}$$

$$\begin{aligned}-\beta &= \epsilon(1 - 2x_2), \\ 1 &= x_2 + x_4,\end{aligned}\tag{34}$$

$$\begin{aligned}\frac{1}{2} \left(1 - \frac{\beta}{\epsilon} \right) &= x_4, \\ \frac{1}{2} \left(1 + \frac{\beta}{\epsilon} \right) &= x_2,\end{aligned}\tag{35}$$

with bifurcations at $\beta = 0$ and $\epsilon = \beta$.

We will facilitate analysis of this system with the usual transformation of variables

$$\begin{aligned}A &= x_1 + x_2, \\ B &= x_1 + x_3, \\ D &= x_1x_4 - x_2x_3,\end{aligned}\tag{36}$$

with the reverse transformation (using $x_1 + x_2 + x_3 + x_4 = 1$)

$$\begin{aligned}x_1 &= AB + D, \\ x_2 &= A(1 - B) - D, \\ x_3 &= (1 - A)B - D, \\ x_4 &= (1 - A)(1 - B) + D,\end{aligned}\tag{37}$$

so that we get

$$\begin{aligned}\dot{A} &= \frac{1}{\bar{w}} A\beta(1-A)(2B-1) + \frac{\epsilon}{\bar{w}} ((1-A)(x_1^2 + x_2^2) - A(x_3^2 + x_4^2)), \\ \dot{B} &= \frac{\mu}{\bar{w}} [(\gamma - \beta)B(1-2A)(1-B) + \gamma(2B-1)D], \\ \dot{D} &= \frac{\mu}{\bar{w}} [A(A-1)(B-1)B(\beta - \gamma) - D((1-2A)(1-2B)\beta + \delta) + D^2(\gamma - \beta)].\end{aligned}\tag{38}$$

3.6. Projection function

The function used to project the trajectories in Figure 2 is used by Ashwin and Postlethwaite (2013) and is given by

$$R(t) = \frac{1}{n_v} \sum_{k=1}^n x_k^2 \exp \left[i\pi \frac{2(k-1)}{n_v} \right].\tag{39}$$

It projects the edges of the m -simplex onto the edges of a regular m -gon on the unit circle in the complex plane. As our dynamics are typically following on or nearby one of the heteroclinic connections, which almost all lie in one or two dimensional space, this projection works very effectively. More complex heteroclinic networks, with connections in higher dimensions, would have more information lost with such a projection function.

3.7. Additional materials

The additional materials to accompany this paper can be found at the following shared Dropbox folder: <https://tinyurl.com/y6caeto6>. Alternatively, if preferred, they can be found at the following private GitHub repository <https://github.com/thimotei/thesis-additional-materials>. Access to the private repository can be granted on request by sending an email to timothywilliamrussell@gmail.com. The materials include: an animation of the dynamics of the spatial model and the Mathematica notebook in which the model is implemented, dynamics are simulated and plotted and the invariance of the heteroclinic connections is verified. All of the exact parameters and initial conditions used for the figures can also be found in either the Mathematica notebooks or the C++ code.

References

- Akin, E., 1982. Cycling in simple genetic systems. *Journal of Mathematical Biology* 13, 305–324.
- Arnold, L., Wihstutz, V., 1986. Lyapunov exponents: Proceedings, bremen 1984. *Lecture Notes in Mathematics* 1186.
- Ashwin, P., Postlethwaite, C., 2013. On designing heteroclinic networks from graphs. *Physica D: Nonlinear Phenomena* 265, 26–39.

- Bürger, R., 2000. The mathematical theory of selection, recombination, and mutation. volume 228. Wiley Chichester.
- Camacho, J., Shaw, M., López-León, M., Pardo, M., Cabrero, J., 1997. Population dynamics of a selfish b chromosome neutralized by the standard genome in the grasshopper *eyprepocnemis plorans*. *The American Naturalist* 149, 1030–1050.
- Charlesworth, B., Hartl, D.L., 1978. Population dynamics of the segregation distorter polymorphism of *drosophila melanogaster*. *Genetics* 89, 171–192.
- Eldon, B., Riquet, F., Yearsley, J., Jollivet, D., Broquet, T., 2016. Current hypotheses to explain genetic chaos under the sea. *Current zoology* 62, 551–566.
- Ewens, W.J., 2012. Mathematical population genetics 1: theoretical introduction. volume 27. Springer Science & Business Media.
- van der Gaag, M., Debets, A.J., Oosterhof, J., Slakhorst, M., Thijssen, J.A., Hoekstra, R.F., 2000. Spore-killing meiotic drive factors in a natural population of the fungus *podospira anserina*. *Genetics* 156, 593–605.
- Goddard, M.R., Burt, A., 1999. Recurrent invasion and extinction of a selfish gene. *Proceedings of the National Academy of Sciences* 96, 13880–13885.
- Haig, D., Grafen, A., 1991. Genetic scrambling as a defence against meiotic drive. *Journal of theoretical Biology* 153, 531–558.
- Hammond, T.M., Rehard, D.G., Xiao, H., Shiu, P.K., 2012. Molecular dissection of neurospora spore killer meiotic drive elements. *Proceedings of the National Academy of Sciences* 109, 12093–12098.
- Hastings, A., 1981. Stable cycling in discrete-time genetic models. *Proceedings of the National Academy of Sciences* 78, 7224–7225.
- Jansen, V.A., Lloyd, A.L., 2000. Local stability analysis of spatially homogeneous solutions of multi-patch systems. *Journal of mathematical biology* 41, 232–252.
- Karlin, S., Feldman, M.W., et al., 1970. Linkage and selection: two locus symmetric viability model. *Theoretical population biology* 1, 39–71.
- Kirk, V., Lane, E., Postlethwaite, C.M., Rucklidge, A.M., Silber, M., 2010. A mechanism for switching near a heteroclinic network. *Dynamical Systems* 25, 323–349.
- Le Rouzic, A., Deceliere, G., 2005. Models of the population genetics of transposable elements. *Genetics Research* 85, 171–181.
- Lindholm, A.K., Dyer, K.A., Firman, R.C., Fishman, L., Forstmeier, W., Holman, L., Johannesson, H., Knief, U., Kokko, H., Larracuente, A.M., et al., 2016. The ecology and evolutionary dynamics of meiotic drive. *Trends in ecology & evolution* 31, 315–326.

- May, R.M., 1976. Simple mathematical models with very complicated dynamics. *Nature* 261, 459.
- Núñez, M.A.B., Nuckolls, N.L., Zanders, S.E., 2018. Genetic villains: killer meiotic drivers. *Trends in Genetics* 34, 424–433.
- Rodrigues, A.A., Labouriau, I.S., Aguiar, M.A., 2011. Chaotic double cycling. *Dynamical Systems* 26, 199–233.
- Russell, T.W., Russell, M.J., Úbeda, F., Jansen, V.A., 2019. Stable cycling in quasi-linkage equilibrium: fluctuating dynamics under gene conversion and selection. *Journal of theoretical biology* .
- Smale, S., 1967. Differentiable dynamical systems. *Bulletin of the American mathematical Society* 73, 747–817.
- Stadler, B.M., 1996. Heteroclinic cycles and segregation distortion. *Journal of theoretical biology* 183, 363–379.
- Úbeda, F., Russell, T.W., Jansen, V.A., 2019. Prdm9 and the evolution of recombination hotspots. *Theoretical population biology* 126, 19–32.
- Vogan, A.A., Ament-Velásquez, S.L., Granger-Farbos, A., Svedberg, J., Bastiaans, E., Debets, A.J., Coustou, V., Yvanne, H., Clavé, C., Saupe, S.J., et al., 2019. Combinations of spok genes create multiple meiotic drivers in *podospira*. *eLife* 8, e46454.
- Werren, J.H., 2011. Selfish genetic elements, genetic conflict, and evolutionary innovation. *Proceedings of the National Academy of Sciences* 108, 10863–10870.
- Yahara, K., Fukuyo, M., Sasaki, A., Kobayashi, I., 2009. Evolutionary maintenance of selfish homing endonuclease genes in the absence of horizontal transfer. *Proceedings of The National Academy of Sciences* 106, 18861–18866.

Chapter 7

Conclusion

Contents

7.1	Summary	166
7.1.1	Overview of the models used: their novelty and complexity .	166
7.1.2	Details of the analyses	167
7.2	Further work	168
7.3	Concluding remarks	169

7.1 Summary

The two central aims of this thesis were: to develop models in population genetics including novel biological details and extensions or capable of non-equilibrium and complex dynamics; and to analyse them, if necessary, to a point beyond that of linear stability — the standard endpoint for many models in specific cases within theoretical population genetics. Here, we list all of the models derived and presented in this thesis and describe briefly how each satisfies the central aims.

7.1.1 Overview of the models used: their novelty and complexity

Focusing on the first aim, these are the model we derived and presented in the thesis:

1. A two-locus n -allele non sex-specific model of the evolution of recombination hotspots in Chapter 3;
2. A sex-specific extension of the model from Chapter 4;
3. Chapter 5 saw the assumptions on the parameters of the non sex-specific model of the evolution of recombination hotspots from Chapter 3 relaxed (described in detail in Chapter 2), showing how it fits as a special case of the discrete-time selection-recombination equations;
4. Chapter 6 develops a model of the evolution of a genetic element known as a meiotic driver. The novelty here was allowing three-allelic variants within subpopulations to exist, producing very complex dynamics.

The models of the evolution of recombination hotspots in Chapters 3 and 4 included recent details of the molecular action of PRDM9 on its target site. Furthermore, extending the model to allow for two distinct sexes, as in Chapter 4, was motivated by strong empirical evidence that recombination hotspot evolution had many attributes which are sex-specific. Deriving a heteroclinic cycle, producing persist evolutionary behaviour of recombination hotspots in the non sex-specific model and a sex-specific level of linkage disequilibrium at a stable polymorphic equilibrium in the sex-specific model supports many of the empirical advances the models were motivated by.

The novelty and advances in Chapter 5 were primarily through the level of analysis undergone and therefore refer to the next section (7.1.2) about depth of analysis.

The novelty of the model in Chapter 6 came in two ways. First, we extended an existing model to allow for n -alleles of a meiotic driver. This process manifests itself by the way of index-based rules for the interaction between any number of alleles of a driver-target haplotype undergoing arbitrary levels of selection and recombination. Primarily

though, the advances given by this chapter are in the way of novel behaviours in models in theoretical population genetics — heteroclinic network and nearby chaos — and the resulting in-depth numerical and analytic analysis.

The final chapter is a framework and review chapter. Chapter 2 discusses clearly and verbosely the general model known as the selection-recombination equation. We show how some of the models used in this thesis are special cases of the selection-recombination equation and which genetic assumptions are required for this to be the case — allowing easily for other theoretical population genetic models to determine whether they too are members of this system. The chapter does not provide any new models. However, it reviews many of the known results from the literature about the general system and discusses some of the techniques used to establish these results. Its novelty comes in the way of a clear and expansive overview of the widely used general model.

Next, we describe the analyses carried out on the models, mentioning specific technical details which can be thought of as going beyond linear stability.

7.1.2 Details of the analyses

Chapter 5 was devoted to the global dynamics of discrete and continuous-time models inspired by the model of recombination hotspot evolution from Chapter 3. We noticed the model had a stable heteroclinic cycle and polymorphic equilibrium, both on the same surface within the state space. This surface, a well-known manifold in theoretical population genetics, is known as the *quasi-linkage equilibrium manifold*. We were able to determine an approximate closed-form expression for this surface in our model and, using the expression, we were able to determine the stability of the heteroclinic cycle bounded by the manifold. We also found a Lyapunov function for the continuous-time analogous system — proving global stability (for the subspace of the state space for which $D \leq 0$) for the interior equilibrium in continuous-time. Bistability, especially if studied using invariant manifold theory, a Lyapunov function and involves determining the stability of a heteroclinic cycle are beyond the standard levels of analysis.

The dynamics of the three-allele model presented in Chapter 6 are most easily interpreted as an extension the heteroclinic cycle from the two-allele models of recombination hotspot evolution via a three-fold symmetry, producing three such heteroclinic cycles joined together. However, allowing three allelic variants at each loci did more than this, it gave birth to three novel heteroclinic cycles of a different type — they did not only travel around the edges of the state space. Three quarters of the heteroclinic connections each of the new cycles are comprised of lie within the *interior* of the state space — something which was not possible in the two-allele version of the model. In total, the

model includes six heteroclinic cycles, with paths from one to another other point, producing a complex attracting heteroclinic network. As is common with such topologies within dynamical systems, the nearby dynamics were chaotic. We numerically computed which saddle along the network trajectories hit first, showing the dependency on initial conditions to be highly sensitive. Furthermore, we produced a coupled metapopulation implementation of the model. This metapopulation implementation exhibits highly complex patterns, including selective sweeps, divergence between subpopulations giving rise to patches of individuals with the same allele at fixation within the patch and a shifting mosaic pattern with what seem to be travelling wave solutions across the lattice. There is plenty more analysis possible on the spatial model, discussed at length in the next section about Further work.

7.2 Further work

It is the results of Chapters 5 and 6 that I believe have the clearest potential for further work. The QLE manifold in Chapter 5 was derived for a special case of the model, with a specific, but not too restrictive parameterisation of the fitness matrix. A separation of timescales existed, allowing for relatively simple approximation techniques to be used to find the closed-form expression for the QLE manifold. How generic is this separation of timescales? After transforming coordinates, using highly non-intuitive variables, we could isolate distinct timescales. Do these coordinate transformations isolate timescales in the most general formulation of the system? Exact conditions on the parameters for the existence of the QLE manifold were derived in [Seymenoglu \(2019\)](#). Inspecting these conditions under the coordinate transformations used in this thesis could elucidate if and when a separation of timescales exists in the two-locus two-allele equations.

Another interesting question comes from the stochastic implementation of the model describing the evolution of recombination hotspots in Chapter 3. Specifically, now it is clear there can exist a separation of timescales in this model, how close is the stochastic implementation of the model to manifold in general. I.e. are the stochastic models dynamics well approximated by the dynamics of a stochastic model constrained to the QLE manifold? This approach would use techniques developed in [Constable and McKane \(2017\)](#), whereby certain stochastic models are constrained to surfaces extracted from a deterministic analogue and results on the convergence of their stationary distributions are proved, showing the constrained dynamics to be very accurate. We predict that will be the case with the stochastic model in Chapter 3.

More abstractly, it would be a worthwhile, yet difficult endeavour, to try and derive conditions within the two-locus two-allele model which produce heteroclinic cycles.

Much like many models from mathematical biology, the edges of the state space are invariant, even in the most general formulation of the system (see a proof of the invariance of the edges of the tetrahedron in the two-locus two-allele model in Chapter 2). This would be best attempted by finding all of the sets of parameters which give the equations the type of intrinsic symmetries that give rise to heteroclinic cycles. Systems possessing such symmetries are known in as *equivariant dynamical systems* — systems where their solutions under the action of some Lie group are also solutions.

Finally, it would be fascinating to derive a version of the metapopulations model in Chapter 6 that varies continuously through space. This would involve taking a continuum limit and using the limit to derive a PDE. It would look like a reaction-diffusion equation. However, its coefficients would depend on the nine-dimensional system of difference (or differential) equations (for discrete and continuous-time respectively). This would mean it would be a highly complex and nonlinear PDE. However, as the numerical simulations suggest, the system seems to possess travelling wave solutions. Using this as an ansatz, it might be possible to make progress analytically, possibly finding certain sets of solutions to this highly complex PDE.

7.3 Concluding remarks

Studying the world of genetics and changing gene frequencies using complex mathematics has provided enough food-for-thought to keep theoretical population geneticists interested for over a century. This is the case as both the mathematical understanding required to study such systems, or the biological processes the systems represent, is sufficient for a career of wonderment. Furthermore, as the dynamics tend to be nonlinear and therefore complex dynamics are not just possible but quite likely. Indeed, the more and more realistic the models become, the more interesting and rich the dynamics are sure to be. Systems with enough complexity to represent the dynamics of genes in empirical populations are of dimension well high enough for the complexities observed in, for example, Chapter 6. It is the richness of both the mathematics and the biology — and the intimate connections between the two — which make theoretical population genetics a highly appealing avenue for research.

Bibliography

- Baudat, F., Buard, J., Grey, C., Fledel-Alon, A., Ober, C., Przeworski, M., Coop, G., De Massy, B., 2010. Prdm9 is a major determinant of meiotic recombination hotspots in humans and mice. *Science* 327, 836–840.
- Boulton, A., Myers, R.S., Redfield, R.J., 1997. The hotspot conversion paradox and the evolution of meiotic recombination. *Proceedings of the National Academy of Sciences* 94, 8058–8063.
- Buiting, K., Saitoh, S., Gross, S., Dittrich, B., Schwartz, S., Nicholls, R.D., Horsthemke, B., 1995. Inherited microdeletions in the angelman and prader–willi syndromes define an imprinting centre on human chromosome 15. *Nature genetics* 9, 395.
- Burt, A., Koufopanou, V., 2004. Homing endonuclease genes: the rise and fall and rise again of a selfish element. *Current opinion in genetics & development* 14, 609–615.
- Charlesworth, B., Hartl, D., 1978. Population dynamics of the segregation distorter polymorphism of *drosophila melanogaster*. *Genetics* 89, 171–192.
- Coddington, E.A., Levinson, N., 1955. *Theory of ordinary differential equations*. Tata McGraw-Hill Education.
- Constable, G.W., McKane, A.J., 2017. Exploiting fast-variables to understand population dynamics and evolution. *Journal of Statistical Physics* , 1–41.
- Darwin, C., 2004. *On the origin of species*, 1859. Routledge.
- Dawkins, R., 1976. *The Selfish Gene*. Oxford University Press, Oxford, UK.
- DeVries, P.L., Wolf, R.P., 1994. A first course in computational physics. *Computers in Physics* 8, 178–179.
- Grey, C., Baudat, F., de Massy, B., 2018. Prdm9, a driver of the genetic map. *PLoS genetics* 14.

- Haig, D., Grafen, A., 1991. Genetic scrambling as a defence against meiotic drive. *Journal of theoretical Biology* 153, 531–558.
- Hamilton, W.D., 1963. The evolution of altruistic behavior. *The American Naturalist* 97, 354–356.
- Hamilton, W.D., 1964. The genetical evolution of social behaviour. ii. *Journal of theoretical biology* 7, 17–52.
- Larracuente, A.M., Presgraves, D.C., 2012. The selfish segregation distorter gene complex of *drosophila melanogaster*. *Genetics* 192, 33–53.
- Lichten, M., Goldman, A.S., 1995. Meiotic recombination hotspots. *Annual review of genetics* 29, 423–444.
- Lindholm, A.K., Dyer, K.A., Firman, R.C., Fishman, L., Forstmeier, W., Holman, L., Johannesson, H., Knief, U., Kokko, H., Larracuente, A.M., et al., 2016. The ecology and evolutionary dynamics of meiotic drive. *Trends in ecology & evolution* 31, 315–326.
- Mendel, G., 1866. Versuche über pflanzenhybriden. *Verhandlungen des naturforschenden Vereines in Brünn* 4, 3–47.
- Myers, S., Bottolo, L., Freeman, C., McVean, G., Donnelly, P., 2005. A fine-scale map of recombination rates and hotspots across the human genome. *Science* 310, 321–324.
- Myers, S., Spencer, C., Auton, A., Bottolo, L., Freeman, C., Donnelly, P., McVean, G., 2006. The distribution and causes of meiotic recombination in the human genome.
- NIH, 2015. National human genome research institute. talking glossary of genetic terms. Retrieved from genome. gov at <http://www.genome.gov/glossary>.
- Núñez, M.A.B., Nuckolls, N.L., Zanders, S.E., 2018. Genetic villains: killer meiotic drivers. *Trends in Genetics* 34, 424–433.
- Paigen, K., Petkov, P., 2010. Mammalian recombination hot spots: properties, control and evolution. *Nature Reviews Genetics* 11, 221–233.
- Pittendrigh, C.S., 1958. Adaptation, natural selection, and behavior. *Behavior and evolution* 390, 416.
- Ponting, C.P., 2011. What are the genomic drivers of the rapid evolution of *prdm9*? *Trends in Genetics* 27, 165–171.

- Roach, J.C., Glusman, G., Smit, A.F., Huff, C.D., Hubley, R., Shannon, P.T., Rowen, L., Pant, K.P., Goodman, N., Bamshad, M., et al., 2010. Analysis of genetic inheritance in a family quartet by whole-genome sequencing. *Science* 328, 636–639.
- Rodgers, K., McVey, M., 2016. Error-prone repair of dna double-strand breaks. *Journal of cellular physiology* 231, 15–24.
- Russell, T.W., Russell, M.J., Úbeda, F., Jansen, V.A., 2019. Stable cycling in quasi-linkage equilibrium: Fluctuating dynamics under gene conversion and selection. *Journal of theoretical biology* 477, 84–95.
- Seymenoglu, B., 2019. Invariant manifolds of models from Population Genetics. Ph.D. thesis. UCL (University College London).
- Stadler, B.M., 1996. Heteroclinic cycles and segregation distortion. *Journal of theoretical biology* 183, 363–379.
- Úbeda, F., Russell, T.W., Jansen, V.A., 2019. Prdm9 and the evolution of recombination hotspots. *Theoretical population biology* 126, 19–32.
- Ubeda, F., Wilkins, J., 2011. The red queen theory of recombination hotspots. *Journal of evolutionary biology* 24, 541–553.
- Weiling, F., 1991. Historical study: Johann gregor mendel 1822–1884. *American journal of medical genetics* 40, 1–25.
- Wikimedia Commons, 2013. Illustration of the nucleotides in dna. URL: https://commons.wikimedia.org/wiki/File:DNA_Nucleotides.jpg.
- Williams, G., 1966. *Adaptation and natural selection* princeton university press. Princeton, NJ .
- Yahara, K., Fukuyo, M., Sasaki, A., Kobayashi, I., 2009. Evolutionary maintenance of selfish homing endonuclease genes in the absence of horizontal transfer. *Proceedings of The National Academy of Sciences* , pnas–0908404106.